THE COLUMNAR TO EQUIAXED TRANSITION

IN Pb-Sn AND Sn-Pb ALLOYS

by

Geoffrey T. Lowe

B.A.Sc.(Metallurgical Engineering), University of British Columbia, 1978

A THESIS IN PARTIAL FULFILMENT OF
THE REQUIREMENT FOR THE DEGREE OF
MASTER OF APPLIED SCIENCE

in

THE FACULTY OF GRADUATE STUDIES

Department of Metals and Materials Engineering

We accept this thesis as conforming
to the required standard

THE UNIVERSITY OF BRITISH COLUMBIA

March, 1990

In presenting this thesis in partial fulfilment of the requirements for an advanced degree at the University of British Columbia, I agree that the Library shall make it freely available for reference and study. I further agree that permission for extensive copying of this thesis for scholarly purposes may be granted by the head of my department or by his or her representatives. It is understood that copying or publication of this thesis for financial gain shall not be allowed without my written permission.

Department of Metals and Materials Engineering

The University of British Columbia
Vancouver, Canada

Date April 4, 1990

DE-6 (2/88)

ABSTRACT

The columnar to equiaxed transition has been studied experimentally using accurate temperature measurements and with a heat transfer mathematical model in Pb-1.5%Sn and Sn-10%Pb alloys. The behaviour of the two alloys was markedly different. In the Pb-1.5%Sn alloy, the transition did not occur until a large portion of the liquid thermally supercooled. At this point the temperature gradient in the liquid is very low, approximately 0°C/mm. For Sn-10%Pb, the transition occurred at a positive temperature gradient of approximately 0.12°C/mm which confirms earlier work by Mahapatra and Weinberg. Supercooling was also found to occur in this alloy but it is not certain whether the supercooling is constitutional or thermal. The difference in the behaviour of the two alloys is related to the density of nuclei prior to directional solidification. Altering the method to release latent heat by using the Scheil equation or the Lever rule instead of the traditional linear assumption in the mathematical model did not have a significant effect on the predicted temperatures or temperature gradients in the Pb-1.5%Sn alloy. The effect was seen when the Sn-10%Pb alloy was considered. The difference is attributed to the total amount of latent heat to be released by a particular alloy.

TABLE OF CONTENTS

LIST OF FIGURES

LIST OF TABLES

ACKNOWLEDGEMENTS

I would like to thank the Natural Science and Research Council for the support in putting this thesis together. In addition, I would like to express my heartfelt thanks to Dr. Fred Weinberg for his patience and understanding while this document was being prepared. Finally, this thesis could not have been done without the support of my fellow students whom I owe a great deal of thanks as well as to my family and friends.

This thesis is dedicated to the memory of my father, Robert A. Lowe.

Chapter 1

1.1 INTRODUCTION

The columnar to equiaxed transition, (CET), is a classical problem in the study of the solidification behaviour of cast alloys. The problem lies in the inability to fully understand why the structure changes abruptly from columnar to equiaxed along a plane, parallel to the mould wall, at some distance from the mould wall as shown by the example in Figure 1.1. The CET is sensitive to many of the parameters associated with the casting process, including the alloy composition, cooling rate, mould material, trace elements present in the melt, casting size and others. The transition from columnar to equiaxed may be sharp or gradual, the position of the transition can vary widely with respect to the mould wall, and the size of the columnar grains can vary appreciably. Since the mechanical properties of the casting are directly related to the cast structure all of these variables are important. At present there is no quantitative way of predicting the

cast structure from first principles, and particularly the CET. Even on a qualitative basis, the mechanism accounting for the CET is not clearly established.

Optimum mechanical properties are usually associated with an equiaxed fine grained structure. This is generally the case for ferrous or non ferrous permanent mould castings, as well as the continuous casting of steel and the DC casting of Al slabs. In particular for the continuous casting of steel, cracking of the billet or slab often occurs at the grain boundaries between columnar grains during casting[33]. As a result, casting conditions are adjusted to minimize the size and length of the columnar structure starting at the mould wall by electromagnetic stirring of the melt during casting. A fine grain structure in the DC casting of Al is promoted, to obtain better mechanical properties, by adding a nucleating agent to the melt such as TiB_2.

An attempt is being made to establish the mechanism which accounts for the CET and to define a parameter or equation which can be used to predict the position of the CET by examining the CET in a simple binary alloy and using a heat transfer model to define the complex thermal field which occurs during the solidification of a cast alloy.

1.2 LITERATURE REVIEW

The structure of castings, which includes the CET, has been examined and reported on for many years. Most of the reports are described and reviewed in standard textbooks on casting[1,2] and will not be considered here. A number of mechanisms have been proposed for the CET which are described and considered below. All of the models assume that the critical parameter in the CET is the presence and growth of nuclei ahead of the advancing columnar grains. The models then consider the source of the nuclei from

which the equiaxed grains grow. There are four mechanisms to account for the presence of the nuclei in the equiaxed zone. These are, constitutional supercooling, the big bang theory, dendrite remelting and dendrite showering.

1.2.1 CONSTITUTIONAL SUPERCOOLING

A columnar to equiaxed transition is not observed in pure metals under growth conditions where the structure is initially columnar. As a result, the CET must be associated with the alloying element. This led Winegard and Chalmers[4] to propose that the structure changes from columnar to equiaxed as a result of the entire central region becoming constitutionally supercooled. This would enable the existing heterogeneous nuclei to grow in a supercooled melt. The sequence of events as postulated by the authors is shown in Figure 1.2. Further consideration by Chalmers[5] led him to discard the concept of the entire central region becoming constitutionally supercooled. Solute is concentrated in a relatively small region ahead of the advancing columnar grains, as a result of segregation of the solute during solidification. The thickness of the region is in the order of microns, and remains essentially constant with a constant growth rate and constant fluid flow. As a result the entire central region cannot be constitutionally supercooled. In addition there is no clear evidence that heterogeneous nuclei grow more readily in a constitutionally supercooled liquid.

1.2.2 BIG BANG THEORY

Experimental observations showed that both the length of columnar grains and equiaxed grain size increased with increasing pouring temperature, Figure 1.3. In addition, the columnar length decreased with increasing solute concentration, Figure 1.4. These observations suggested that nuclei were present in the melt and led to the Big Bang theory. In this theory, the effective nuclei in the melt are generated at the mould wall as the chill mould is filled. Small solid grains are generated at the chill and are swept into the melt by the vigorous fluid flow in the melt at the start of solidification. At high pouring temperatures most of the grains do not survive and therefore there is a small equiaxed zone. The CET occurs when the melt supercools and allows the surviving grains to grow. The equiaxed grains ahead of the columnar grains block the columnar growth and the CET occurs.

1.2.3 SHOWERING OF DENDRITES

Southin[6] suggested that the presence of nuclei is the important step in the formation of the equiaxed zone. The nuclei are produced by the showering of dislodged surface dendrites which generally have a higher density than the melt. The surface dendrites result from a loss of heat to the ambient temperature by the air/melt surface. Preventing the loss of heat by hot topping or preventing the dendrites from showering into the central region of the casting by using a basket produced a predominantly columnar structure This mechanism for the CET is unique in that Southin proposes that supercooling is not a

necessary criteria for equiaxed grain growth. The equiaxed grains can grow after they touch the advancing columnar dendritic front. The latent heat of solidification is carried away by conduction through the solid columnar dendrites

1.2.4 DENDRITE REMELTING

To test the big bang theory and the constitutional supercooling theory Walker[7] conducted tests on Ni-Cu alloys and showed that these alloys could be supercooled 200°C and still produce an equiaxed zone during chill casting. This was contrary to what was expected for both theories. Jackson et Al[8] proposed a new theory based on observations made with transparent "metal like" materials. They showed that the secondary branches of the advancing columnar dendrites can become detached during growth, Figure 1.5. The detachment of the secondary branches is attributed to the melting of the solute enriched base of the secondary branch by currents of slightly hotter melt. The secondary branches move into the central region of the melt as a result of fluid flow or buoyancy forces. The secondary branches form the nuclei necessary for equiaxed growth. This mechanism produces a transition which is gradual rather than abrupt. The growth of nuclei into equiaxed grains was considered to occur in constitutionally supercooled liquid as postulated by Winegard and Chalmers[4].

1.2.5 THE INFLUENCE OF FLUID FLOW ON THE CET

Cole and Bolling[9,10] examined the effect of fluid flow on the formation of the CET in a number of alloys. They found that by suppressing the fluid flow due to natural

convection in the liquid by placing physical barriers to flow in the melt that columnar growth dominated. Increasing fluid flow in the melt by using rotating magnetic and electric fields reduced columnar growth producing a structure that was primarily equiaxed grains. Fluid flow was believed to change the structure and the CET by lowering the temperature gradient in the liquid, G_L, to a point where the nuclei that are present can survive and grow into equiaxed grains. A secondary effect of fluid flow is the enhancement of dendrite remelting following Jackson et Al[8].

1.2.6 CRYSTAL SEPARATION AT THE MOULD WALL

Ohno[11] proposed that nuclei for the equiaxed grains originate on the mould wall prior to solidification which is similar to the "Big Bang theory". However, Ohno explains that growth occurs along the mould wall in the fashion shown in Figure 1.6. Due to solute rejection a neck forms at the junction between the equiaxed grain and the mould wall. The equiaxed grain breaks at the neck and drifts into the central zone which is constitutionally supercooled. Support for this mechanism came from direct observation of the solidification of Sn-Bi in which small grains were observed to leave the mould surface on top of the melt.

1.2.7 COMPETITIVE GROWTH: EQUIAXED VERSUS COLUMNAR GROWTH

A completely different approach to the problem of the CET has been taken by Hunt and his co-workers[12-17]. Hunt recognized that for equiaxed grains to grow they must

release the latent heat of solidification into liquid that is cooler than the equiaxed grain. In other words, the liquid has to be supercooled. Since the CET occurs only in alloys, supercooling is constitutional. While most of the other studies consider constitutional supercooling, they have not considered how the constitutional supercooling develops. Hunt has examined in detail how constitutional supercooling is produced in the melt and the resultant structure on solidification based on nucleation and growth models.

The CET model developed by Hunt is based on the results of Burden and Hunt[16,17] who measured the columnar dendrite tip temperature in an Al-Cu alloy under different imposed temperature gradients, G, and growth velocities, V. The columnar dendrite tip temperature was determined by directionally solidifying the alloy in a small rod containing a thermocouple. When the leading edge of the solidifying front passed the thermocouple, the rod was rapidly quenched. The rod was then sectioned and the distance from the quenched solid interface and the thermocouple measured. The temperature of the solid/liquid interface was determined at the time when the interface was coincident with the thermocouple by back calculating using the growth velocity, the distance between the interface and the thermocouple at the time of the quench, and the cooling curve obtained from the thermocouple. This is shown in Figure 1.7. They used calibrated Pt-Pt/Rh thermocouples and measured temperatures to an accuracy of $\pm 0.1^{\circ}C$.

The results showed that the columnar dendrite tip is supercooled and varies depending on the imposed temperature gradient, G, and growth velocity, V, as shown in Figure 1.8, and the alloy composition as shown in Figure 1.9.

An equation was developed to calculate the amount of supercooling at the dendrite tip using the above variables and is given below.

$$\Delta T = \frac{GD}{V} + A'(C_o V)^{\frac{1}{2}} \tag{1.1}$$

where:

ΔT = Columnar dendrite tip supercooling

G = Temperature gradient in the liquid

D = Liquid diffusion coefficient

V = Velocity of the columnar dendrite tip

C_o = Alloy composition

A' = Constant

The Hunt model only considers the case where:

$$\frac{GD}{V} << A'(C_o V)^{\frac{1}{2}} \tag{1.2}$$

Which gives the supercooling at the dendrite tip as.

$$\Delta T = \left(\frac{VC_o}{A'}\right)^{\frac{1}{2}} \tag{1.3}$$

Nucleation and growth of the nuclei into equiaxed grains are then assumed to occur in the supercooled zone ahead of the dendrite tip. Hunt assumes that the nucleation rate is given by the expression.

$$I = (N_o - N) I_o \exp\left\{-\frac{u}{(\Delta T)^2}\right\} \tag{1.4}$$

where:

I = Nucleation rate per unit volume.

N_o = Total number of heterogeneous nuclei available per unit volume.

N = Number that have already produced grains.

ΔT = Supercooling at the dendrite tip.

u = A constant for a given nuclei.

I_o = A constant = 10^{20} estimated using the liquid diffusion coefficient of the melt.

The value of u is calculated on the basis of the heterogeneous nucleation temperature, ΔT_N, and is given by:

$$u = -(\Delta T)^2 \ln(N_o \times 10^{20}) \tag{1.5}$$

The competitive process Hunt considers in the model involves the competition between equiaxed grain growth and columnar grain growth in a constitutionally supercooled zone just ahead of the columnar dendrite tip.

For the model to predict the growth of equiaxed grains in the supercooled zone, the concept of an extended volume fraction is used to account for the impingement of equiaxed grains. The extended volume fraction is then used to determine whether or not at a specific columnar dendrite tip supercooling the structure is equiaxed or columnar by introducing an arbitrary criteria which states that a structure is fully equiaxed when:

$$\phi_E > 0.66 \tag{1.6}$$

where: ϕ_E = The extended volume fraction.

The extended volume fraction, ϕ_E, is calculated using the following equation.

$$\phi_E = \frac{4\pi r^3 N_o}{3} \tag{1.7}$$

where: r = Radius of the equiaxed grain.

The radius of the equiaxed grain is determined by relating the growth velocity of the equiaxed dendrite tips, V_e, at supercoolings greater than the heterogeneous nucleation supercooling, ΔT_N, so that :

$$r = \frac{A'[(\Delta T)^3 - (\Delta T_N)^3]}{3VGC_o} \tag{1.8}$$

Equation 1.8 is rearranged so that the velocity of the dendrite tip, V, and the alloy composition, C_o, are removed by substituting $(A'\Delta T_c)^2$ for VC_o from equation 1.3. In addition the radius of the equiaxed grain, r, is removed by using equation 1.7 at ϕ_E greater than 0.66 to give the criteria for fully equiaxed growth as a function of the dendrite tip supercooling, the heterogeneous nucleation supercooling, the nuclei density, and the temperature gradient giving the following expression.

For fully equiaxed growth:

$$G < 0.617 N_o^{\frac{1}{3}} \left\{ 1 - \frac{(\Delta T_N)^3}{(\Delta T_c)^3} \right\} \Delta T_c \tag{1.9}$$

Columnar growth is determined in a similar fashion except that it is taken to dominate when $\phi_E < 0.0066$ giving the following equation for fully columnar growth.

$$G > 0.617 (100 N_o)^{\frac{1}{3}} \left\{ 1 - \frac{(\Delta T_N)^3}{(\Delta T_c)^3} \right\} \Delta T_c \tag{1.10}$$

The structure is predicted by assuming N_o is $1/mm^3$ and ΔT_N is 0.75 K, which gives the columnar and equiaxed regions in a directionally solidified Al-3%Cu alloy shown in Figure 1.10 as a function of G and V. The CET using Hunt's model is assumed to be gradual as shown schematically in Figure 1.11.

1.2.8 CRITICAL TEMPERATURE GRADIENT

Mahapatra and Weinberg[18] investigated the CET in Sn-Pb alloys. They observed that the position of the CET was dependent on the rate of heat extraction on the bottom of a directionally solidified ingot, Figure 1.12. Experimental observations indicated that the position of the CET was independent of the melt superheat, as shown in Figure 1.13 contrary to previous reports, (Figure 1.3). As shown in Figure 1.13 the CET is abrupt and the transition plane flat contrary to the model proposed by Hunt.

The temperature field during solidification was determined for a directionally solidified Sn-Pb melt using a one dimensional heat transfer model. The model assumes the linear release of latent heat, negligible radial heat loss, and negligible melt/air heat loss. The model determined a specific temperature gradient in the liquid, G_L, that occurred at the position of the CET. For example, for a Sn-10%Pb alloy, the CET occurred at a G_L of 0.11°C/mm as shown in Figure 1.14. Thus, it was termed to be a critical temperature gradient for the formation of the CET in Sn-Pb alloys. There was very little composition dependence on the value of the critical temperature gradient as G_L for a Sn-5%Pb alloy was 0.10°C/mm and for a Sn-15%Pb alloy G_L was 0.13°C/mm.

The authors proposed that the CET occurred when the constitutionally supercooled region ahead of the advancing dendrite tip was sufficiently large enough to allow a

heterogeneous nucleus in the melt to grow. This region increased as the temperature gradient ahead of the melt decreased. Once equiaxed grains formed ahead of the advancing columnar dendrite tip, columnar dendritic growth would stop, producing a CET.

In a similar study, Ziv and Weinberg[19] showed that the CET occurs when G_L = 0.06°C/mm for an Al-3%Cu alloy. The CET is also very sharp for this alloy as shown in Figure 1.15 when directionally solidified. The experimentally determined value of 0.06°C/mm agreed generally with the theoretical prediction of 0.073°C/mm using the Hunt model assuming a nuclei density of 4.6/cm^3 and a calculated columnar dendrite tip supercooling of 0.71°C.

Increasing the number of nuclei in the melt by adding up to 100 ppm TiB_2 did not change the position of the CET as seen in Figure 1.16. Adding 171 ppm of TiB_2 produced a fine grained structure at a very high G_L of 0.88°C/mm. From these observations the authors proposed that there is a minimum large number of nuclei required to have an effect on the position of the CET. Below that number, the nucleant has very little effect on the CET and its position is determined by the temperature gradient in the liquid.

1.2.9 THEORIES OF DENDRITIC GROWTH INTO SUPERCOOLED ALLOY MELTS

Equiaxed and columnar grains are both manifestations of dendritic growth. As such it is felt to be worthwhile to discuss some of the theories of dendritic growth into supercooled alloy melts even though at the present time they do not explain the CET. They do however have potential to explain the CET if the critical parameters controlling

the CET are fully defined. A model by Lipton, Glicksman, and Kurz[20], assimilates the current theories very well to describe the behaviour of free dendritic growth in a supercooled liquid. The model splits the total supercooling at a dendrite tip into three components, so that:

$$\Delta T = \Delta T_t + \Delta T_c + \Delta T_R \tag{1.11}$$

where:

ΔT = The total supercooling

ΔT_t = Thermal supercooling

ΔT_c = Constitutional supercooling

ΔT_R = Supercooling associated with the curvature of the dendrite tip.

The three components of the total supercooling are illustrated in Figure 1.17 relative to a schematic phase diagram, and in Figure 1.18 relative to the temperature of the dendrite tip and the liquidus temperature of the alloy for a given solute composition profile ahead of the dendrite tip. The three components of the total supercooling in Figure 1.18 are contrasted with the case of a pure metal where $C_o = 0$ and the total supercooling consists of only two components, the thermal component and the component associated with the curvature of the dendrite tip.

Lipton, Glicksman, and Kurz developed expressions which give the growth rate, V, and the dendrite tip radius, R, of a free growing dendrite for a given alloy having a specified supercooling.

One expression is the Ivantsov equation which is the general solution for the diffusion field around a shape preserving paraboloid of revolution. This shape approximates the shape of a dendrite tip. For a steady state dendrite tip radius, the Ivantsov equation is:

$$\Omega = P\,\mathrm{EXP}(P)E_1(P) \equiv I_v(P) \tag{1.12}$$

where:

Ω = Dimensionless supersaturation

$E_1(P)$ = Exponential integral function

$I_v(P)$ = Ivantsov function

P = Peclet number

For the thermal field, the Peclet number is:

$$P_t = \frac{VR}{2a} \tag{1.13}$$

where:

V = Interface growth rate

R = Dendrite tip radius

a = Thermal diffusivity

For the solutal field ahead of a dendrite tip:

$$P_c = \frac{VR}{2\bar{D}} \tag{1.14}$$

where: $\tilde{D}$ = The interdiffusion coefficient

The dimensionless supersaturation, Ω, is given a thermal and solutal component. The thermal component, Ω_t is given by:

$$\Omega_t = \frac{\Delta T_t c_p}{\Delta H} \tag{1.15}$$

where: $\Delta H/c_p$ = The designated unit thermal supercooling

Combining equations 12 to 15, gives the thermal supercooling:

$$\Delta T_t = \frac{\Delta H}{c_p} I_v(P_t) \tag{1.16}$$

where:

ΔH = Latent heat

c_p = Specific heat

It can also be shown that the constitutional supercooling is given by:

$$\Delta T_c = mC_o\left\{1 - \frac{1}{(1-k_o)I_v(P_c)}\right\} \tag{1.17}$$

where:

m = Liquidus slope

C_o = Initial alloy composition

k_o = The equilibrium partition coefficient

The depression of the liquidus temperature due to the curvature of the tip is given by:

$$\Delta T_R = \frac{2\Gamma}{R} \tag{1.18}$$

where:

Γ = The Gibbs-Thomson parameter

Combining equations 16 to 18 gives:

$$\Delta T = \Delta\frac{H}{c_p} I_v(P_t) + mC_o\left\{1 - \frac{1}{(1-k_o)I_v(P_c)}\right\} + \frac{2\Gamma}{R} \tag{1.19}$$

This equation relates the product of the growth velocity, V, and the dendrite tip radius, R, to the supercooling, ΔT. To obtain unique values for V, and R, a stability criterion is introduced.

$$\lambda_i = \left\{\frac{\Gamma}{\sigma^*(mG_c - G)}\right\}^{\frac{1}{2}} \tag{1.20}$$

where:

λ_i = Shortest wavelength which can form at the tip

σ^* = Stability constant

G_c = Concentration gradient

G = Temperature gradient

Mean gradients were assumed in the model and defined as:

$$\overline{G} = -\frac{P_t \Delta H}{c_p R} \tag{1.21}$$

$$\overline{G_c} = -\frac{P_c C^* (1 - k_o)}{R} \tag{1.22}$$

where: C^* = the solute concentration at the dendrite tip

Thus, the stability criterion is written in the form.

$$R = \frac{\Gamma/\sigma^*}{\frac{P_t \Delta H}{c_p} - \frac{P_c m C_o (1 - k_o)}{1 - (1 - k_o) I_v(P_c)}} \tag{1.23}$$

The equations for the tip radius and the total supercooling were used to determine how the growth rate, V, and the tip radius, R, varied with total supercooling and solute concentration for a succinonitrile-acetone solution.

The model results agreed well with the experimental measurements as shown in Figure 1.19 and Figure 1.20. In the CET, a necessary condition for the equiaxed grains to grow ahead of the advancing columnar dendrites is that the liquid be supercooled. The model and analysis of the growth of dendrites described above is the most recent attempt to quantify the dendritic growth process. The model develops expressions for the dependence of supercooling at the dendrite tip on growth rate, tip curvature, and solute segregation. Since the dependence is a basic component of the CET process, the analysis could be of value in developing a model for the CET from basic principles.

1.2.10 DISCUSSION

It appears that the temperature gradient in the liquid, G_L is a critical factor in the development of the CET in cast alloys considering the work by Hunt[12-17], Weinberg[18,19], and the earlier work by Cole and Bolling[9,10]. To predict the position of the CET using Hunt's model requires specific knowledge on the number of nuclei present in the supercooled zone, the heterogeneous nucleation temperature of the nuclei, and the amount of supercooling at the columnar dendrite tip. These values are not readily available which limits the applicability of the Hunt model to predict the CET under normal casting conditions. In addition Hunt's model is for a gradual transition from columnar to equiaxed which has been shown not to be the case in work by Weinberg.

The concept of a critical temperature gradient, G_L, in the melt in front of the columnar dendrite tip requires detailed knowledge of the temperature field in a casting during solidification and the thermophysical properties of the metal. Heat transfer mathematical models are being developed extensively for castings and can be validated with temperature measurements. This can provide the detailed thermal field during the solidification which can be used to establish where in the casting the critical G_L will occur. The values of G_L for Sn-Pb are different from the Al-Cu alloys, which indicates G_L is different for different alloy systems. However, there is no mention of thermocouple calibration reproducibility by Mahapatra and Weinberg[18] in the Sn-Pb work while the G_L for Al-Cu alloys could not be determined by a mathematical model due to the poor fit between experimental temperatures and predicted temperatures. The values for G_L were

taken from the cooling curves which would have to be produced by thermocouples with a known accuracy relative to each other and an absolute accuracy relative to the melting point of the pure Al.

1.2.11 OBJECTIVES OF THE PRESENT INVESTIGATION

The nucleation theories to account for the CET are not clearly established, and cannot be used to predict when the CET will occur in a casting. The Hunt model, as it stands, requires information concerning the density and effective nucleating temperature of nuclei in the melt as well as the supercooling at the dendrite tip, all of which are generally not known in most alloys. In addition, the theory assumes a gradual transition at the CET which is generally not the case. The model which associates the CET with a critical temperature gradient ahead of the dendrite tip is critically dependent on accurate temperature measurements and a precise heat transfer mathematical model since the gradients are continuously changing and are very small at the CET. The result for Sn-Pb in which the experimental measurements were not fitted well by the heat transfer model indicate that better measurements are required as well as a better heat transfer model, particularly in establishing boundary conditions used in the model. Similar problems were present in the Al-Cu observations.

The objectives of the present investigation are:

1. Experimentally determine the temperature distribution in the liquid ahead of the columnar dendritic front for Pb-Sn alloys using accurate temperature measurements.

2. Determine if a critical temperature gradient, G_L, in the melt exists for Pb-Sn alloys at the CET and establish the value of the gradient.

3. Investigate various procedures used to account for the release of latent heat in a one dimensional heat transfer model. These procedures for releasing the latent heat include the following, 1) Linear release of latent heat using the specific heat method, 2) Release proportional to fraction solid determined by the Scheil equation, 3) Release proportional to fraction solid determined by the Lever rule.

4. With the mathematical model, establish the temperature gradient in the melt as a function of distance from the chill. Determine the critical temperature gradient, G_L, at the CET.

Examining the Pb-Sn system will establish G_L for a third alloy system. In addition it will consider the possibility of equiaxed grain movement during solidification. When Sn-Pb solidifies, the initial grains are Sn rich and as a result are lighter than the melt. In the Pb-Sn system, the initial grains are heavier than the melt and they will not rise. Accordingly if upward movement of grains is significant in the CET, the results for Pb-Sn should be markedly different than Sn-Pb.

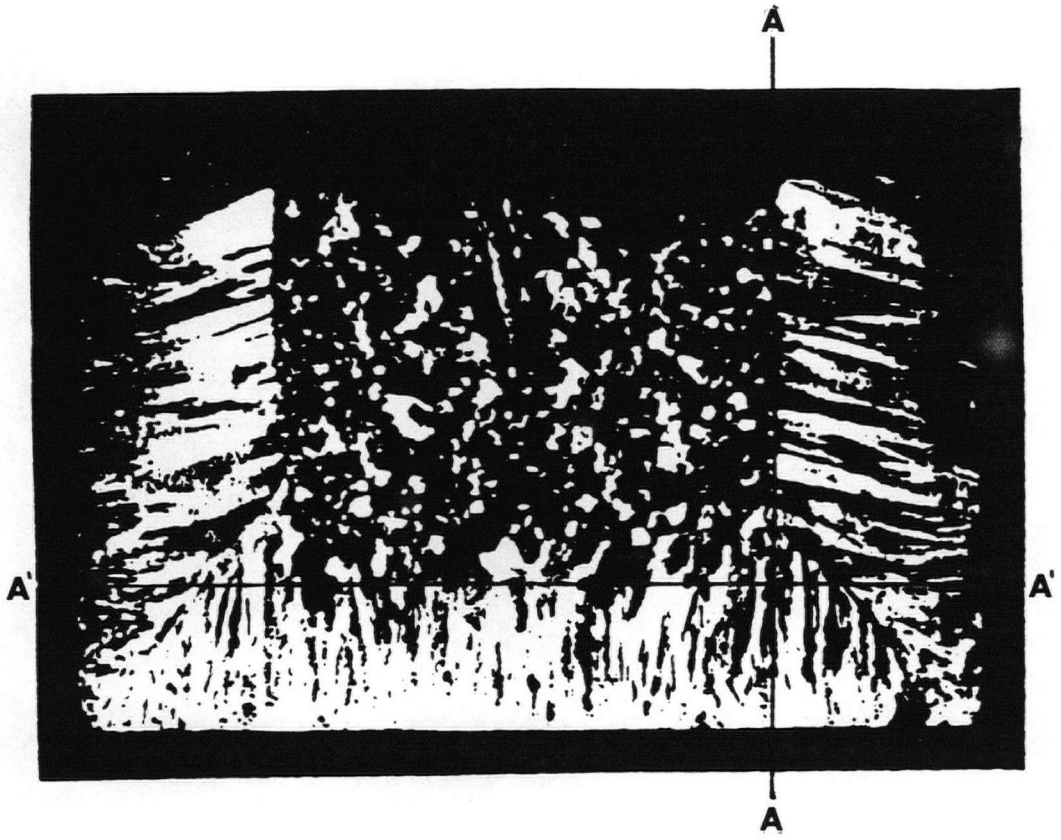

Figure 1.1

The columnar to equiaxed transition in a cast Pb- %Sb alloy at planes A-A and $A'-A'$

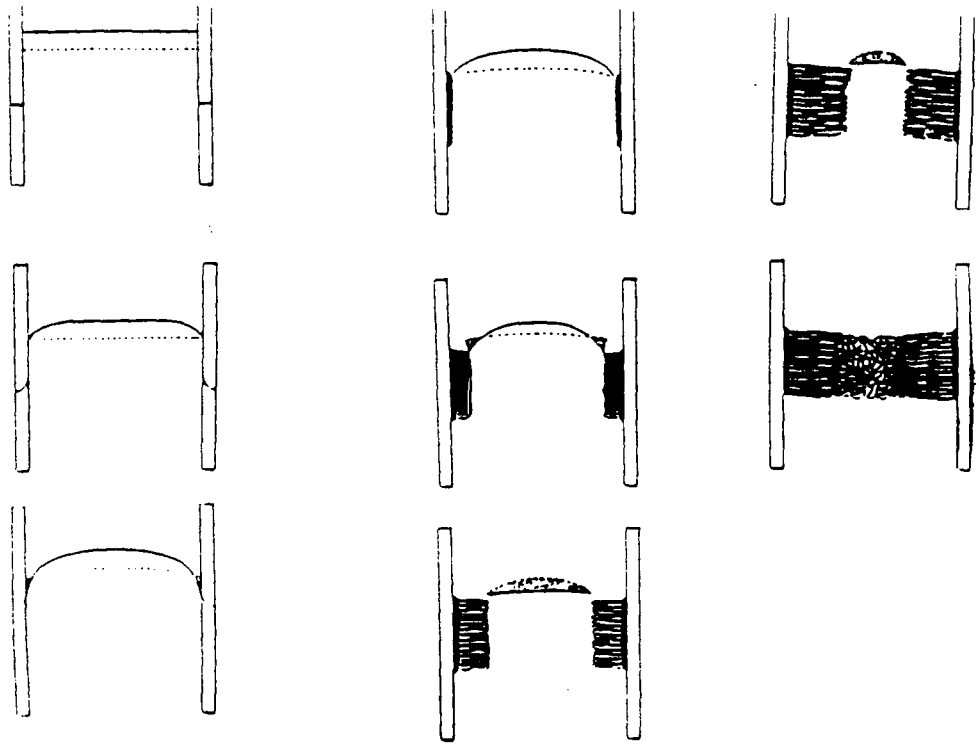

Figure 1.2

The sequence of events for the CET according to the constitutional supercooling theory.

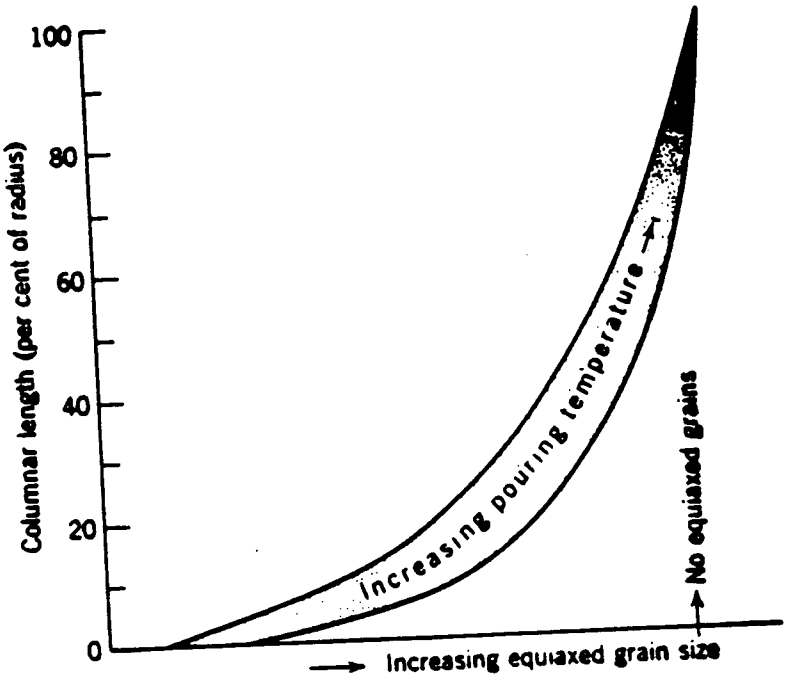

Figure 1.3

Variation in grain size and columnar length with pouring temperature.

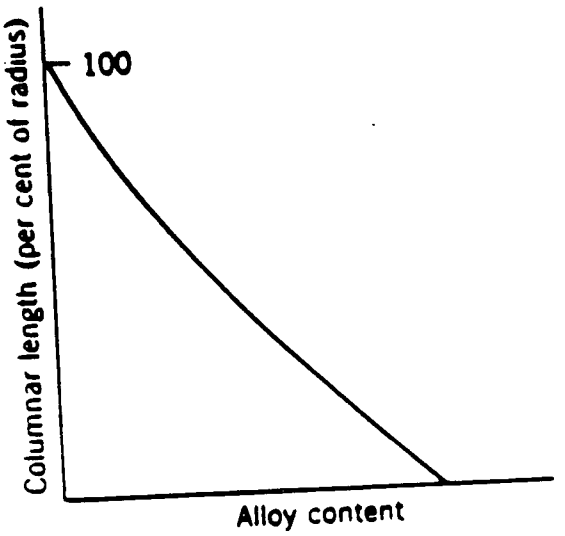

Figure 1.4

Variation in grain size with alloy content.

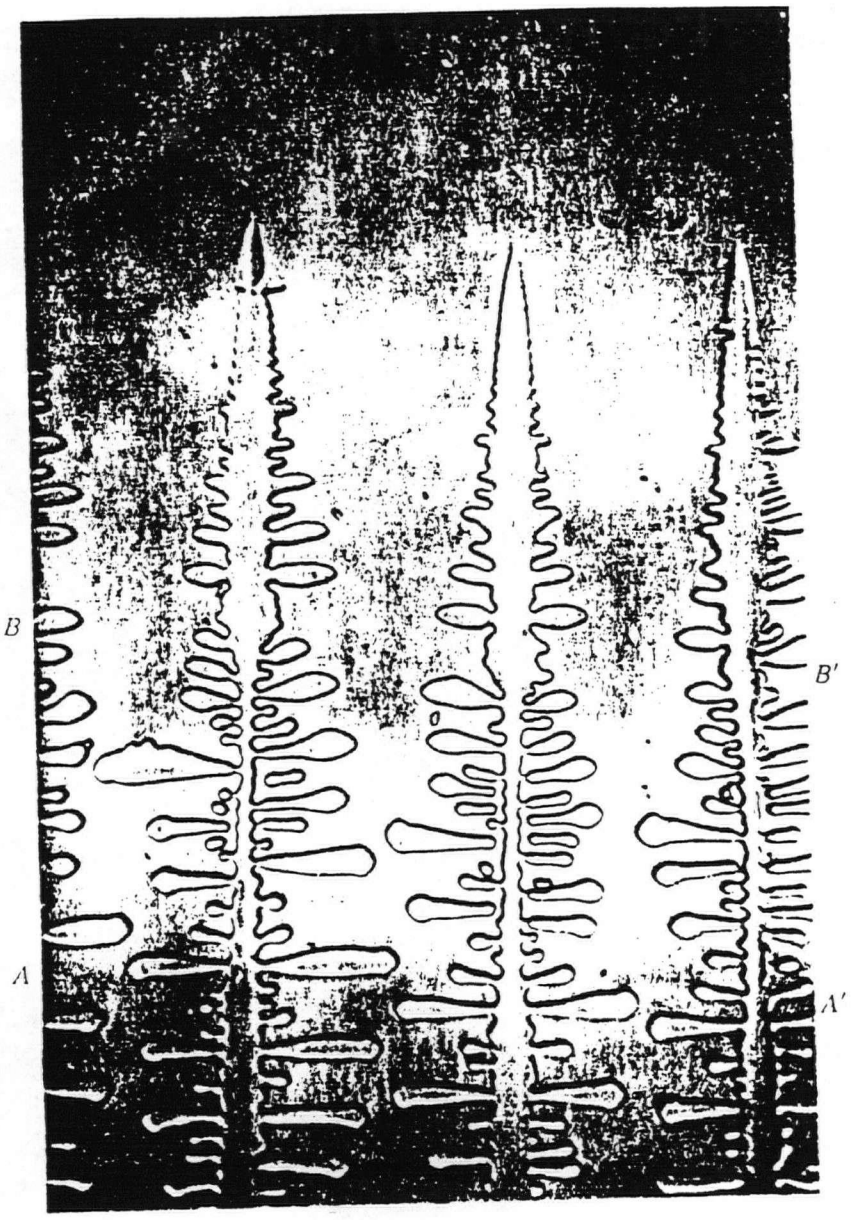

Figure 1.5

Secondary dendrite branches showing neck formations and detachment during growth.

Carbon tetrabromide with added salt. Mag. X75

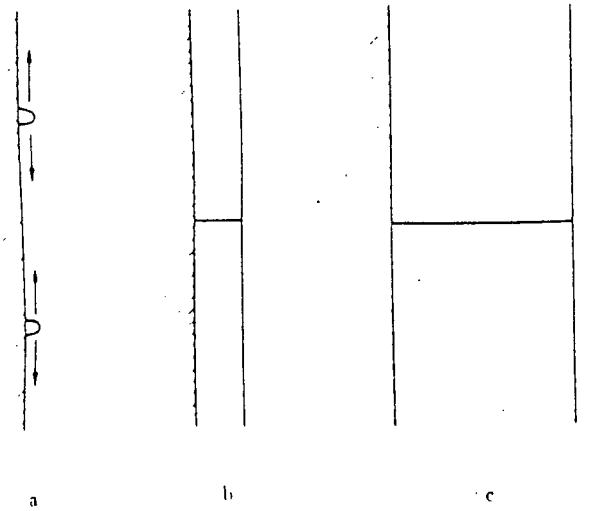

Fig. 5. Solidification phenomenon of a pure metal at the mold wall

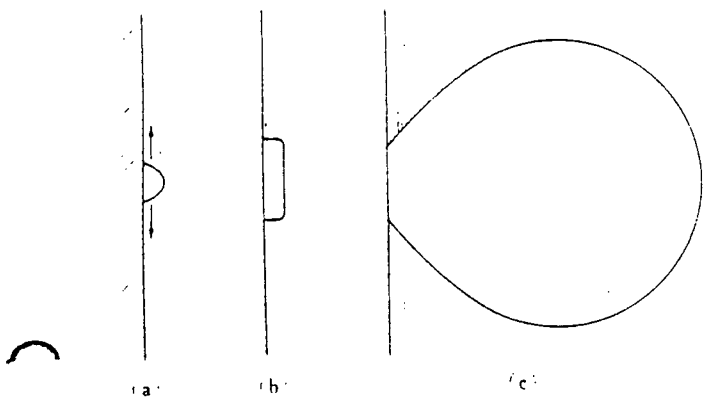

Figure 1.6

Mechanism for the formation of the equiaxed grains initiating at the mould wall following Ohno.

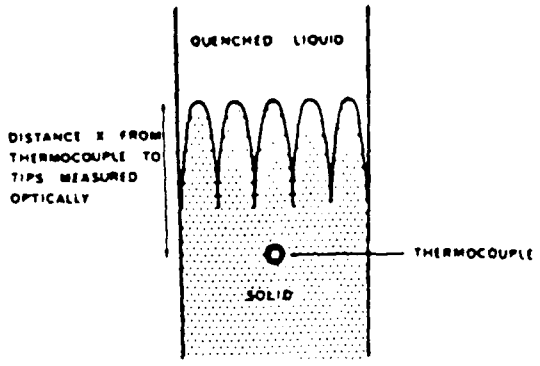

Specimen grown at constant velocity v and quenched

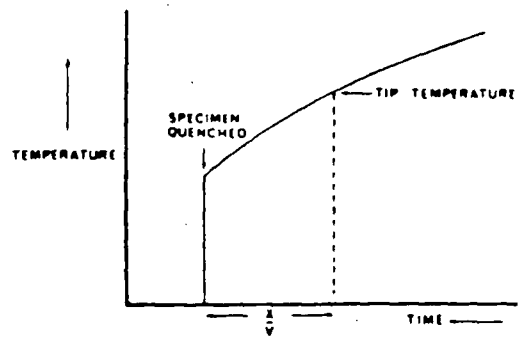

Fig. 1. A temperature/time trace of thermocouple in specimen.

Figure 1.7

Measurement of temperature of dendrite tips at constant velocity, V, and quenching the sample during growth.

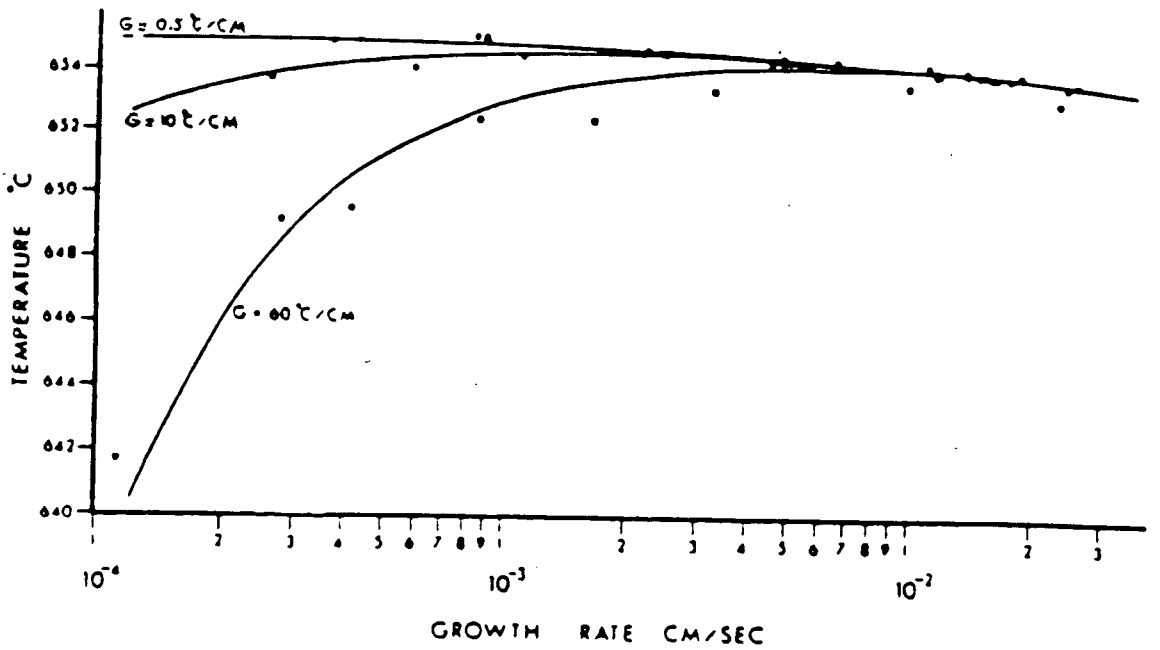

Figure 1.8

Dendrite tip temperature vs. growth rate at three temperature gradients.

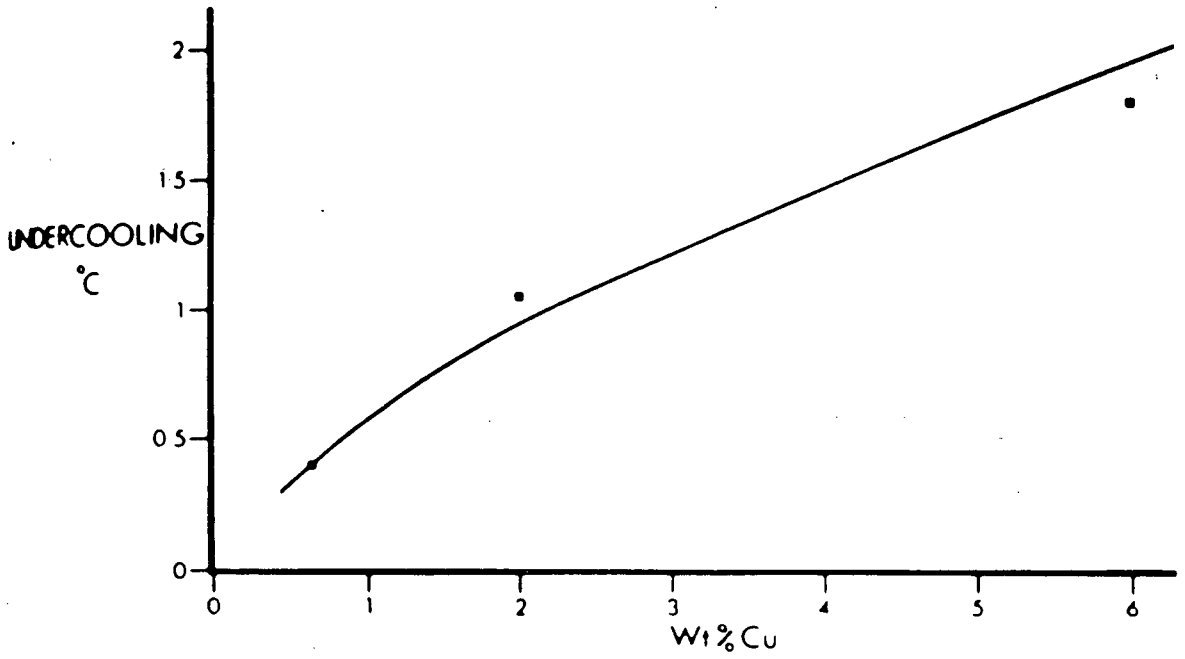

Figure 1.9

Supercooling at dendrite tip vs. weight percent Cu.

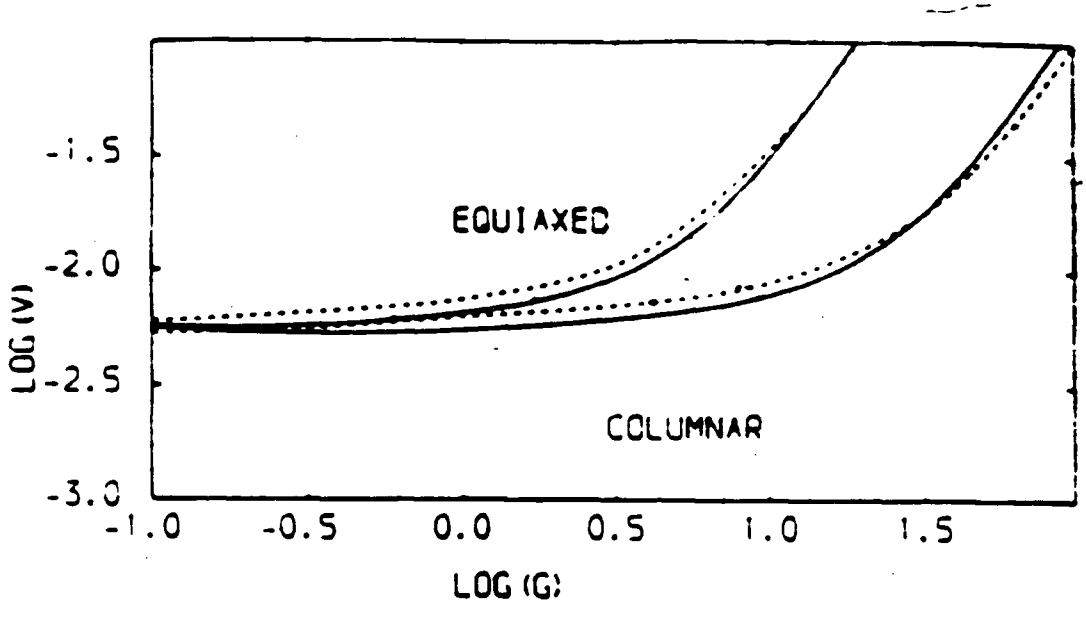

Figure 1.10

Predicted columnar and equiaxed regions in a directionally solidfied Al-3%Cu alloy as a function of the growth velocity V and temperature gradient G. The dotted lines use a more accurate analysis than the solid lines.

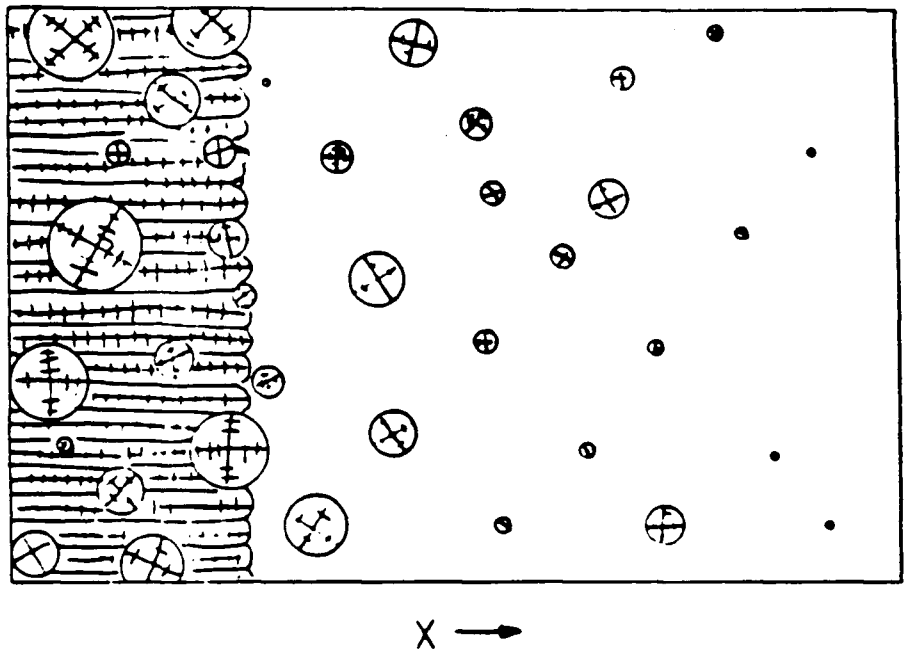

Figure 1.11

Gradual transition from columnar to equiaxed structure following the model by Hunt.

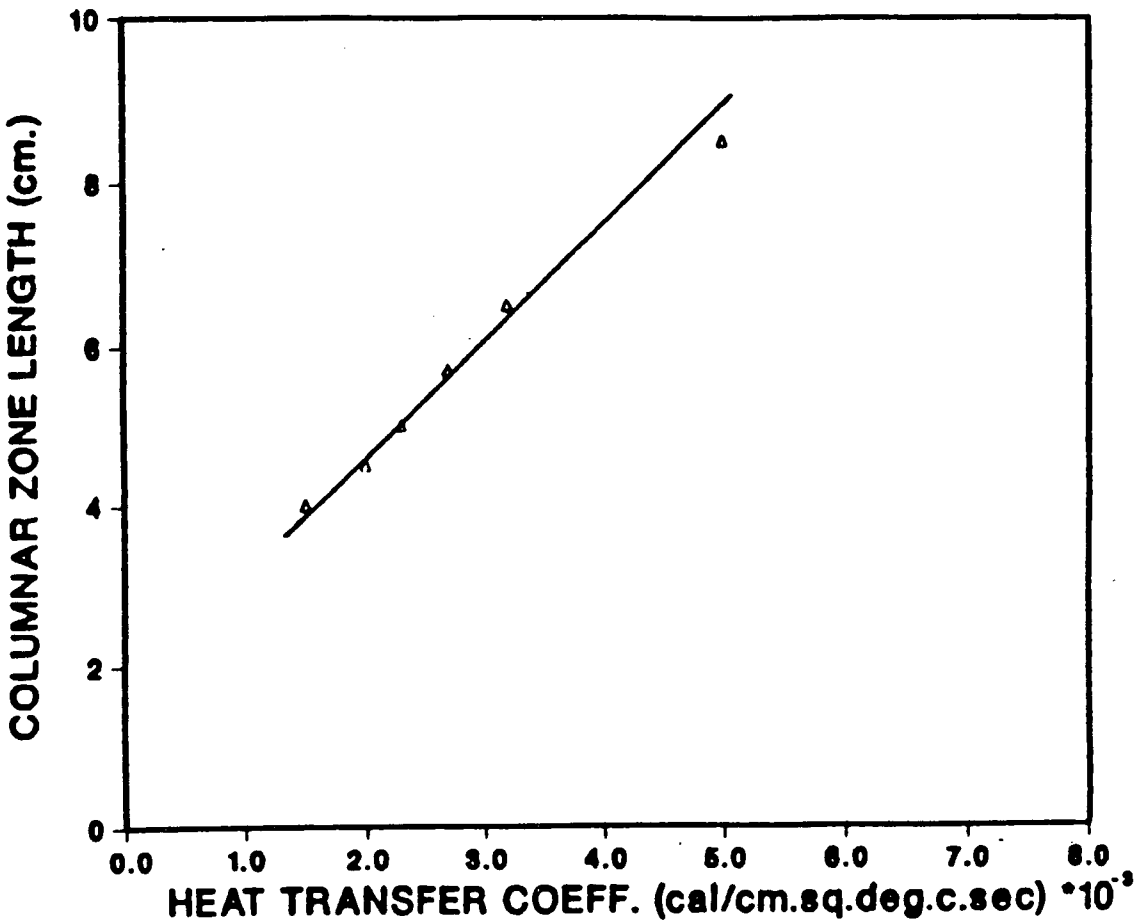

Figure 1.12

Columnar zone length vs. heat transfer coefficient for Sn-10%Pb

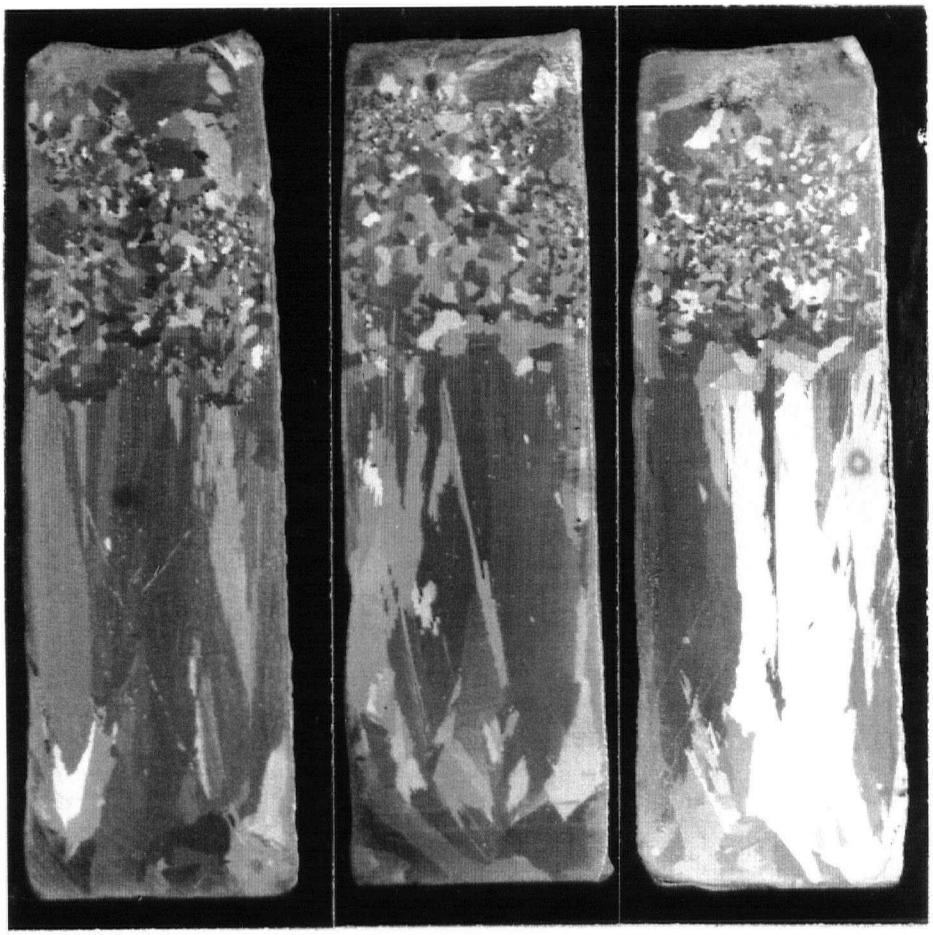

(a) 19°C (b) 31°C (c) 36°C

Figure 1.13

The independence of the CET position on superheat for Sn-10%Pb.

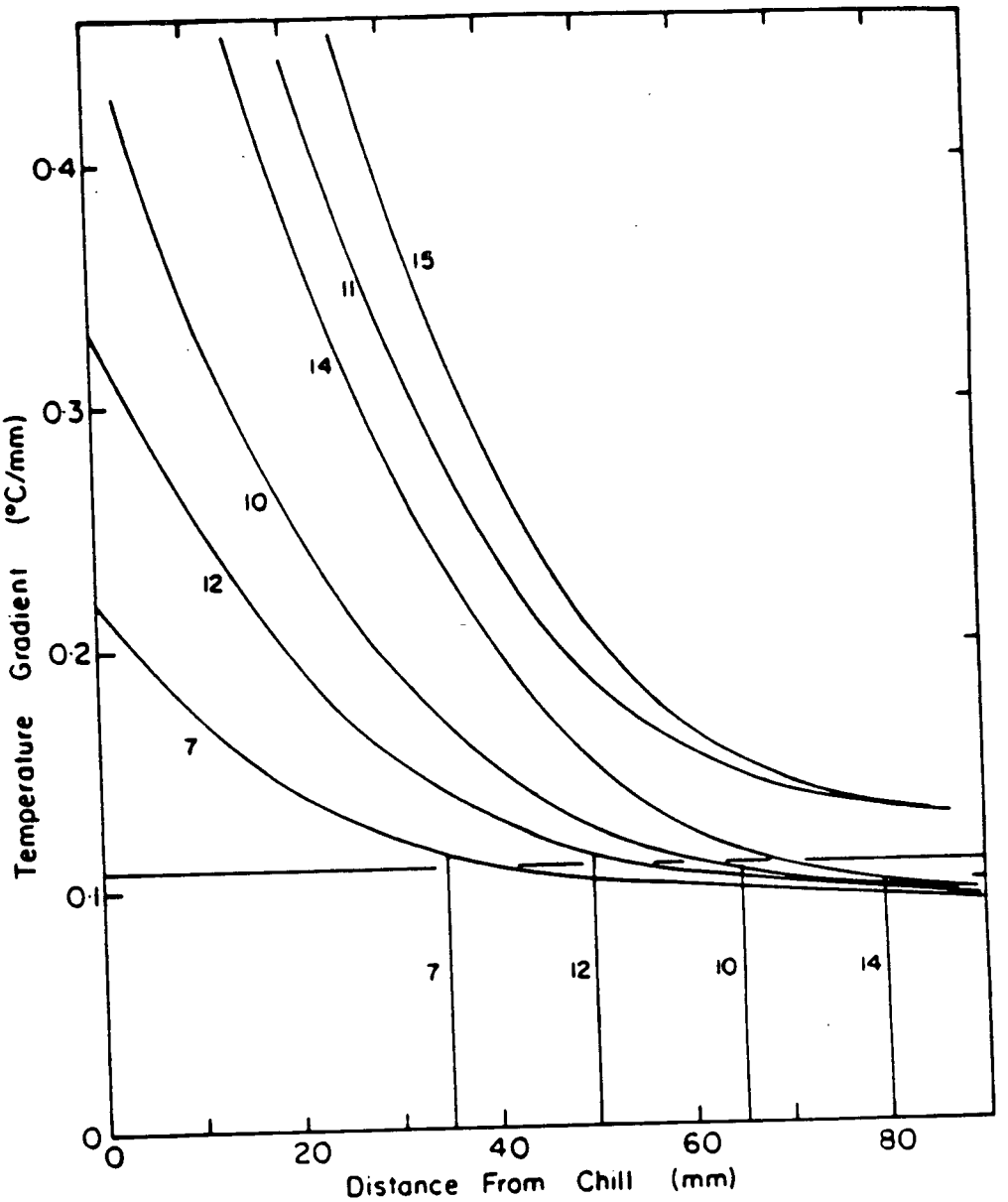

Figure 1.14

G_L vs. distance from the chill for Sn-10%Pb. The four vertical lines are CET positions for tests 7,12,10, and 14.

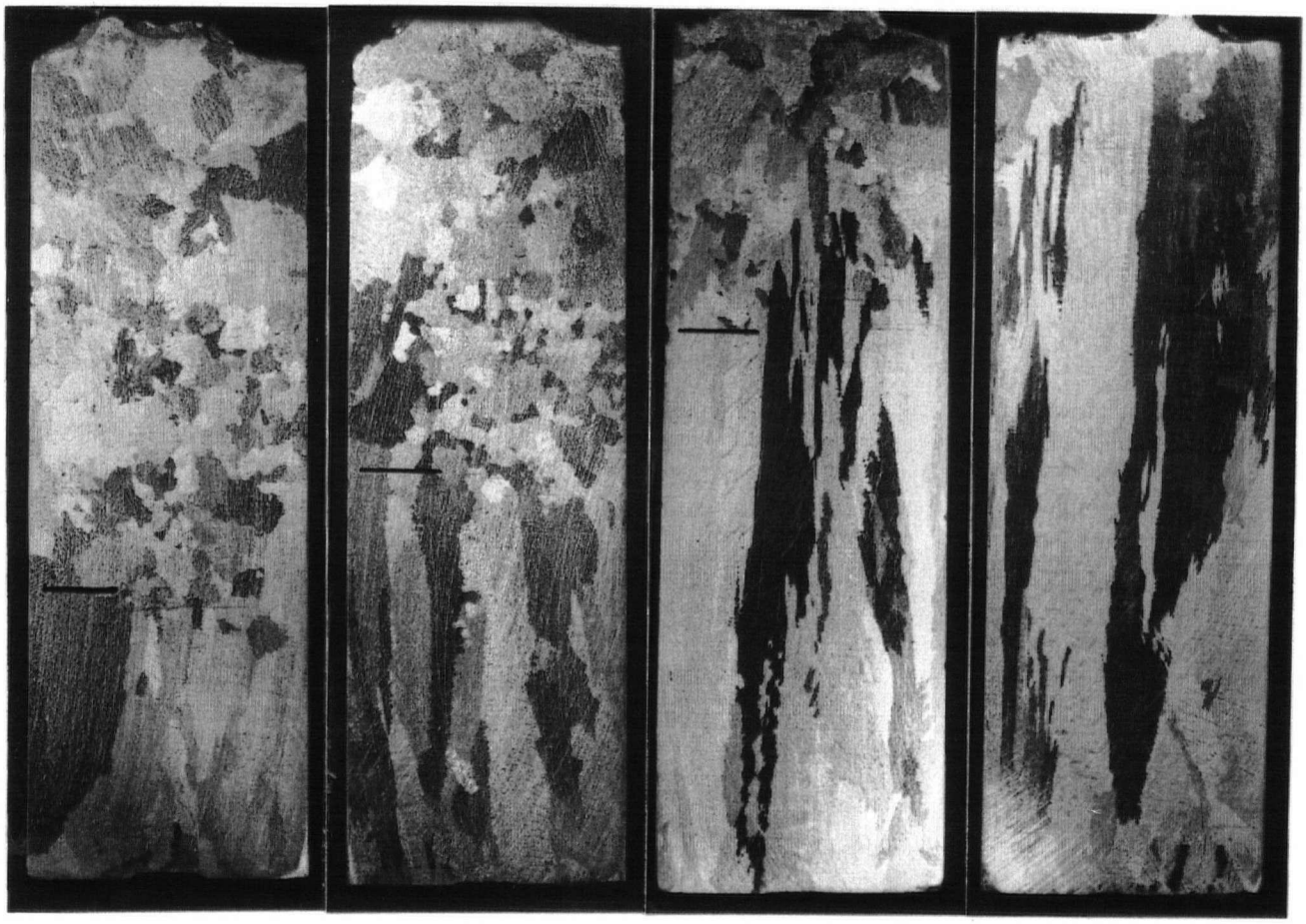

Figure 1.15

The CET in an Al-3%Cu alloy directionally solidified for various bottom heat transfer coefficients. The transition is very sharp in each case.

Figure 1.16

The influence of TiB_2 concentration on the CET in an Al-3%Cu alloy.

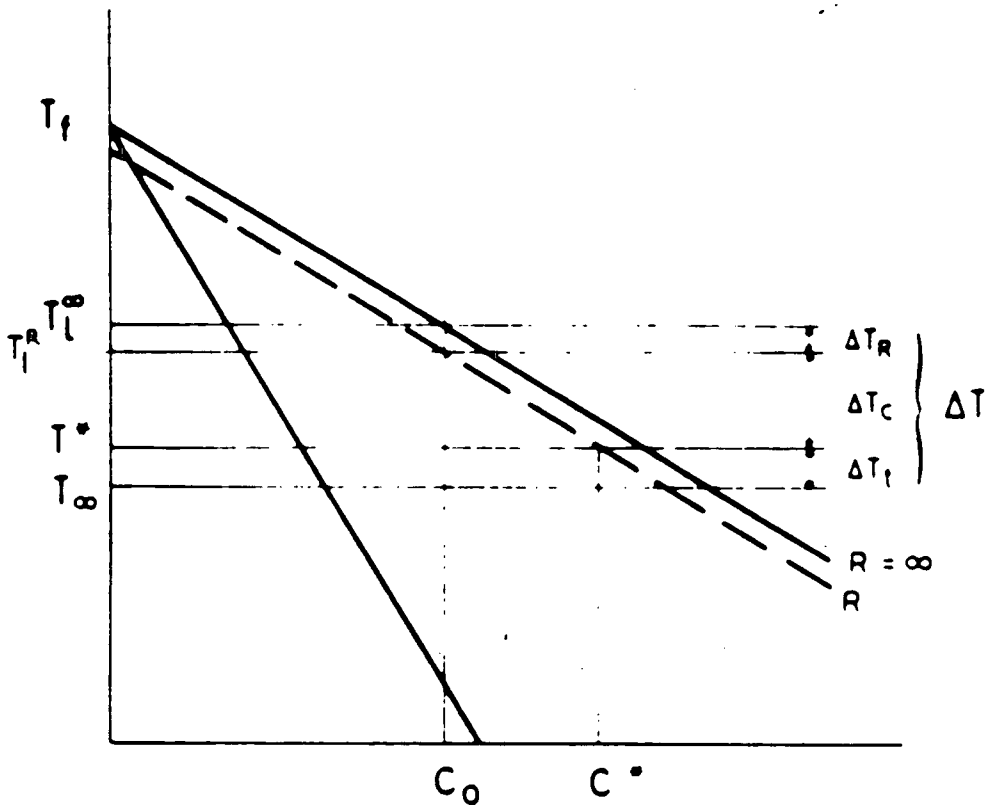

Figure 1.17

Phase diagram showing the elements of supercooling.

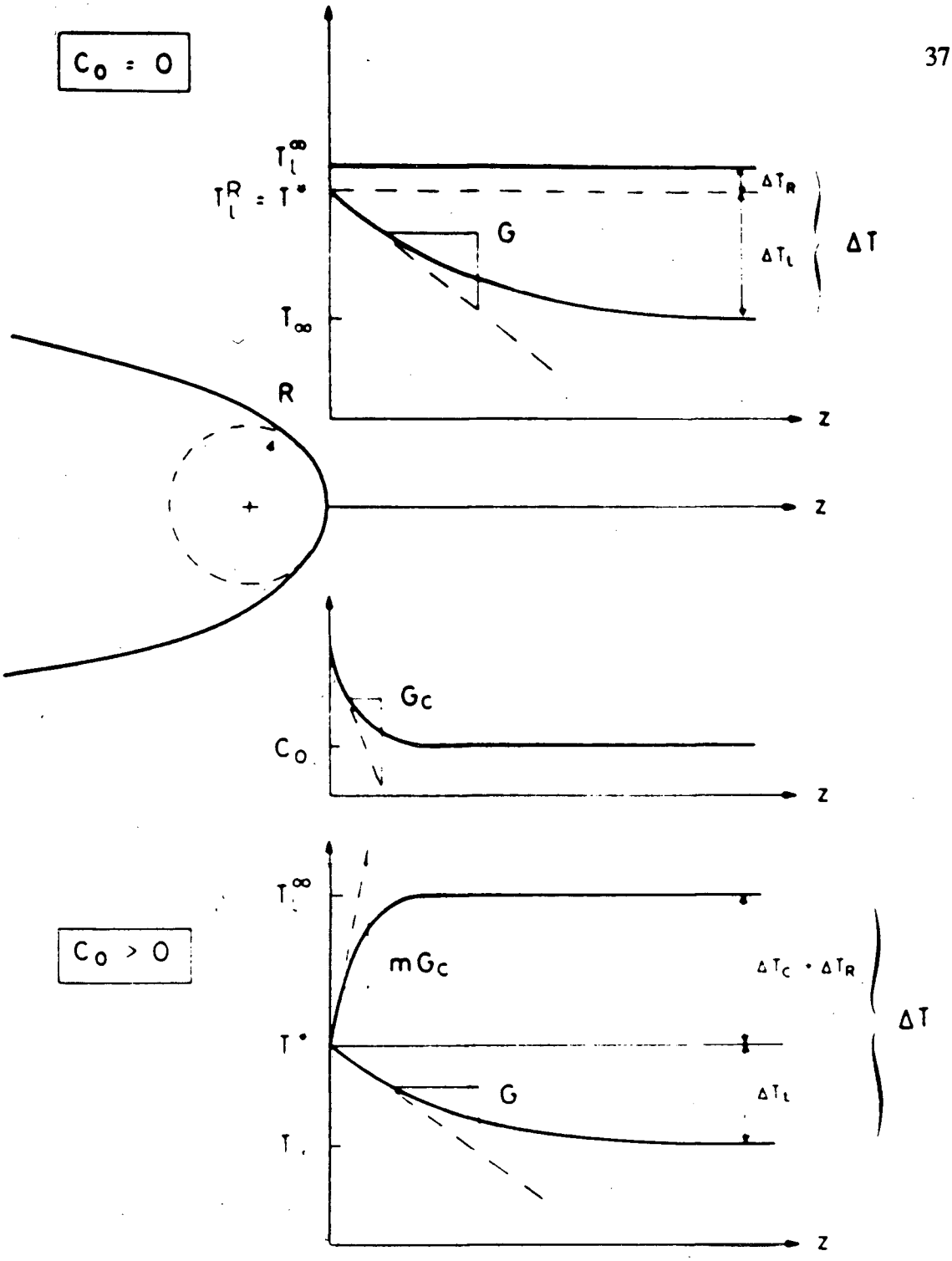

Figure 1.18

Concentration and temperature fields ahead of the dendrite tip.

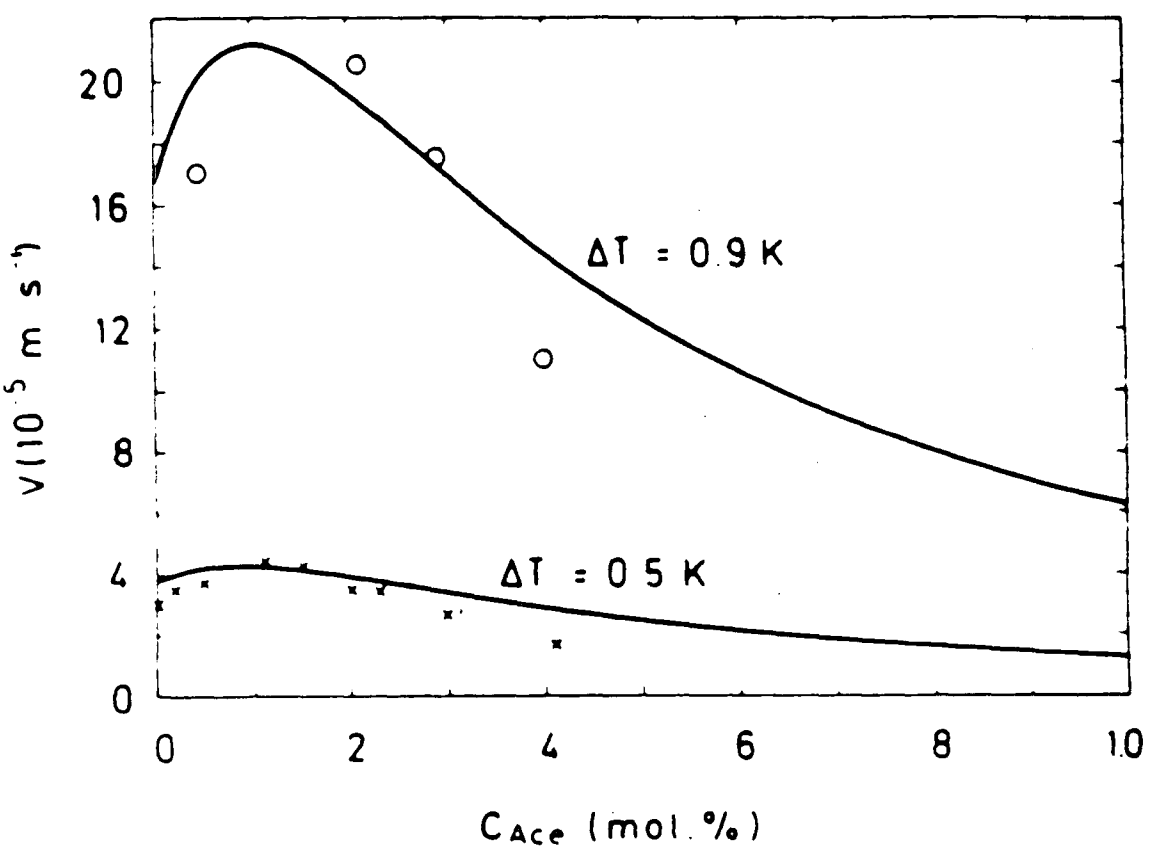

Figure 1.19

Growth rate V for two supercoolings as a function of acetone concentration C_{ACE} (=C_0) in succinonitrile-acetone alloys, symbols are measured values and the line is calculated.

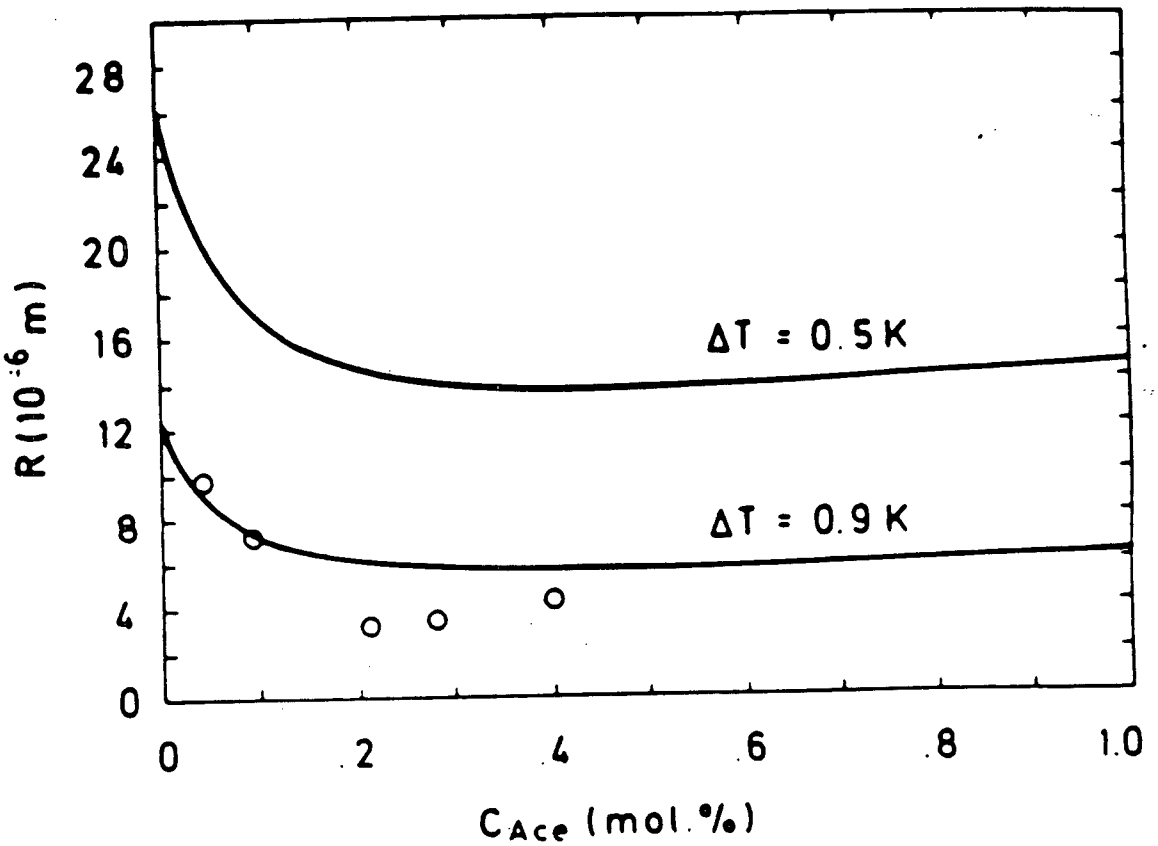

Figure 1.20

Dendrite tip R for two supercoolings as a function of acetone concentration C_{ACE} (=C_0) in succinonitrile-acetone alloys, symbols are measured values and the line is calculated.

Chapter 2

EXPERIMENTAL PROCEDURES

2.1 COLUMNAR TO EQUIAXED TRANSITION

Four directional solidification tests were carried out to establish that a columnar to equiaxed transition,(CET),occurred in a Pb-1.5%Sn alloy. The experiments were performed using the apparatus shown in Figure 2.1.

The apparatus consists of a copper mould filled with a Pb-1.5%Sn alloy and contained in a quartz tube. The quartz tube is surrounded by a resistance heating furnace. The bottom of the mould is cooled by a water cooled copper chill block. The rate of cooling is controlled by layers of 1 mm thick stainless steel sheets between the mould and the copper chill block.

The mould is made from copper pipe with a copper plate brazed on one end. The outside and inside diameter of the mould are 42 and 37 mm respectively and the height of the mould is 110 mm for tests 1 to 3 and 200 mm for test 4. The inside of the mould is coated with a dispersion of graphite in alcohol,(Acheson DAG 154). The inside and outside vertical walls are lined with 3 mm thick Fibrefrax sheet to minimize radial heat flow during solidification.

Weighted amounts of 99.99%Pb and 99.89%Sn are melted in the mould to produce a Pb-1.5%Sn alloy. The alloy is homogenized by vigorously stirring the melt for six minutes using a stainless steel plunger.

Temperature measurements are made in the alloy during solidification with thermocouples at equidistant positions along the vertical axis of the mould. The thermocouples are held in position by a rubber bung and brass cap as shown in Figure 2.1. Four thermocouples are used in test 1 at approximately 20, 40, 60, and 80 mm from the mould bottom. Three thermocouples are used in tests 2, 3, and 4 located at approximately 25, 50 and 75 mm from the bottom.

The thermocouples are made from chromel and alumel wires of 0.00254 mm (0.0001") diameter, separated by ceramic sleeves and sheathed in a 3 mm O.D. Pyrex tube. The thermocouples are calibrated against the temperature plateau at the freezing point of 99.99%Pb using an ice water cold junction.

The voltage signal from the thermocouples is measured with two Kipp and Zonen chart recorders for test 1 and an HP 3480A digital voltmeter for tests 2, 3, and 4. With the digital voltmeter, measurements are made at 1 second intervals for the three thermocouples in a single scan. The time interval between scans was dependent on the temperature being measured.

For a test, the number of stainless steel sheets is selected and placed between the chill block and the copper mould. The mould is then filled with weighted amounts of Pb and Sn to produce a Pb-1.5%Sn alloy and the furnace turned on. After the metal has melted, it is stirred and the system equilibrated to the required temperature. The furnace is then turned off and water passed through the chill block to initiate solidification. For test 3, the furnace power is reduced to 50% instead of being turned completely off. The test is completed when all the thermocouples show a temperature below the liquidus temperature of the alloy. The solid metal is removed from the mould, the position of the thermocouples measured, and the height of the ingot determined. The height varied between 75 to 110 mm.

The ingot is sectioned on a vertical plane containing the central axis. The cut surface is filed flat with an aluminum type A file, and etched to remove the worked material on the surface. The etch used is 4-3-16 part solution of nitric acid, acetic acid, and distilled water at 40°C. Etching is continued until the grain structure is clearly delineated. The surface is then ground on 80 to 400 SiC paper, lubricated with paraffin saturated kerosene, and given a final polish on a 5μ alumina polishing wheel. The surface is then lightly etched using the same etching solution used to remove the cold worked material.

2.2 TEMPERATURE MEASUREMENT

It became evident in the initial tests that the accuracy of the temperature measurements is a critical factor in the observations since attempts are being made to measure very small temperature differences in a transient temperature field over relatively long time periods. As a result, a series of tests are conducted to calibrate the thermocouples more accurately and to determine the reproducibility of the temperature measurements.

Accurate temperature measurements are made using the apparatus shown in Figure 2.2. The apparatus consists of a copper mould similar to that described in Figure 2.1 with graphite coating and fibrefrax insulation on the inside and outside walls. The bottom of the mould is thermally insulated with two, 3 mm thick sheets of fibrefrax. The mould height is 200 mm.

The thermocouples are calibrated against the temperature plateau at the freezing point of 99.999%Pb (327.502°C[42]). The thermocouple to be calibrated is positioned in the centre of the melt and its voltage signal referenced to 0 °C using an ice-water cold junction.

The voltage signal from the thermocouple is measured and recorded with a 16 bit analog to digital,(A/D), data acquisition board in an IBM PC. Temperatures are recorded intermittently at time intervals dependent on the temperature being measured. Each temperature measurement recorded is the average of 32 individual measurements made at 10 ms intervals.

For a normal test, the entire system is equilibrated at a specified melt temperature, and the furnace turned off. The melt slowly cools and solidifies from the outer vertical walls to the center of the mould. The cooling curve exhibits a clearly defined and flat temperature plateau at the freezing point of pure Pb which is related to the thermocouple output. The Pb is remelted and the procedure repeated. This is done a number of times to establish the accuracy and reproducibility of the measurements. Three calibration measurements are also made using 99.99%Pb and 99.89%Sn to establish the change in the shape and temperature of the temperature plateau using these metals.

2.3 DIRECTIONAL SOLIDIFICATION

Directional solidification tests are carried out to carefully measure the temperature gradient in the liquid ahead of the solid/liquid interface,G_L, in the vicinity of the CET during solidification. The metals examined are pure Pb(99.999%), alloys of Pb-1.5%Sn, Pb-3%Sn, Pb-6%Sn, and Sn-10%Pb.

The apparatus for these tests is shown in Figure 2.3 which is a modification of the apparatus shown in Figure 2.2. In Figure 2.3, a brass support ring is brazed to the bottom of the mould, the ring resting on an alumina sleeve which supports the mould in the furnace. In this way, the mould is separated from the chill block by an air space while the alloy is being melted and the furnace equilibrated. Cooling water flows through the chill block at all times.

The chill system consists of a water cooled copper chill block and three copper discs which are positioned on top of the copper chill block, (Figure 2.4) This configuration is referred to as CA1 in this thesis. Each disc is 45 mm in diameter and 6.4

mm thick. The top and bottom discs contain a keyhole slot to accommodate a thermocouple. The center disc is reduced in cross sectional area by 39 holes of 3 mm diameter evenly distributed in the disc which reduces the rate of heat transfer from the mould. This basic configuration is altered by inserting a 6.4 mm thick stainless steel disc on top of the bottom copper disc, (Figure 2.4), and is referred to as CA2. The final alteration of the chill system consists of an additional 5, 1 mm stainless steel sheets inserted on top of the bottom copper disc, (Figure 2.4), and is referred to as CA3. The chill system is altered in some tests to further reduce the rate of heat transfer from the mould bottom.

The thermocouples in the top and bottom discs are made from chromel and alumel wires of 0.00254 mm (0.0001") diameter and are sheathed in ceramic tubes, positioned to measure the surface temperature in the center of the disc. The temperature difference, ΔT, between the top and bottom copper disc is used to estimate the heat flux from the bottom of the mould.

Tests were carried out following three procedures.

1. Weighted amounts of Pb and Sn are added to the mould and melted. After vigorous stirring, three thermocouples are positioned in the melt at approximately 35, 65 and 95 mm from the bottom of the mould. No insulation is used at the top of the melt. When the melt has reached equilibrium at the desired melt temperature, the chill is raised with a laboratory jack until it comes into firm contact with the bottom of the mould. The current to the furnace is then reduced to a predetermined level and left at that position until solidification is complete. In this procedure, each temperature recorded on the (A/D) board from each thermocouple, including the 3 in the melt and the 2 in the chill system, is

the average of 8 measurements taken 50 ms apart.

2. Comparing the temperature measurements to predicted temperatures from a heat transfer model indicated that heat is being lost from the vertical side walls of the mould and from the top of the melt. To determine the extent of radial heat loss and heat lost from the top of the melt, the apparatus shown in Figure 2.3, is modified to that shown in Figure 2.5. The melt is prepared using procedure 1 except that loosely packed insulation is added to the top of the melt, and a graphite cap placed on top of the copper mould. The graphite cap has 6, 3 mm diameter holes drilled through it as shown in Figure 2.6. This allows thermocouples to be located at the positions in the melt shown in Figure 2.7, to measure both the vertical and the radial temperature gradients during directional solidification. Temperature measurements are made using those in procedure 1.

3. To further improve the accuracy and reproducibility of the temperature measurements, the calibration and measuring procedure is modified in the following way.

A melt was prepared in a graphite crucible in the furnace and thoroughly stirred. The melt is then poured into a copper mould and allowed to solidify. Fibrefrax insulation is then loosely packed on top of the ingot and the graphite cap, containing the thermocouples, is placed on top of the mould. A quartz tube is positioned around the mould and the entire assembly lowered into the furnace to remelt the alloy. The three thermocouples are then lowered into the melt to a position approximately 65 mm from the mould bottom and the system allowed to reach equilibrium at the desired melt temperature. The furnace is then turned off and cooling curves are obtained for each thermocouple using the A/D data acquisition board and IBM PC. In this case, each temperature recorded from each thermocouple in the melt is the average of 8

measurements taken at 30 ms intervals.

The alloy is then remelted and the three thermocouples positioned at approximately 35, 65, and 95 mm from the bottom of the mould The alloy is then resolidified directionally using procedure 1 described above. After solidification, the ingots are removed from the mould, sectioned vertically along the ingot axis, etched, ground, polished and reetched in the manner described previously.

A Sn-10%Pb alloy is directionally solidified following procedure 3 used for the Pb-Sn alloys. In this case, after directional solidification, the ingot is removed, sectioned vertically, the surface is ground, polished and etched in a solution of 80-10-10 glycerol, nitric acid, and acetic acid. The sample is immersed in the solution for 10 minutes at 40°C.

2.4 MATHEMATICAL MODELLING

The experimental temperature measurements during directional solidification are confined to three positions in the metal at which the three thermocouples are located. What is required is the full temperature field as a function of time and position as the metal solidifies. In particular, local temperatures and temperature gradients are required at the moving solid/liquid interface. This information can be obtained by developing a heat transfer model for the directionally solidified alloy system. The mathematical model predictions can then be compared to the experimental temperature measurements to verify the model. Additionally, the temperature measurements can be used to establish the boundary conditions required for the model.

2.4.1 OBJECTIVES

The objective of the mathematical model is to predict the temperature in the metal as a function of time and distance during the directional solidification. From the temperature field, the temperature gradient at the solid/liquid interface, G_L, can be determined as well as the growth velocities.

2.4.2 SOLUTION METHOD

A one dimensional mathematical model in cylindrical coordinates is used to determine the temperature distribution in the directionally solidifying ingot.

The governing heat conduction equation is:

$$k\left(\frac{\partial^2 T}{\partial z^2}\right) = \rho C_p \frac{\partial T}{\partial t} \tag{2.1}$$

where:

k = the thermal conductivity of the alloy

T = the temperature of the alloy

z = the distance from the bottom of the mould

ρ = the density of the alloy

C_p = the specific heat of the alloy

t = time

Equation 1 is solved using the implicit finite difference method for the node configuration scheme shown in Figure 2.8. The development of the finite difference equations based on a heat balance is outlined in Appendix 1.

2.4.3 ASSUMPTIONS

The following simplifying assumptions are made to solve equation 2.1.

1. Heat flow is axisymmetric.

$$\frac{\partial^2 T}{\partial \theta^2} = 0 \tag{2.2}$$

where: θ = the angular direction

2. The radial heat flow is zero.

$$\frac{\partial T}{\partial r} = 0 \tag{2.3}$$

where: r = the radial direction

3. There is no convection in the liquid ahead of the solid/liquid interface.

4. There is no melt supercooling prior to solidification.

5. The thermophysical parameters, k, ρ, and C_p, are linear functions of temperature between the liquidus and solidus temperatures.

6. The thermophysical parameters, k, ρ, and C_p, for the alloy can be determined from the parameters of Pb and Sn on the basis of the weighted averages of the Pb and Sn in the alloy.

2.4.4 BOUNDARY CONDITIONS

Two boundary conditions need to be defined to solve the governing heat conduction equation, one at the top of the ingot where z = 1 and the other at the bottom of the ingot where z = N. At both boundaries, a constant heat transfer coefficient is used to calculate the heat flux from the corresponding surface.

1. At the bottom of the ingot where z = N:

$$-k\frac{\partial T}{\partial z} = H_B(T'_N - T_{AMB}) \tag{2.4}$$

2. At the top of the ingot where z = 1:

$$-k\frac{\partial T}{\partial z} = H_{Top}(T'_1 - T_{Furn}) \tag{2.5}$$

where:

H_B = the heat transfer coefficient at the bottom of the ingot

H_{Top} = the heat transfer coefficient at the top of the ingot

T'_N = the temperature of the bottom node

T'_1 = the temperature of the top node

T_{AMB} = the ambient temperature taken to be 25°C

T_{Furn} = the furnace temperature immediately above the top node

The furnace temperature, T_{Furn}, is determined experimentally using the thermocouple configuration shown in Figure 2.9. Thermocouple 1 is in the loose fibrefrax insulation 10 mm above the melt surface; thermocouple 2 is in the melt 95 mm from the bottom of the mould; and thermocouple 3 is at the same height as thermocouple 2

adjacent to the furnace wall. The temperature difference between thermocouples 1 and 2, and thermocouples 3 and 2, as a function of time during solidification with the furnace power off, is shown in Figure 2.10. The results show that there are both vertical and radial temperature gradients between the melt and the furnace which change with time in a non-linear fashion. For the first 1500 seconds, there is a positive temperature gradient in both directions indicating heat is flowing into the melt from furnace. After 1500 seconds, the vertical temperature gradient is zero and continues to drop becoming negative at which point heat is flowing out of the melt. The radial temperature gradient decreases more rapidly than the vertical temperature gradient and becomes zero at 960 seconds after which it is negative again indicating that heat flows out into the furnace.

This thermal behavior is incorporated into the model by assuming the temperature difference between the top of the melt and the insulation above the melt changes with time as shown in Figure 2.11. This is a simplified form of the experimental results. The radial heat losses are not incorporated in the model as it is assumed that the radial isotherms in the alloy during directional solidification are flat.

2.4.5 INITIAL CONDITIONS

The initial temperature distribution in the melt at the start of cooling in the model is taken from the temperatures recorded by the three thermocouples in the melt immediately after the chill block contacts the bottom of the mould. A typical temperature distribution used in the model is shown in Figure 2.12. The temperature at the bottom and top of the melt is taken as the extrapolation of lines 1 and 2 respectively. Each line can be represented by the linear equation:

$$T_i = Slope(Dist_i) + Axis \tag{2.6}$$

where;

T_i = the temperature of any node i

Slope = the slope of the line

$Dist_i$ = distance between the node i and the bottom of the mould

Axis = the temperature of the bottom node or the intercept of line 2

2.4.6 LATENT HEAT RELEASE

Any mathematical model involving solidification must account for the latent heat of solidification. While there are a number of well established techniques to incorporate the latent heat into mathematical models[41], these techniques still assume that the latent heat is released linearly between the liquidus and the solidus lines. Like any assumption, releasing latent heat linearly may take the model away from reality. The assumption's validity or usefulness is only tested by comparing the model's predicted temperatures to experimental temperatures. As such, the assumption on how the latent heat is released can be changed and tested in the same manner.

In this investigation the assumption of how the latent heat is released is changed by assuming that the alloy solidifies according to the Scheil equation, and then changed again to assume that the alloy solidifies according to the Lever rule. Thus, there are three basic methods on how the latent heat is released. Each method incorporates the latent heat of solidification into the model in different ways. For example, to release the latent heat linearly the specific heat of the alloy is artificially raised following equation 2.7.

$$C_p(eff) = C_p(mushy) + \frac{L}{T_{liq} - T_{sol}} \tag{2.7}$$

where:

C_p(eff) = the effective specific heat of the alloy in the mushy zone

C_p(mushy) = the specific heat of the alloy in the mushy zone

L = the latent heat of solidification of the alloy

T_{liq} = the liquidus temperature of the alloy

T_{sol} = the solidus temperature of the alloy

The Scheil equation and the Lever rule do not directly release the latent heat but are used to calculate the fraction solidified within a single node. The latent heat is released in proportion to the change in the fraction solidified as the node cools through the mushy zone.

The Scheil equation, shown in equation 2.8, assumes that during solidification, there is complete solute mixing in the liquid and no mixing in the solid.

$$C_S = kC_0(1-g)^{k-1} \tag{2.8}$$

where: C_S = solute concentration in the solid

C_0 = the bulk alloy composition

$k = \frac{C_s}{C_l}$ = the equilibrium partition coefficient

g = the fraction solid

The Lever rule, equation 2.9, assumes that solidification is at equilibrium in which:

$$g = \frac{C_L - C_0}{C_L - C_S} \tag{2.9}$$

where the solid and liquid are homogeneous during solidification with solute concentrations of C_S and C_L respectively.

The fraction solid as a function of temperature during solidification for the linear method, the Scheil Equation, and the Lever Rule are shown in Figure 2.13 for a Pb-1.5%Sn alloy between the liquidus and solidus temperatures only. In Figure 2.13, the fraction solid given by the Scheil equation at the solidus temperature is only 0.75. The node does not completely solidfy until the temperature reaches 183°C. This is not shown in Figure 2.13 for the sake of clarity. There is a significant difference in the shape and position of the curves for the three alternative procedures for releasing latent heat in the model.

2.4.7 POST ITERATIVE HEAT BALANCE

To incorporate the Scheil equation and the Lever rule into the implicit finite difference mathematical model to release latent heat requires including three more unknown variables directly into the each nodal equation, namely, C_S, C_L, and g. Inserting these unknown variables directly into the nodal equations would make the simultaneous solution of the equations impossible since there are now too many unknowns per nodal equation. To overcome this problem, a correction technique is employed whereby the nodal equations are first solved simultaneously without latent heat being introduced and then the temperatures corrected afterwards to account for the latent heat. The correction

technique revolves around two heat balance equations to account for a node going from liquid to mushy or for a node going from one mushy state to another. For a node going from liquid to mushy, the heat balance is given by:

$$T_3 - \left(\frac{L}{C_2}\right)\Delta g = T_{liq} - \frac{C_1}{C_2}(T_{liq} - T_2) \tag{2.10}$$

After the initial solidification step, further solidification through the mushy zone is corrected using the following heat balance.

$$T_3 - \left(\frac{L}{C_2}\right)\Delta g = T_2 \tag{2.11}$$

where:

T_3 = the new corrected temperature after the latent heat has been brought in.

T_2 = the new temperature after the time has been advanced a single time step, but no latent heat has been accounted for.

T_{liq} = the liquidus temperature of the alloy.

C_2 = the specific heat of the node in the mushy state.

C_1 = the specific heat of the node in the liquid state.

Δg = the change in the fraction solidified of the node

L = the latent heat of solidification

The development of the post iterative heat balance equations is shown in Appendix 1.

The Secant convergence technique is used to arrive at the new corrected temperature for the Lever rule and the Scheil equation method.

2.4.8 REPRESENTATION OF THE PHASE DIAGRAM

Equations for the liquidus and solidus lines from the Pb-Sn phase diagram are required in the model to calculate C_S, and C_L for a node which is solidifying. The liquidus and the solidus lines are represented as a series of linear equations connected by two boundary temperatures. For the liquidus line in the Pb rich end of the phase diagram between the eutectic temperature, 183°C and the melting point of Pb, 327.5°C, the following linear equations apply.

Between 183°C and 207° C

$$C_L = 61.9 - 0.29(T_i - 183°C) \tag{2.12}$$

Between 207°C and 300°C

$$C_L = 55.0 - 0.48(T_i - 207°C) \tag{2.13}$$

Between 300°C and 327.5°C

$$C_L = 0.37(T_i - 300°C) \tag{2.14}$$

For the solidus lines the following linear equations apply.

Between 183°C and 269°C

$$C_S = 19.2 - 0.11(T_i - 183°C) \tag{2.15}$$

Between 269°C and 327.5°C

$$C_S = 10.0 - 0.17(T_i - 269°C) \tag{16}$$

For the Sn rich end of the phase diagram, with the melting point of 232 °C, the following linear equations apply for the liquidus line.

Between 223°C and 232°C

$$C_L = 5.0 - 0.56(T_i - 223°C) \tag{2.17}$$

Between 215°C and 223°C

$$C_L = 10.0 - 0.63(T_i - 215°C) \tag{2.18}$$

Between 209°C and 215°C

$$C_L = 15.5 - 0.92(T_i - 209°C) \tag{2.19}$$

Between 183°C and 209°C

$$C_L = 38.1 - 0.87(T_i - T_{EUT}) \tag{2.20}$$

The following linear equations apply for the solidus line.

Between 217°C and 232°C

$$C_S = 1.5 - 0.1(T_i - 217°C) \tag{2.21}$$

Between 200°C and 217°C

$$C_S = 1.9 - 0.024(T_i - 200°C) \tag{2.22}$$

Between 183°C and 200 °C

$$C_S = 2.5 - 0.035(T_i - 183°C) \tag{2.23}$$

where:

T_i = the temperature of the node i.

C_L = the solute concentration in the liquid phase within a node.

C_S = the solute concentration in the solid phase within a node.

2.4.9 DEFINITION OF G_L AND VELOCITY CALCULATIONS

In order to calculate G_L, the temperature gradient in the liquid immediately ahead of the advancing solid/liquid interface, the position of the interface must be located. With the assumption that there is no supercooling at the interface, the front of the interface can be associated with the liquidus temperature, T_{LIQ}. However, as a node begins to solidify, the predicted temperature may not be at the liquidus temperature exactly, but, because of the length of the time step, it may be slightly lower. Therefore, to ensure that the position of the solid/liquid interface is determined to within a single node, the following criteria is used to define its position, measured from the bottom of the mould and given the arrangement shown in Figure 2.14.

The solid/liquid interface is at node i when:

$$T_i > T_{LIQ}$$

$$T'_i < T_{LIQ}$$

$$T'_{i+1} < T_{LIQ}$$

$$T'_{i-1} > T_{LIQ}$$

where:

T_i = the temperature of node i at the current time step

T'_i = the temperature of node i at the future time step

T'_{i+1} = the temperature of node i+1 at the future time step

T'_{i-1} = the temperature of node i-1 at the future time step

The temperature gradient in the liquid ahead of the solid/liquid interface is then given by:

$$G_L = \frac{T'_{i-1} - T'_i}{\Delta Z} \tag{2.24}$$

where:

ΔZ = the nodal distance of 0.5 mm.

The velocity of the solid/liquid interface, V, is calculated by first assuming that its position at any time, t, is given by:

$$x = A + B\sqrt{t} \tag{2.25}$$

where:

x = the position of the solid/liquid interface measured from the bottom of the mould

A and B are constants

t = time

The velocity is therefore given by:

$$V = \frac{dx}{dt} \tag{2.26}$$

$$\frac{dx}{dt} = \frac{1}{2} B t^{-\frac{1}{2}} \tag{2.27}$$

To obtain B in equation 2.27, the interface position, as determined by the model, is plotted first as a function of $\sqrt{time}$. A best fit line is used to determine the slope of the line which is B.

2.4.10 VALIDATION OF THE MODEL

The mathematical model is validated by considering that the heat transfer coefficients are constant at the top and bottom of the mould during solidification The two constants are adjusted until a good fit is obtained between the experimental temperatures and the calculated temperatures for each of the three thermocouple positions for the entire cooling and solidification period. Good fit is taken as ±1°C in the region near the liquidus temperature and ±3°C in the remaining regions.

The validation was made first for the model using the specific heat method and then, with the same heat transfer coefficients and thermophysical parameters, with the Scheil equation, and finally with the Lever rule. The values of the parameters used in the model calculations are listed in Table 2.1 .

TABLE 2.1
VALUES OF PARAMETERS USED IN MODEL CALCULATIONS

INPUTS	ALLOY							
	Pb-1.5%Sn		Pb-3%Sn		Pb-6%Sn		Sn-10%Pb	
	LIQUID	SOLID	LIQUID	SOLID	LIQUID	SOLID	LIQUID	SOLID
THERMAL CONDUCTIVITY J/sec-cm °C	0.164	0.305	0.168	0.313	0.177	0.328	0.324	0.585
SPECIFIC HEAT J/°Cgm	0.155	0.141	0.158	0.144	0.163	0.150	0.251	0.251
DENSITY gm/cm^3	10.46	11.27	10.36	11.16	10.18	10.96	7.18	7.47
LATENT HEAT J/gm	24.50		24.82		25.32		56.02	
LIQUIDUS TEMPERATURE °C	322.9		318.9		310.8		215.0	
SOLIDUS TEMPERATURE °C	318.3		309.6		292.2		183.0	
NODE SIZE cm	0.05		0.05		0.05		0.05	
TIME STEP sec	0.5		0.5		0.5		0.5	
TOP HEAT TRANSFER COEFFICIENT J/cm^2-°C-sec	0.02		0.02		0.02		0.02	
BOTTOM HEAT TRANSFER COEFFICIENT J/cm^2-°C-sec	0.01		0.01		0.01		0.01	

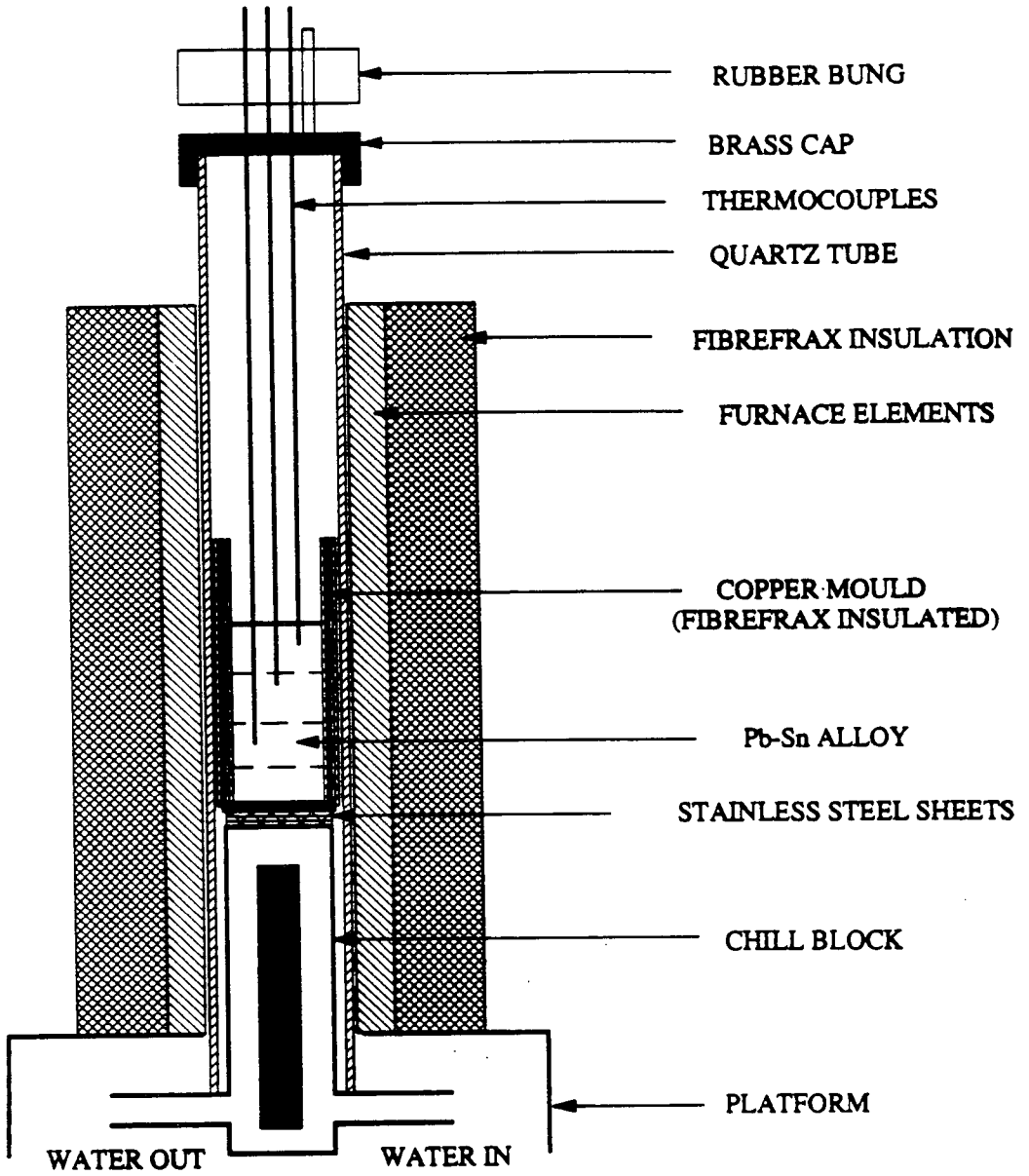

Figure 2.1

Experimental apparatus for columnar/equiaxed transition observations

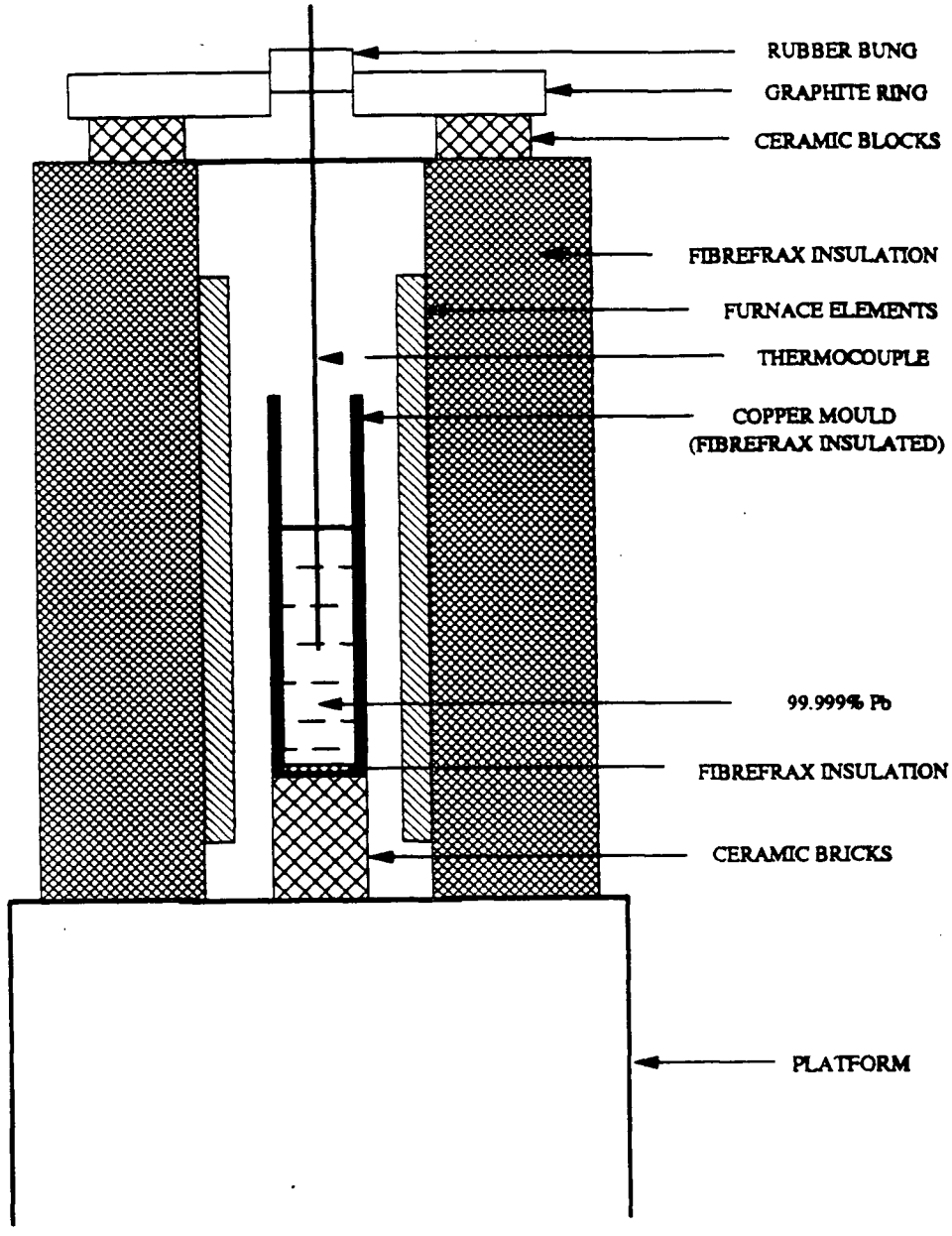

Figure 2.2

Experimental apparatus for thermocouple calibration and reproducibilty experiments

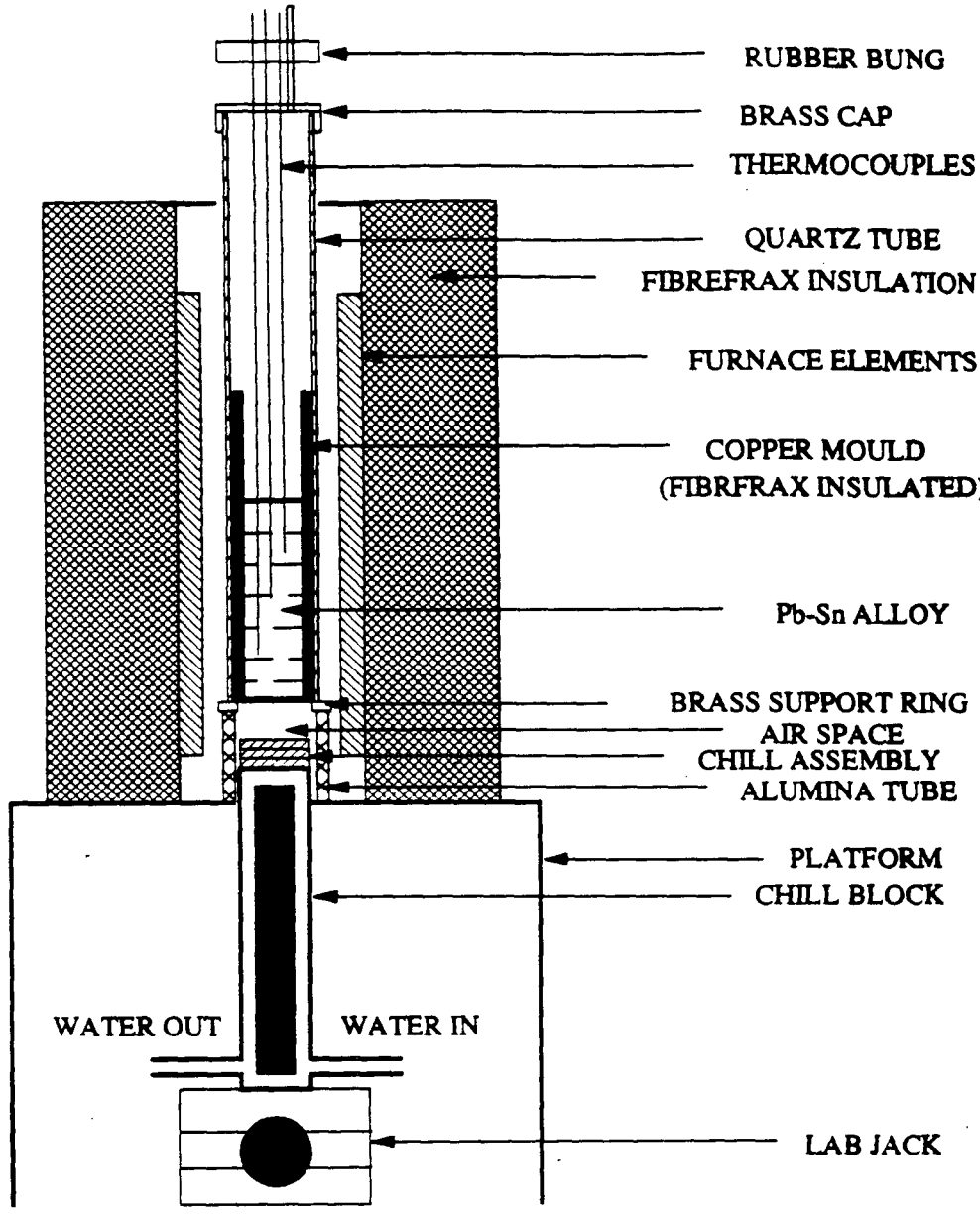

Figure 2.3

Experimental apparatus for directional solidification

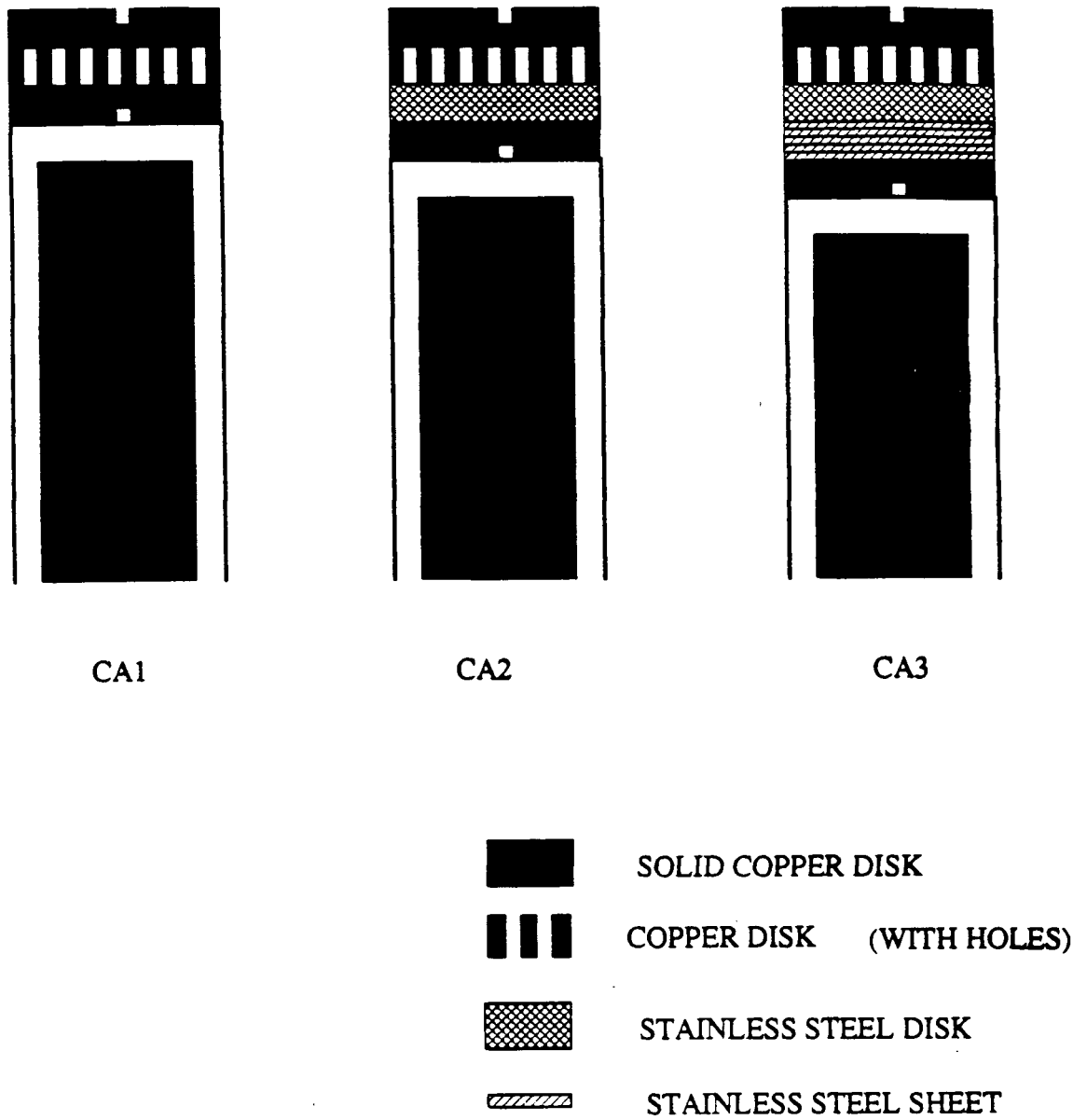

Figure 2.4

Various chill assemblies used for directional solidification

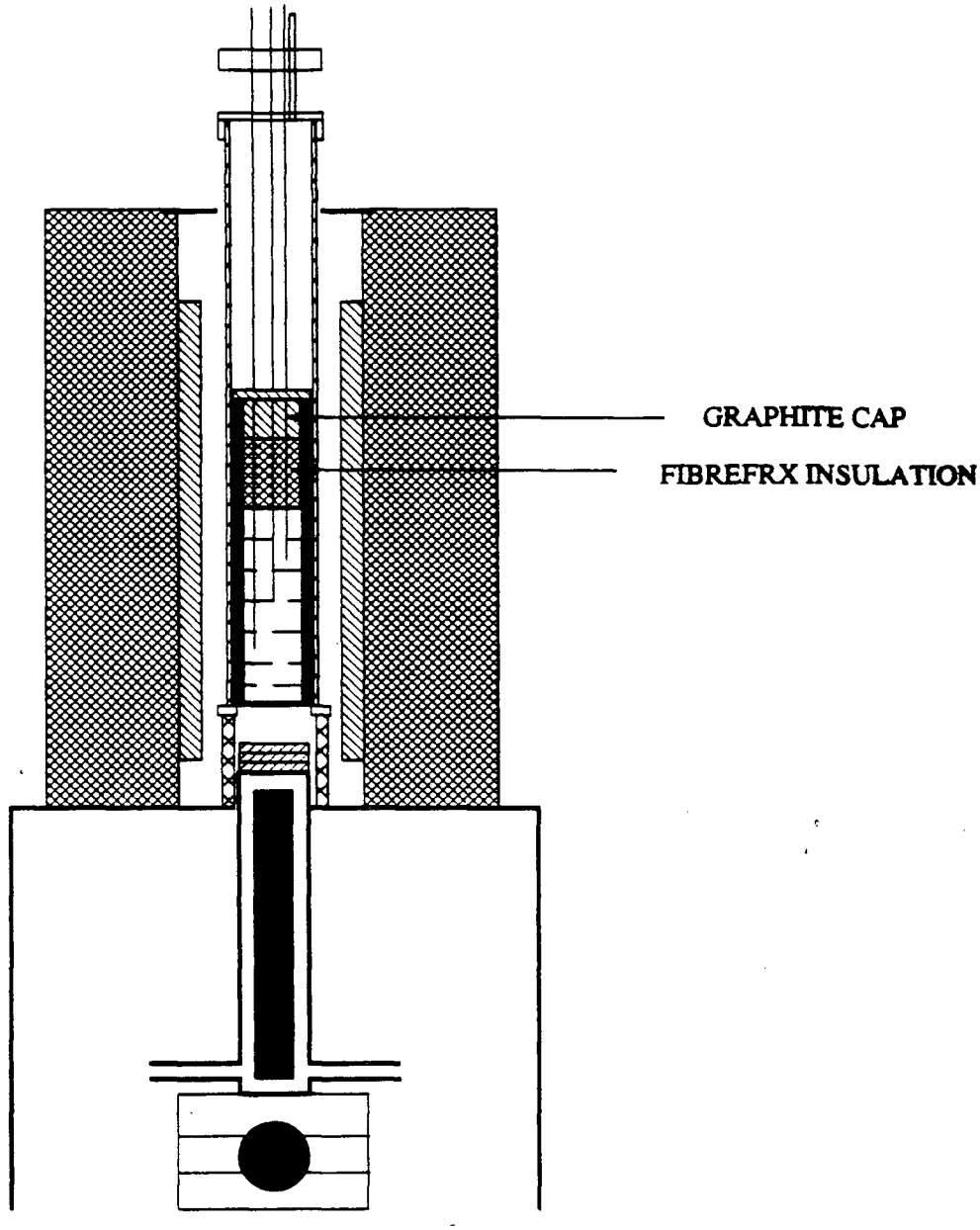

Figure 2.5

Modified experimental apparatus for directional solidification

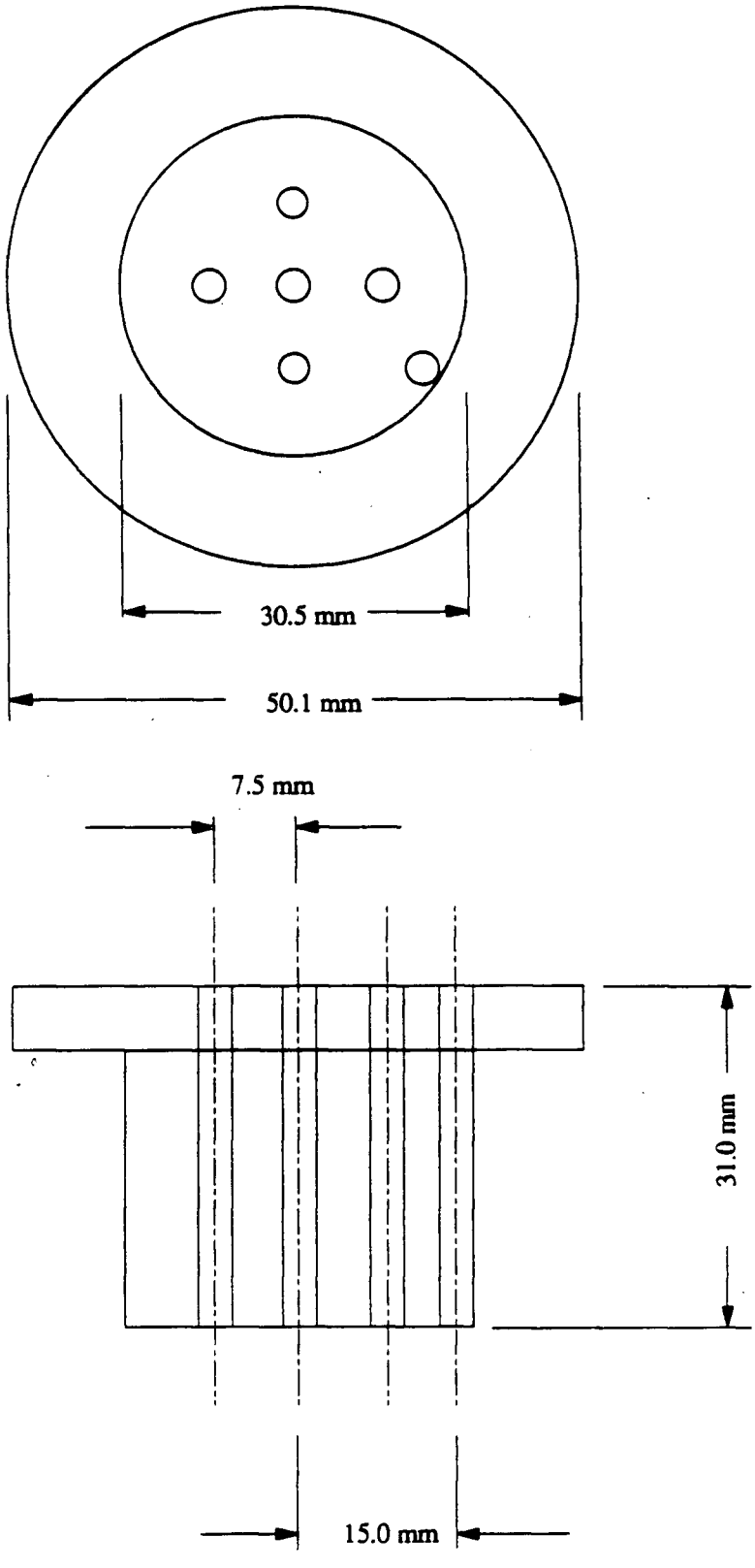

Figure 2.6

Dimensions of graphite cap and positions of holes to accommodate thermocouples

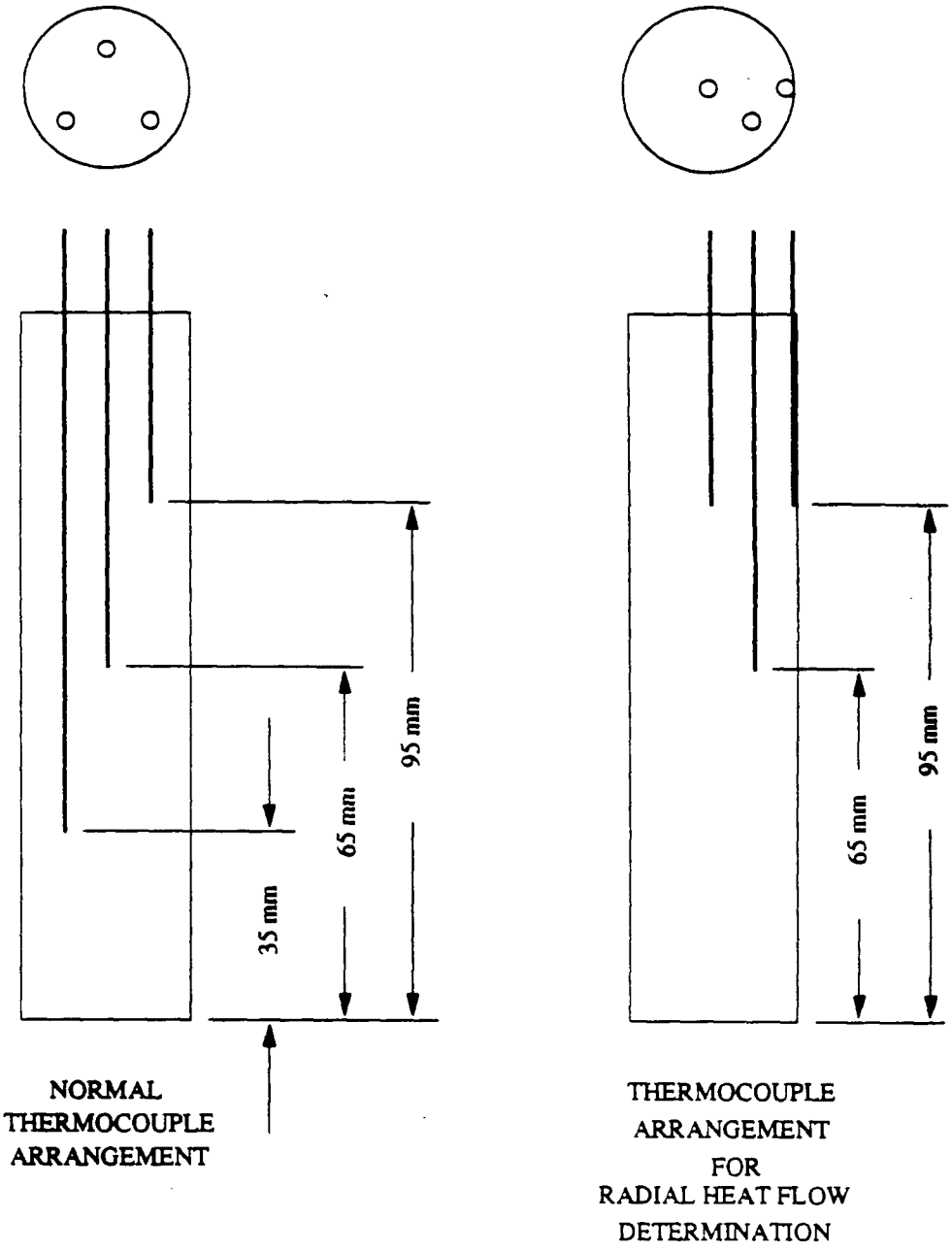

Figure 2.7

Thermocouple arrangement for radial heat flow determination and for normal temperature measurements

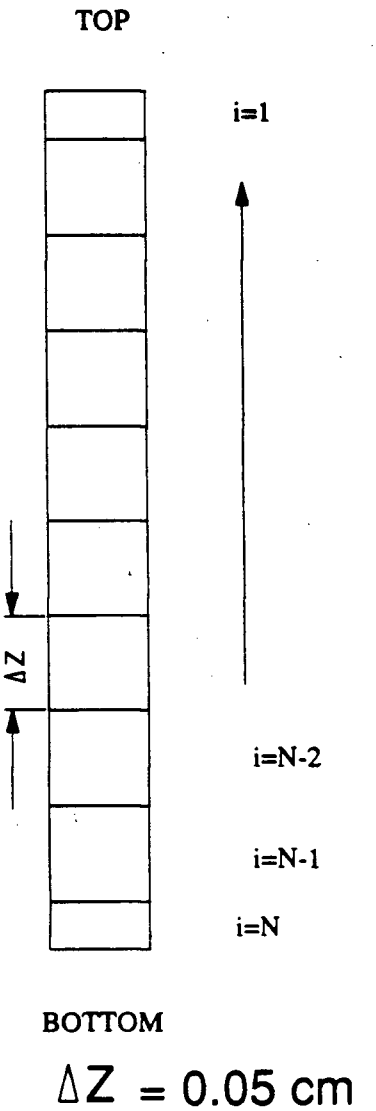

Figure 2.8

Node configuration scheme used for one dimensional heat transfer model

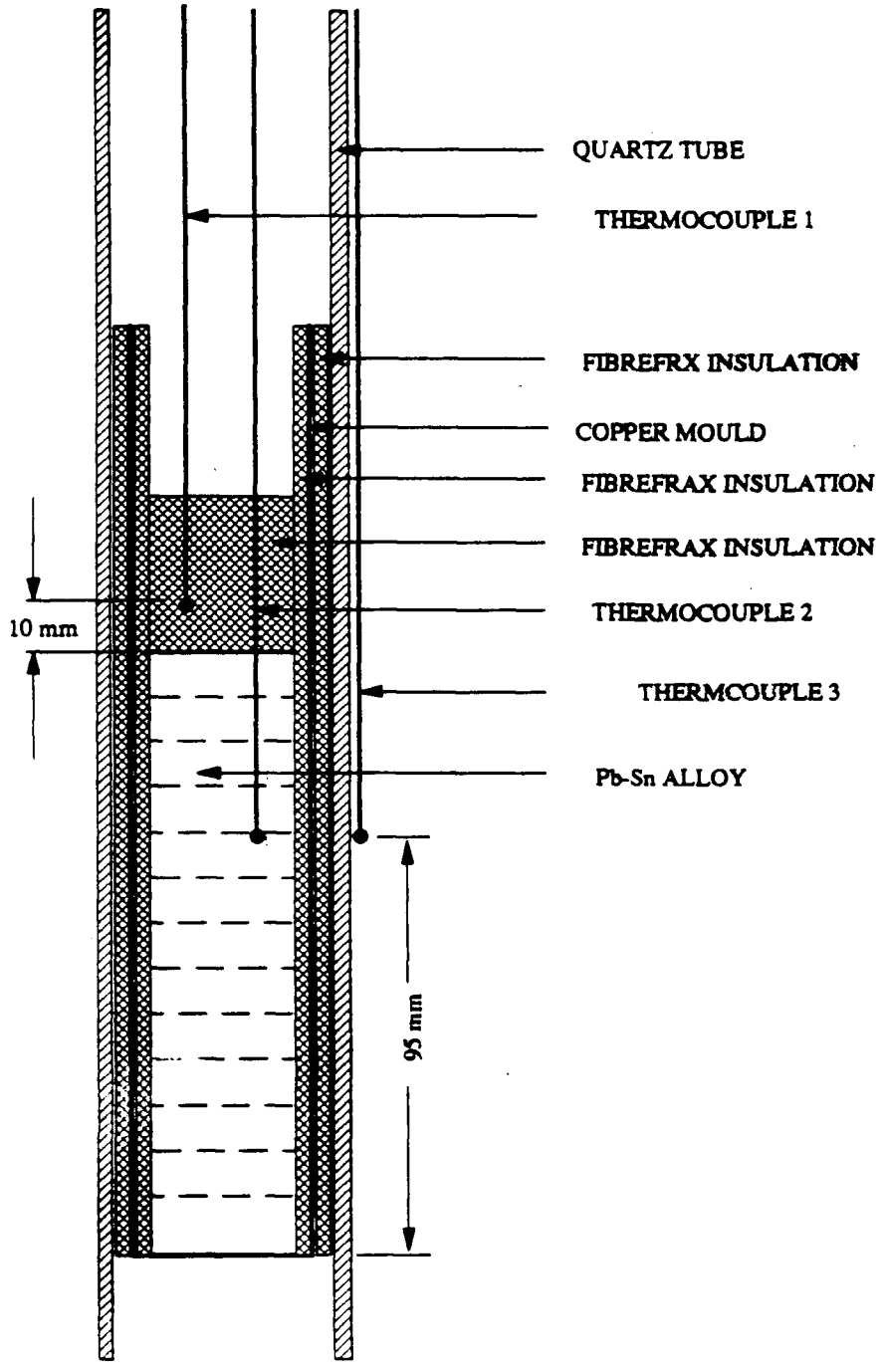

Figure 2.9

Thermocouple positions for measurement of vertical and radial temperature gradients at the top of the Pb-Sn alloy during solidification

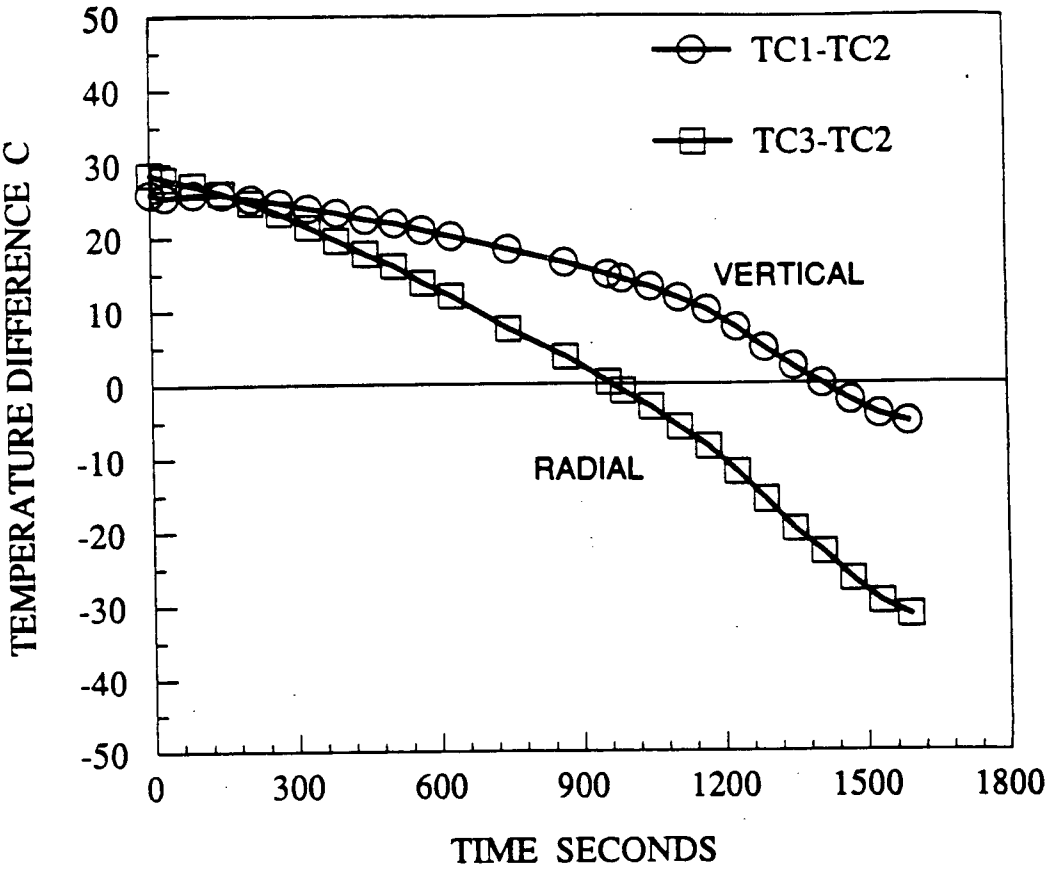

Figure 2.10

Vertical and radial temperature gradients in the top part of a Pb-Sn alloy as a function of time during directional solidification

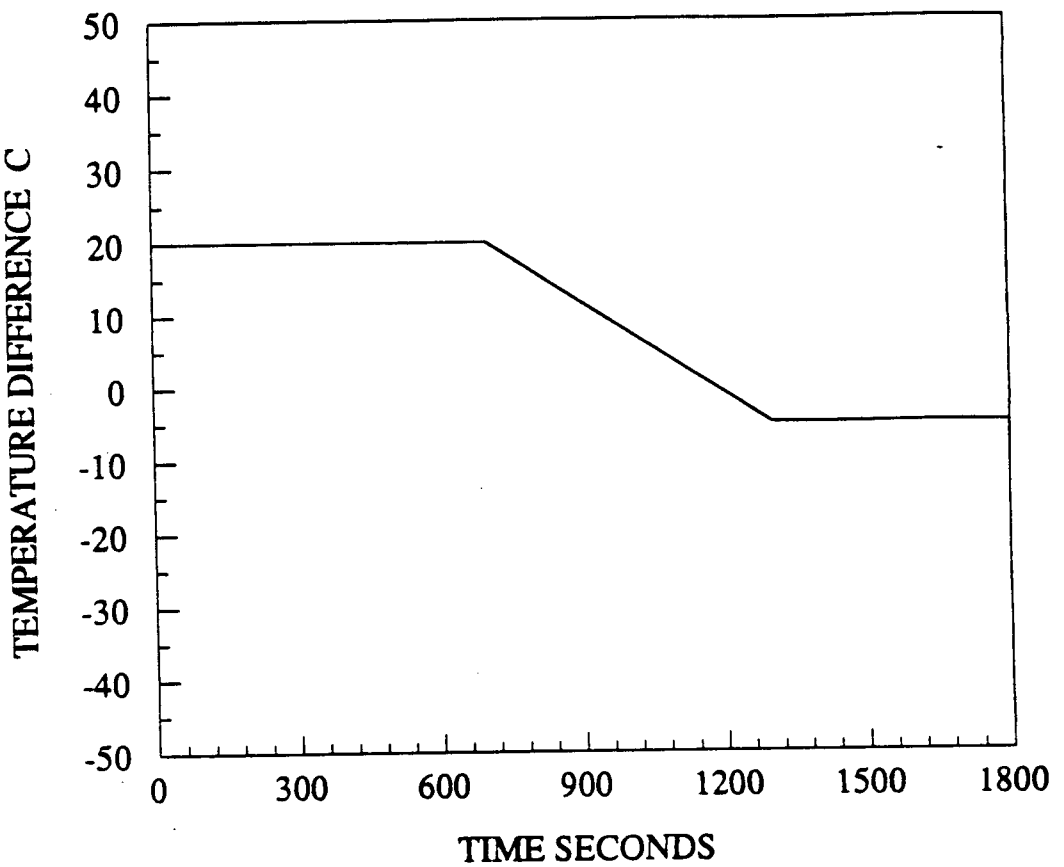

Figure 2.11

Assumed vertical temperature gradient at the top of the melt for the heat transfer model

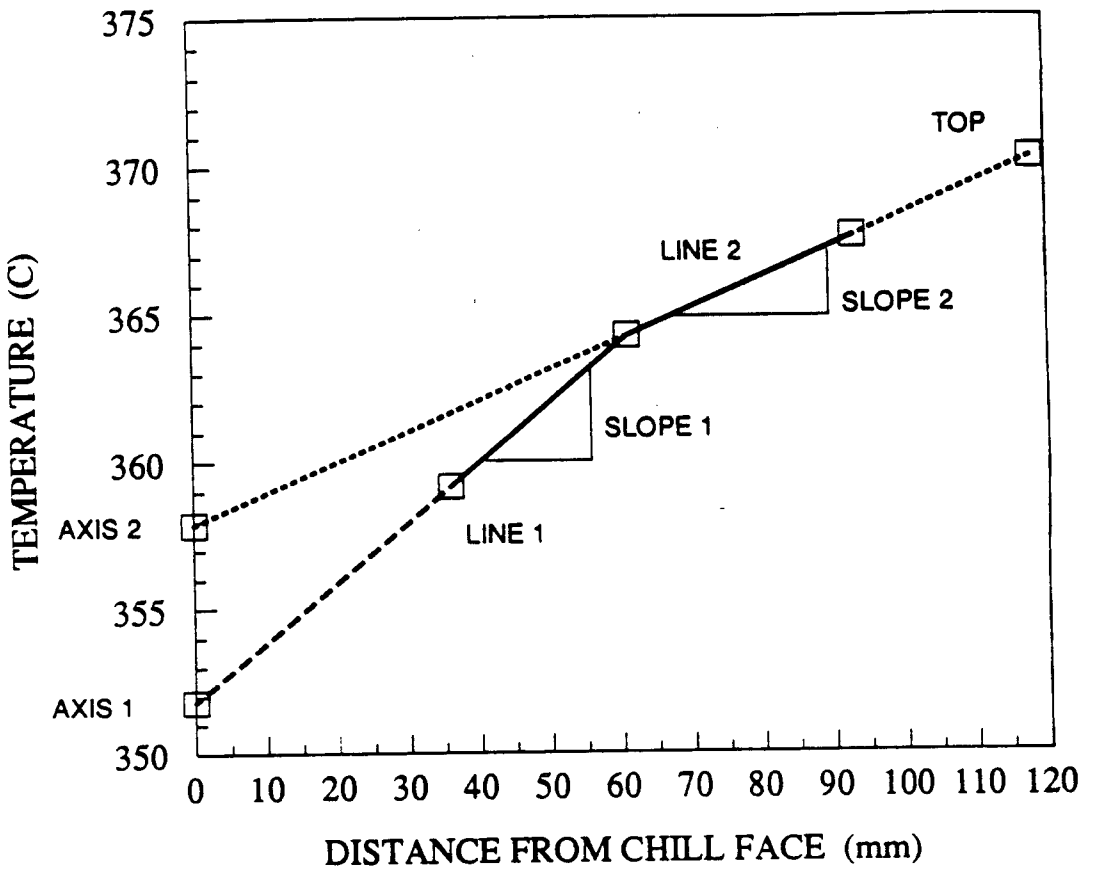

Figure 2.12

Temperature distribution in the melt at the start of cooling

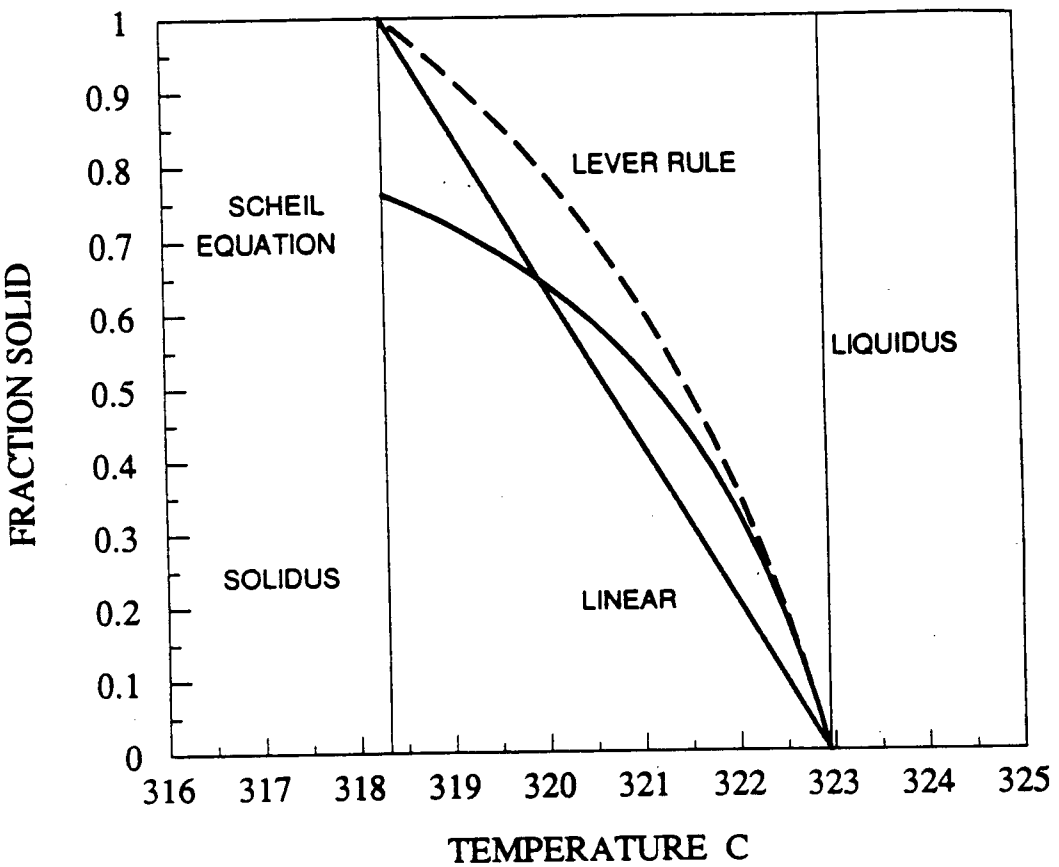

Figure 2.13

Fraction solid as a function of temperature for a Pb-1.5%Sn alloy calculated using the Scheil equation, the Lever rule, and assuming a linear function

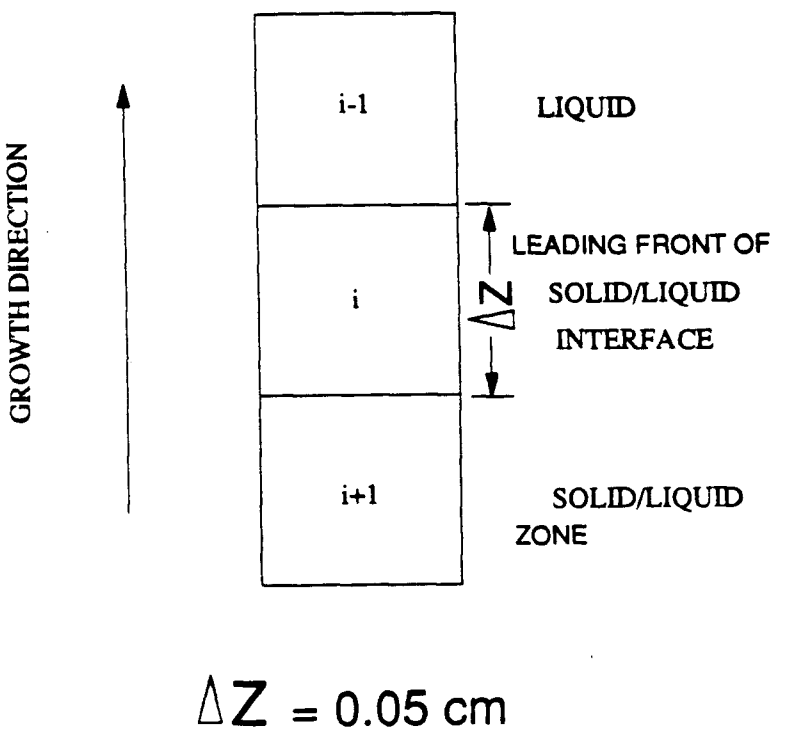

Figure 2.14

Nodal arrangement about the solid/liquid interface

Chapter 3

EXPERIMENTAL RESULTS

3.1 COLUMNAR TO EQUIAXED TRANSITION

To establish that a columnar to equiaxed transition, (CET), occurred in the Pb-1.5%Sn alloy, four directional solidification tests were carried out as listed in Table 3.1. Stainless steel inserts were used between the chill and the mould to change the cooling rate from one test to the next.

At the slowest cooling rate, (test 1), with 7 stainless steel sheets, no CET is observed. A completely equiaxed structure is produced as shown in Figure 3.1. Increasing the cooling rate by decreasing the number of stainless steel sheets to 3, (test 2), results in the cast structure shown in Figure 3.2. A CET is observed to occur sharply on a plane that is approximately perpendicular to the vertical plane containing the central

31 mm from the chill face. Increasing the cooling rate further by not using any stainless steel sheets, (test 4), results in the cast structure shown in Figure 3.3. A CET is seen to occur on the left hand side approximately 85 mm from the chill face.

For these four tests, the distance between the CET and the chill face decreases as the number of stainless steel sheets between the mould and the chill block increases in the manner shown in Figure 3.4.

TABLE 3.1
DIRECTIONALLY SOLIDIFIED Pb-1.5%Sn ALLOY RESULTS

TEST N°	ΔT_H °C	INGOT HEIGHT mm	N° OF STAINLESS STEEL SHEETS	%FURNACE POWER ON DURING COOLING	CET		N° OF EQUIAXED GRAINS/cm^2
						DISTANCE FROM CHILL mm	
1	40	92	7	0	NO	-	1
2	25	75	3	0	YES	34	6.7
3	25	80	3	50	YES	31	9.1
4	45	111	0	0	YES	85	12.5

The equiaxed grains in the region beyond the CET change in grain size with different cooling rates. The average number of grains per cm^2, (N), measured on the polished samples for the four tests are also listed in Table 3.1. The value of N is observed to increase appreciably from test 1 to test 4 accompanying an increase in cooling rate for tests 1, 2, and 4. Test 3 should have a slower cooling rate than test 2 since the furnace power is kept on but it is not clear why N is larger in test 3.

Cooling curves are obtained in each test using the melt thermocouples (TC). At the slowest cooling rate, test 1, with the furnace power off during cooling, the cooling curves from the four TC's unexpectedly show four distinct temperature plateaus as seen in Figure 3.5. This is unexpected as all the plateaus should coincide since they are from TC's measuring temperature in the same alloy. If there are thermal second order effects this might result in a progressive change in the plateau with distance from the chill face but this is not the case.

The duration of the plateau as a function of distance is shown in Figure 3.6. The duration of the plateau is seen to increase, then remain constant before unexpectedly decreasing as the distance is increased from 23, to 43, to 62, to 81 mm from the chill face.

The cooling curves for test 2 are shown in Figure 3.7. The increased cooling rate in this test eliminates the plateau at 27 mm from the chill face. A plateau is obtained for the TC at 51 mm from the chill face. The temperature of the plateau, (T_p), at this position is 324°C which is above the liquidus temperature, (T_{LIQ}), for the alloy and lasts for 240 seconds, appreciably shorter than the plateaus in test 1. At 77 mm from the chill face a plateau is obtained at 321°C, well below T_{LIQ} with a short duration of 60 seconds.

The results for test 3 with 50% furnace power on but the same number of stainless steel inserts as test 2 are shown in Figure 3.8. In this case, plateaus are observed at 27, 54, and 71 mm from the chill with T_p being nearly coincident with T_{LIQ} at 27 and 54 mm but appreciably higher than T_{LIQ} at 54 mm from the chill face. The duration of each plateau increases with distance from the chill in this case as shown in Figure 3.9, as might be anticipated.

The cooling curves for test 4, having the highest cooling rate are shown in Figure 3.10. The curves do not exhibit a temperature plateau for any of the thermocouples. The cooling curves do exhibit a positive temperature gradient in the melt as the temperature increases with distance from the chill throughout cooling and solidification.

Considering the cooling curves from tests 1-3 which have plateaus, the T_p recorded are not consistent with each other or what might be expected from the phase diagram. The T_p as a function of distance from the chill are plotted in Figure 3.11. For equilibrium conditions, one would expect the start of the plateau should occur at the liquidus and the curve should slope downward terminating at the solidus. This is clearly not the case since the plateaus are horizontal and T_p for tests 1 and 3 are above or at T_{LIQ}. Also in test 1, T_p varies in a cyclic manner between 326°C and 323.5°C with distance from the chill in the same Pb-1.5%Sn alloy. These results may be attributed to either errors in the temperature measurements of at least several degrees, or non-equilibrium solidification. In the case of non-equilibrium solidification, this would require the melt composition to be reduced to Pb-1.1%Sn for a liquidus temperature of 326°C. It is difficult to account for a reduction in the melt composition to 1.1%Sn at 43 mm from the chill, and to assume no fluid flow during solidification. Accordingly the results indicate appreciable absolute and relative deviations of the measured temperatures during solidification. Following this conclusion a series of calibration and reproducibility tests were undertaken to delineate the errors in the temperature measurements for the specific thermocouples used in the measurements.

3.2 TEMPERATURE MEASUREMENTS

3.2.1 HIGH PURITY LEAD (99.999%)

In the previous section in which the CET was examined, it was concluded that the measured temperatures were not sufficiently accurate or reproducible to determine the low temperature gradients associated with the CET. As a result, a series of careful measurements were undertaken to calibrate the thermocouples used and establish their accuracy and reproducibility. This was done by obtaining cooling curves for pure lead (99.999%) and comparing the freezing point, (T_{MP}), determined from the plateau in the cooling curve to that of pure lead, defined as 327.502°C. The cooling curves were obtained from a thermocouple positioned in the center of a cylindrical graphite mould containing the molten lead, which was slowly cooled as previously described in section 2.2.

A typical cooling curve for TC1 is shown in Figure 3.12. The liquid initially supercools to 328.1°C, then the temperature rises to 328.5°C and remains constant for approximately 660 seconds. Compared to the melting point of pure Pb, the TC in this case, registers a temperature which is high by 328.5-327.5=1.0°C. This experiment, repeated 11 times for TC1, gives the results listed in Table 3.2. In all the tests, the melt supercooled for about 210 seconds before solidification with an average supercooling of 0.6°C, the supercooling varying between 0.2°C and 1.1°C. Horizontal temperature plateaus are observed in all cases with the scatter in the plateau within ± 0.1°C in each test. The average plateau temperature, T_P, for all 11 tests is 328.5°C, 1.0°C above the T_{MP} for pure lead. The difference between T_P and T_{MP} varied between 0.6°C and 1.3°C.

TABLE 3.2
COOLING CURVE DATA FOR TC1 WITH 99.999% Pb.

TEST N°	SUPERCOOLING		PLATEAU		T_P-T_{MP}
	ΔT_s °C	DURATION SECS.	T_P °C	DURATION SECS.	°C
5	0.6	240	328.7	960	1.2
6	0.6	180	328.6	1080	1.1
7	0.9	180	328.7	1080	1.2
8	1.1	210	328.2	780	0.7
9	1.0	240	328.3	990	0.8
10	0.6	180	328.1	720	0.6
11	0.7	240	328.1	660	0.6
12	0.5	180	328.4	750	0.9
13	0.7	240	328.5	810	1.0
14	0.4	240	328.6	690	1.1
15	0.2	210	329.2	780	1.7
16	0.3	210	328.8	480	1.3
AVG.	0.6	210	328.5	810	1.0

The results shown in Table 3.3 pertain to TC2 using the same procedure to obtain the results for TC1 except the experiment was repeated only seven times. As with TC1, the melt supercools before solidification an average of 0.6°C. Horizontal temperature plateaus are observed in all cases which last for an average of 690 seconds. Unlike the case for TC1, the average T_P is 328.3°C, 0.2°C lower than the average T_P for TC1. The variation in the difference between T_P and T_{MP} for TC2 is also different as T_P-T_{MP} for TC2 varies from -0.1°C in test 19 to 1.5°C in test 21. The average difference is 0.8°C.

TABLE 3.3
COOLING CURVE DATA FOR TC2 WITH 99.999% Pb

TEST N°	SUPERCOOLING		PLATEAU		T_P-T_{MP}
	ΔT_s °C	DURATION SECS.	T_P °C	DURATION SECS.	°C
17	0.6	240	328.6	750	1.1
18	0.7	240	328.6	900	1.1
19	0.7	180	327.4	720	-0.1
20	0.8	180	327.5	780	0.0
21	0.3	180	329.0	780	1.5
22	0.4	240	328.8	510	1.3
23	0.4	180	328.3	480	0.8
AVG.	0.6	210	328.3	690	0.8

In a similar manner, nine repeat experiments were performed to obtain the results shown in Table 3.4 for TC3. This thermocouple registers an identical average supercooling to TC1 and TC2 of 0.6°C but indicates a higher average T_P than the previous two thermocouples at 328.8°C which is higher than the T_{MP} for pure Pb. The difference between T_P and T_{MP} for TC3 is always positive and varies between 0.9°C and 1.9°C with an average difference of 1.3°C which is the largest difference of the three thermocouples tested.

In summary, the three thermocouples indicate absolute temperatures which are too high when compared to T_{MP} for pure lead. Using the average values of T_P for TC1, TC2, TC3 as listed in Tables 3.2, 3.3 and 3.4 respectively, the corrections would be -1.0°C, -0.8°C, and -1.3°C. Even with these corrections, an individual test would not produce highly accurate results as the scatter of individual measurements is close to 0.7°C from

the average values.

These results indicate that each thermocouple should be calibrated prior to a test since the absolute correction is in the order of 1°C, and varies between thermocouples. The correction should be subtracted from any experimentally measured values.

TABLE 3.4
COOLING CURVE DATA FOR TC3 WITH 99.999% Pb

TEST N°	SUPERCOOLING		PLATEAU		T_P-T_{MP}
	ΔT_s .C	DURATION SECS.	T_P °C	DURATION SECS.	°C
24	0.9	180	328.7	840	1.2
25	0.9	180	328.5	840	1.0
26	0.6	180	328.4	660	0.9
27	0.8	180	329.2	1170	1.7
28	0.5	180	328.9	690	1.4
29	0.5	210	329.0	660	1.5
30	0.2	240	329.4	780	1.9
31	0.3	180	329.1	540	1.6
32	0.4	300	328.4	480	0.9
AVG.	0.6	210	328.8	750	1.3

3.2.2 COMMERCIALLY PURE LEAD (99.99%)

Cooling curves were obtained for commercially pure lead, (99.99%), under the same test procedures as the high purity lead. One cooling was obtained for each of the three thermocouples giving the results shown in Figure 3.13. The liquid is again seen to

supercool but this time to 326.9°C, and then gradually recalesce until the temperature plateau is reached at 327.5°C, which is at the T_{MP} for lead. The plateau lasts for approximately 450 seconds until the temperature decreases. The test results from all three thermocouples are listed in Table 3.5.

TABLE 3.5
COOLING CURVE DATA WITH 99.99% Pb FOR TC1, TC2, TC3

TC N°	SUPERCOOLING		PLATEAU		T_p-T_{mp}
	ΔT_s .C	DURATION SECS.	T_P °C	DURATION SECS.	°C
1	0.6	390	327.5	450	0
2	0.4	300	327.5	360	0
3	N.M.	N.M.	327.7	450	0.2

N.M.= Not Measured

3.2.3 COMMERCIALLY PURE TIN (99.89%)

Cooling curves were measured for commercially pure tin, (99.89%), for the three thermocouples. The cooling curves are shown in Figure 3.14 and the data are given in Table 3.6. For TC1, a supercooling of 1.1°C is measured before the temperature rises to the freezing plateau of 230.3°C which is well below the T_{MP} for high purity tin at 231.97°C[42]. For TC2, and TC3, the measured supercooling is smaller than TC1 while the temperature rises to a freezing plateau slightly above T_{MP} for tin. In these measurements

TC1 is reading abnormally low for reasons unclear at this time.

TABLE 3.6
COOLING CURVE DATA WITH 99.89% Sn FOR TC1, TC2, TC3

TC N°	SUPERCOOLING		PLATEAU		T_P-T_{MP}
	ΔT_s °C	DURATION SECS.	T_P °C	DURATION SECS.	°C
1	1.1	570	230.3	660	-1.7
2	0.8	540	232.1	720	0.1
3	0.6	540	232.3	840	0.3

3.3 DIRECTIONAL SOLIDIFICATION OF Pb-1.5%Sn

3.3.1 FURNACE OFF AND NO INSULATION ON TOP

Twelve tests were carried out following procedure 1 as outlined in section 2.3 using the apparatus shown in Figure 2.3. No insulation was at the top of the melt and the furnace was turned off during cooling. For seven of the tests, (33-39), chill assemblies CA1 and CA2 and a wide range of melt superheats, ΔT_H, varying between 7°C and 42°C were used. The test conditions and results for these tests are listed in Table 3.7. A CET was observed in all the tests at an average distance of 67 mm from the chill face, varying between 62 and 72 mm. The position of the CET is the same for both CA1 and CA2 chill assemblies and is independent of the melt superheat within the range examined. The cast structure of the ingot section from test 34 using the CA1 chill assembly is shown in

Figure 3.15(a) and from test 38 using CA2 in Figure 3.15(b). In both cases the transition from columnar to equiaxed is observed to be irregular, as compared to the CET in Figure 3.2. Some columnar grains continue to grow into the equiaxed region, which makes the measurement of the distance of the CET from the chill face a little subjective.

The equiaxed grain size is observed to be large with occasional isolated clusters of small grains among the large grains.

Cooling curves were obtained from the output of the three thermocouples. An example of the resulting three cooling curves are shown for test 34 in Figure 3.16. At 34 mm from the chill face, the liquid cooling rate for the first 300 seconds is rapid. After 300 seconds, the cooling rate decreases until solidification starts. A horizontal temperature plateau is not observed from a TC at this distance from the chill face, but only a sharp inflection point at the liquidus temperature. Below the liquidus, the cooling rate is rapid and constant.

The cooling curves for TC2 and TC3 positioned at 63mm and 94 mm from the chill have slower melt cooling rates than TC1 and both exhibit a horizontal temperature plateau very near the liquidus temperature. The temperature at 94 mm from the chill in the melt is higher than at 63 mm, the temperature difference decreasing as the liquidus is approached. At the liquidus, the temperatures at 63 and 94 mm appear to merge for a short time before the temperature at 63 mm decreases rapidly. The temperature at 94 mm remains constant for a longer period of time. This thermal behavior is more clearly illustrated in Figure 3.17 where the temperature scale has been expanded.

The liquid at both TC positions supercools 0.5°C with the liquid at 63 mm from the chill face supercooling first followed quickly by the liquid at 94 mm. At approximately

TABLE 3.7
DATA FOR Pb-1.5%Sn
FURNACE OFF DURING COOLING
NO INSULATION ON TOP

TEST N°	CHILL ASSEMBLY	ΔT_E °C	TC mm	G_{LX} °C/mm	SUPERCOOLING		PLATEAU		CET mm	INGOT HEIGHT mm
					ΔT_S °C	DURATION SECONDS	T_P °C	DURATION SECONDS		
33	CA1	29	3	0.25	-	-	-	-	62	132
			61	0	0.2	120	322.8	120		
			94	-	0.6	210	323.4	240		
34	CA1	42	34	0.06	-	-	-	-	67	130
			63	0.0	0.5	120	323.1	150		
			94	-	0.5	60	323.2	420		
35	CA2	38	38	0.09	-	-	-	-	71	141
			67	0.0	-	-	322.3	120		
			95	-	0.7	150	322.9	60		
36	CA2	9	35	0.12	-	-	-	-	62	134
			72	0.02	-	-	322.6	90		
			104	-	0.3	60	323.4	300		
37	CA2	32	37	0.10	-	-	-	-	67	136
			64	-0.03	0.3	120	322.7	30		
			92	-	0.9	240	322.6	180		
38	CA2	13	30	0.15	-	-	-	-	72	132
			60	0.03	-	-	322.7	30		
			92	-	0.2	90	322.9	210		
39	CA2	7	41	0.17	-	-	-	-	70	135
			65	0.0	-	-	322.5	120		
			98	-	0.3	90	322.7	630		
AVERAGE					0.45	120.0	322.8	180.0	67	134

1200 seconds, the liquid at both TC positions is supercooled. There is a gradual rise in temperature from supercooling to the temperature plateau at both positions. The plateau

at 63 mm from the chill occurs first at 323.1°C, 0.2°C above the liquidus, followed approximately 60 seconds later by the plateau at 94 mm at 323.2°C, 0.3°C above the liquidus. For the next 60 seconds, the temperature at 63 mm and at 94 mm from the chill remain at these two constant values. After this time, the temperature 63 mm decreases rapidly, while the temperature at 94 mm remains at 323.2°C. The temperature at 94 mm from the chill remains constant until approximately 1620 seconds where the temperature starts to decrease rapidly.

Considering the overall results for tests 33-39, listed in Table 3.7, no supercooling is observed in any of the tests for the TC closest to the chill, which is similar to test 34. The amount of supercooling at the other two thermocouples varied between 0.2°C and 0.9°C. The plateau temperatures varied between 322.5°C which is 0.5° below the liquidus temperature and 323.4 which is 0.4°C above the liquidus temperature.

Estimates of the temperature gradient in the liquid ahead of the solid/liquid interface, G_{LX}, were made assuming a linear gradient between TC1 and TC2, and between TC2 and TC3 and assuming the interface is coincident with the liquidus temperature. The results are also listed in Table 3.7, and are observed to be very small. With the interface at TC1, G_{LX} varies between 0.06°C/mm and 0.17°C/mm as measured between TC1 and TC2 for tests 34 to 39. At TC2, G_{LX} varies between -0.03°C/mm and +0.03C/mm, a range which is below the sensitivity of the temperature measurements. At 3 mm from the chill face in test 33, G_{LX} is 0.25°C/mm.

Tests 40-44 were carried out in the same manner as tests 33-39 except that chill assembly CA3 was used and the superheat was kept low. The chill assembly CA3 puts a higher thermal resistance between the chill and the mould compared to CA1 and CA2.

The test conditions and results are listed in Table 3.8. From Table 3.8, the distance from the chill that the CET occurs varies between 39 and 51 mm with an average of 45 mm for tests 41-44. This is appreciably shorter than the corresponding distances for tests 33- 39 with an average distance of 67 mm. The CET position appears to be independent of the melt superheat. The cast structure for tests 40 and 42 are shown in Figure 3.18(a) and (b). A large grained highly irregular structure is observed for test 40, and no clear CET is delineated. The structure for test 42, also does not have a sharply delineated CET, but columnar grains are evident at the bottom and the CET is estimated to be the solid horizontal line drawn in the figure. One columnar grain continues well into the equiaxed region to 100 mm from the chill face.

The cooling curves for tests 41-42 are generally similar to those shown in Figure 3.15 for test 34. as shown in Figure 3.19 for test 43. The curve for TC1 was the same as TC1 in Figure 3.15 with no supercooling and no temperature plateau and therefore is not shown. For TC2 and TC3 at 61 and 94 mm from the chill face, there is 0.2°C supercooling at 61 mm and 0.4°C supercooling at 94 mm. In the other tests in this series listed in Table 3.8 supercooling is only observed at 94 mm distance ranging between 0.2°C and 0.4°C. This is appreciably less than the supercooling observed in tests 33-39.

A temperature plateau is observed for both TC2 and TC3, with the plateau temperature a little below the liquidus for TC2, (0.3°C), and appreciably below the liquidus for TC3 (1-2°C).

It is significant that the plateau temperature at 94 mm is below that at 61 mm and is preceded by supercooling. This was generally the case for tests 40 to 44, but not for tests 33-39 where the plateau temperature near 94 mm was higher than that near 61 mm.

TABLE 3.8
DATA FOR Pb-1.5%Sn
FURNACE OFF DURING COOLING
NO INSULATION ON TOP

TEST N°	CHILL ASSEMBLY	ΔT_E °C	TC mm	G_{LX} °C/mm	SUPERCOOLING		PLATEAU		CET mm	INGOT HEIGHT mm
					ΔT_s °C	DURATION SECONDS	T_P °C	DURATION SECONDS		
40	CA3	6	35	0.04	-	-	322.7	60	0	136
			65	-0.03	-	-	323.3	180		
			98	-	0.2	330	322.4	180		
41	CA3	14	40	0.07	-	-	-	-	51	136
			75	-0.04	-	-	322.9	210		
			101	-	0.2	120	322.1	300		
42	CA3	6	31	0.07	-	-	-	-	44	136
			59	-0.04	-	-	322.7	240		
			94	-	0.4	300	321.9	240		
43	CA3	14	32	0.06	-	-	-	-	47	141
			61	-0.04	0.2	30	322.7	210		
			94	-	0.2	180	321.8	150		
44	CA3	11	36	0.1	-	-	-	-	39	135
			65	-0.04	-	-	322.1	150		
			95	-	0.4	120	321.5	240		
AVERAGE					0.3	180	322.4	210	45	137

Values of G_{LX} for tests 40 to 44 were determined in the same way as tests 33 to 39, giving the results listed in Table 3.8. In general, the values of G_{LX} shown are very low. The region where the CET occurs near 44 mm corresponds to the gradient determined between TC1 and TC2 with values of G_{LX} ranging between 0.04°C/mm and 0.1°C/mm. In the upper part of the casting, between TC2 and TC3 the values of G_{LX} are all negative and range between -0.03°C/mm and -0.04°C/mm.

The low temperatures at the top of the melt suggest that significant heat is being lost from the top of the melt. To overcome this effect a series of tests were carried out with insulation added to the furnace above the melt to reduce or eliminate heat loss from the top of the melt.

3.3.2 FURNACE OFF

TOP OF MELT THERMALLY INSULATED

Four tests, (45-48) were carried out in a manner similar to tests 33 and 34 using chill assembly CA1 but with insulation added to the mould above the melt. In addition, the thermocouples were calibrated "in-situ", following procedure 3 in section 2.3 to improve the accuracy of the temperature measurements. The test conditions are listed in Table 3.9.

A CET was observed in each of the tests at distances from the chill ranging between 60 to 91 mm. The cast structure for tests 46,47 and 48 are shown in Figure 3.20 with the position of the CET indicated by the horizontal dark line. As with the previous tests on Pb-1.5%Sn the transition to equiaxed grains is not flat and well defined. The equiaxed grains have large diameters except for test 48 where clusters of small grains are present among the large grains near the transition.

The cooling curves for tests 45 to 48 were generally similar to the curves for tests 33 to 44. Typical curves for TC2 and TC3 of test 47 are shown in Figure 3.21. For TC2, supercooling and a temperature plateau are not observed. Similar results were obtained for tests 45, and 46. In all cases, no supercooling or plateaus are observed for TC1. The cooling curve for TC3 shows supercooling of 0.4°C and a freezing plateau at 323.2°C,

TABLE 3.9
COOLING CURVE DATA FOR Pb-1.5%Sn
FURNACE OFF DURING COOLING
INSULATION ON TOP
USING CHILL ASSEMBLY CA1

TEST N°	ΔT_H °C	TC mm	G_{LX} °C/mm	SUPERCOOLING		PLATEAU		CET mm	INGOT HEIGHT mm
				ΔT_S °C	DURATION SECONDS	T_P °C	DURATION SECONDS		
45	38	33	0.35	-	-	-	-	76	118
		61	0.07	-	-	-	-		
		91	-	0.3	60	323.1	150		
46	20	-	-	-	-	-	-	91	122
		66	0.09	-	-	-	-		
		95	-	0.4	150	323.0	150		
47	37	35	.34	-	-	-	-	76	126
		66	.11	-	-	-	-		
		95	-	.4	150	323.2	150		
48	41	36	.14	-	-	-	-	60	118
		61	.01	0.6	120	322.7	90		
		93	-	0.5	120	322.9	360		

0.2°C above the liquidus. Similar supercooling between 0.3°C and 0.5°C was observed for tests 45 and 46 and plateaus at a temperature of 323.1°C ±0.1°C which is very close to the liquidus temperature of 323.0°C.

The results for test 48 are a little different than for tests 45-47. The cooling curves for TC2 and TC3 for this test are shown in Figure 3.22. Supercooling is observed at both thermocouples, 0.6°C and 0.5°C respectively. A short freezing plateau is observed for

TC2, 0.3°C below the liquidus, and a much longer plateau for TC3 at 0.1°C below the liquidus. It is not clear why the cooling curves for test 48 differed from the other three tests in the series.

Estimates of the temperature gradient in the melt, G_{LX}, were made using the procedure described previously, giving the results listed in Table 3.9. At 33 mm from the chill, (TC1), two values are near 0.35°C/mm and one at 0.14°C/mm. No value is listed for test 46 due to a defective thermocouple. At about 65 mm from the chill, G_{LX}, is much smaller varying between 0.01°C/mm and 0.11°C/mm. These values are obtained using TC2 and TC3 values covering the region where the CET occurs.

The presence of supercooling in the upper region of the melt in these experiments, even with insulation above the melt suggest that significant radial heat is being lost during cooling. As a result tests were carried out in which the furnace power was reduced instead of being turned off during cooling in an attempt to reduce the radial heat loss.

3.3.3 FURNACE POWER ON DURING COOLING

MELT TOP INSULATED

Tests 49 to 55 were carried out in which the furnace was left on during cooling at various power settings. The Pb-1.5%Sn alloy was solidified following procedure 3 in section 2.3 which includes "in-situ" calibration of the thermocouples, and chill assembly CA1. The top of the melt was thermally insulated. In test 50, thermocouples were positioned at the centre and near the mould wall at the same distance from the chill to measure the radial temperature gradient as described in section 2.3, procedure 2. The test conditions and results are listed in Table 3.10.

TABLE 3.10
COOLING CURVE DATA FOR Pb-1.5%Sn
FURNACE ON DURING COOLING
INSULATION ON TOP
USING CHILL ASSEMBLY CA1

TEST N°	FURNACE CURRENT LEVEL AMPS.	ΔT_H °C	TC mm	G_{LX} °C/mm	SUPERCOOLING		PLATEAU		CET mm	INGOT HEIGHT mm
					ΔT_S .C	DURATION SECONDS	T_P °C	DURATION SECONDS		
49	3.0	43	4	0.32	-	-	-		85	123
			64	0.0	-	-	322.9	120		
			95	-	0.4	210	323.4	240		
50	4.4	46	60	0.11	-	-	-	-	-	119
			89*		-	-	-	-		
			93**		-	-	-	-		
51	5.0	38	31	0.26	-	-	-	-	-	126
			60	0.14	-	-	-	-		
			89	-	-	-	-	-		
52	4.4	40	34	0.28	-	-	-	-	-	119
			64	0.12	-	-	-	-		
			93	-	-	-	-	-		
53	3.5	39	-	-	-	-	-	-	-	137
			67	0.20	-	-	-	-		
			95	-	-	-	-	-		
54	3.0	41	-	-	-	-	-		88	129
			56	.02	0.3	90	323.3	270		
			98	-	0.5	180	323.9	270		
55	5.0	43	29	0.29	-	-	-	-	-	123
			62	0.10	-	-	-	-		
			92	-	-	-	-	-		

*THERMOCOUPLE IN THE MIDDLE OF THE MELT

**THERMOCOUPLE ON THE EDGE OF THE MELT

A CET is observed in only two of the seven tests, 49 and 54. In these tests, the furnace current was set at 3.0 amps, the lowest value used in this series. The structure of the test sample from test 54 is shown in Figure 3.23. The structure consists of very large grains with the CET taken at the marked horizontal line 88 mm from the chill face. The structure for test 49 was similar with the CET at 85 mm from the chill.

The cooling curves for TC2 and TC3 from test 54 are shown in Figure 3.24. Both curves exhibit supercooling (0.3°C and 0.5°C respectively) and temperature plateaus above the liquidus temperature (0.3°C and 0.9°C respectively). Values for TC1 are not included as the thermocouple was defective during cooling. The curves for test 49 were similar to 54.

The value of G_{LX} for test 54 at TC2 was small, 0.02°C/mm. For test 49, G_{LX} is large close to the chill, 0.32°C/mm, 4 mm from the chill, and 0°C/mm at 64 mm from the chill.

The remaining tests in this series 51 to 53 and 55 all had higher power inputs to the furnace during cooling compared to tests 49 and 54 as listed in Table 3.10. The structure of the test samples consisted of large columnar grains. An example is shown in Figure 3.25 for test 55. No CET is evident in the structure.

A typical set of cooling curves for TC1, TC2, and TC3 from test 55 is shown in Figure 3.26. Supercooling and a horizontal temperature plateau are not evident, which is similar to that for tests 50 to 53. As a result, no data is included for these values in Table 3.10. The temperature of TC3 is always higher than TC1 and TC2 during cooling and solidification, and TC2 is always higher than TC1. A positive temperature gradient is thus maintained throughout the sample during cooling. The temperature gradient G_{LX}

listed in Table 3.10 is relatively high nearest the chill for tests 51, 52, and 55 at 0.26°C/mm, 0.28°C/mm and 0.28°C/mm. At about 65 mm from the chill G_{LX} decreases to between 0.1°C/mm and 0.2°C/mm.

Measurements of the radial temperature gradient were made in test 50 with one thermocouple at the centre of the melt, and the second adjacent to the mould wall separated by 15 mm, 90 mm from the chill face. The results are listed in Table 3.11. The maximum radial temperature gradient in the liquid occurs at the start of solidification and is approximately 0.07°C/mm. As the liquid cools and the temperatures approach the liquidus temperature the radial temperature gradient decreases to 0.02°C/mm which is realistically beyond the sensitivity of the present measurements. After the alloy solidified at this vertical position the radial temperature gradient increased to approximately 0.09°C/mm. The test was repeated with the power to the furnace off giving the results listed in Table 3.12. The results are very similar except that the time taken to cool to the liquidus temperature is shorter and now a period of supercooling and a temperature plateau are observed. The decline in the radial temperature gradient follows the pattern in Table 3.11.

TABLE 3.11
TEMPERATURES AND TEMPERATURE DIFFERENCE BETWEEN CENTRE OF MELT AND ADJACENT TO MOULD WALL FURNACE POWER ON AT 4.4 AMPS

TIME (SECONDS)	STATE	TC2 CENTRE °C	TC3 MOULD WALL °C	ΔT °C
277	LIQUID	361.3	362.3	1.0
516	LIQUID	351.9	352.7	0.8
1597	LIQUID	331.7	332.0	0.3
2677	LIQUID	325.3	325.6	0.3
4073	SOLID	317.4	318.8	1.4
4305	SOLID	314.0	315.2	1.2

TABLE 3.12
TEMPERATURES AND TEMPERATURE DIFFERENCE BETWEEN CENTRE OF MELT AND ADJACENT TO MOULD WALL FURNACE OFF DURING COOLING

TIME (SECONDS)	STATE	TC2 CENTRE °C	TC3 MOULD WALL °C	ΔT °C
227	LIQUID	360.2	361.2	1.0
467	LIQUID	352.7	353.7	1.0
1067	LIQUID	332.3	333.1	0.8
1523	SUPERCOOLED LIQUID	321.7	322.1	0.4
1847	FREEZING PLATEAU	323.1	323.4	0.3
2391	SOLID	310.2	311.8	1.6

3.4 DIRECTIONAL SOLIDIFICATION OF PURE LEAD (99.999%) AND Pb-Sn ALLOYS

In this series of experiments the cooling curves and cast structure are discussed for directionally solidified pure Pb and Pb containing 3% and 6% Sn.

3.4.1 DIRECTIONAL SOLIDIFICATION OF PURE LEAD

Pure lead, (99.999%) was solidified using procedure 1 of section 2.3 with no thermal insulation above the melt and with two melt superheats. The test conditions and results are listed in Table 3.13, and the cooling curves for test 57 are shown in Figure 3.27. These results in general are similar to the Pb-1.5%Sn alloy. Since a CET was not expected to occur in pure lead, the sample was not sectioned and etched. The melt supercools 0.5°C at 64 mm from the chill face in both tests and approximately 0.5°C at 93 mm. A short temperature plateau is observed at 64 mm from the chill, and a much longer plateau at 93 mm from the chill. The plateau temperatures are 0.1°C and 0.4°C above the melting point of pure lead for TC2 and TC3 respectively which is within the experimental error of the measurements.

The melt temperature gradient, G_{LX} is relatively steep close to the chill, 0.29°C/mm, between 5 and 64 mm from the chill, and effectively zero between 64 and 93 mm from the chill.

TABLE 3.13
COOLING CURVE DATA FOR PURE LEAD(99.999%)
FURNACE OFF DURING COOLING
USING CHILL ASSEMBLY CA1

TEST N°	ΔT_H °C	TC mm	G_{LX} °C/mm	SUPERCOOLING		PLATEAU	
				ΔT_S °C	DURATION SECONDS	T_P °C	DURATION SECONDS
56	79	5	0.30	-	-	-	-
		64	0.01	0.5	90	327.6	180
		93	-	0.5	120	327.9	510+
57	20	5	0.28	-	-	-	-
		64	0.0	0.5	210	327.6	90
		93	-	0.4	150	327.9	600

3.4.2 DIRECTIONAL SOLIDIFICATION OF Pb-3%Sn AND Pb-6%Sn ALLOYS

Two tests, (58 and 59), were carried out, one on a Pb-3%Sn alloy and the second on a Pb-6%Sn alloy. Procedure 3 of section 2.3 was used in which the thermocouples were calibrated "in-situ", the furnace turned off during cooling, chill assembly CA1 was used and thermal insulation was present above the melt. The test conditions and results are listed in Table 3.14 and the cooling curves for test 59 in Figure 3.28.

The test samples were sectioned and etched to determine the cast structure. Unfortunately, a suitable etch to bring out the cast structure was not found for either alloy so that the presence or position of the CET could not be established. The etching solutions tried, in addition to that described in section 2.3, and are listed in Appendix 3.

TABLE 3.14
COOLING CURVE DATA FOR Pb-3%Sn, AND Pb-6%Sn
FURNACE OFF DURING COOLING
INSULATION ON TOP
USING CHILL ASSEMBLY CA1

TEST N°	SOLUTE CONTENT %Sn	ΔT_B °C	TC mm	G_{LX} °C/mm	SUPERCOOLING		PLATEAU	
					ΔT_S °C	DURATION SECONDS	T_P °C	DURATION SECONDS
58	3.0	20	33	0.19	-	-	-	-
			62	0.0	-	-	318.7	60
			94	-	0.5	150	319.3	210
59	6.0	12	36	0.14	-	-	-	-
			66	0.0	0.2	30	310.5	30
			92	-	0.4	90	311.0	180

In both tests the melt supercools between 0.2°C and 0.5°C before solidification. The supercooling is followed by a short plateau at 66 mm from the chill at 0.3°C below the liquidus, and a much longer plateau at 92 mm from the chill 0.2°C above the liquidus. The cooling curves for test 58 for the Pb-3%Sn alloy were similar to Figure 3.28. With a liquidus temperature for Pb-3%Sn of 318.9°C, the plateau at 62 mm from the chill was below the liquidus by 0.2°C, and above the liquidus at 94 mm from the chill by 0.4°C. The measured temperature gradient, G_{LX} is 0.19°C/mm and 0.14°C/mm for the two alloys at 33 mm from the chill and 0°C/mm in both cases at 62 mm from the chill.

3.5 DIRECTIONAL SOLIDIFICATION OF Sn-10%Pb ALLOY

In a previous investigation[18], the CET in Sn-10%Pb alloys was examined extensively. It was considered desirable to do at least one test with this alloy using the better temperature measuring apparatus developed in this investigation.

One sample of Sn-10%Pb alloy was prepared and directionally solidified with the furnace off during cooling using chill assembly CA1, and with thermal insulation above the melt. The thermocouples were calibrated "in-situ" against the T_{LIQ} of the alloy. The test conditions and results are listed in Table 3.15, while the cast structure is shown in Figure 3.29, and the cooling curves in Figure 3.30.

TABLE 3.15
COOLING CURVE DATA FOR Sn-10%Pb
FURNACE OFF DURING COOLING
INSULATION ON TOP
USING CHILL ASSEMBLY CA1

TC mm	G_{LX} °C/mm	SUPERCOOLING		PLATEAU		CET mm	INGOT HEIGHT mm
		ΔT_s °C	DURATION SECONDS	T_P °C	DURATION SECONDS		
34	0.14	0.3	60	213.6	60	45	127
64	0.10	1.7	240	216.1	210		
93	-	2.8	300	218.8	300		

A clearly defined CET is observed at 45 mm from the chill, as shown in Figure 3.29, the transition occurring sharply on a horizontal plane, similar to that reported previously[18]. The cooling curves in Figure 3.30 show a small supercooling, (0.3°C),

nearest the chill and large supercooling occurring simultaneously, (1.7°C and 2.8°C), at 64 and 93 mm from the chill respectively. Following supercooling the temperature rises to a very short plateau from the TC nearest the chill, and progressively longer plateaus from the TC's away from the chill. Plateau temperatures vary appreciably with respect to the liquidus temperature. At 33 mm the difference is -1.4°C, at 64 mm, +1.1°C and at 93 mm, +3.8°C.

Values of G_{LX}, based on the temperature difference between the thermocouples is always positive. The values are 0.14°C/mm at 34 mm and 0.10°C/mm at 64 mm. Since the transition occurs at 45 mm the gradient at that point should be between these two values. This is consistent, to a first approximation, to the value of the critical gradient at the CET of 0.11°C/mm determined previously for Sn-10%Pb.

3.6 MATHEMATICAL HEAT TRANSFER MODEL

3.6.1 DIRECTIONAL SOLIDIFICATION OF Pb-1.5%Sn

It is necessary to know values for G_L, the temperature gradient in the liquid ahead of the solid/liquid interface, for all points in the melt as the solidification front progress from the chill face to the top of the melt and how it changes with time in order to determine the G_L at the CET. This information cannot be derived solely from cooling curves using thermocouples at fixed positions in the melt. The cooling curves data from the three thermocouples can only provide two measured values assuming a linear gradient

in the liquid between each thermocouple. In addition, the position of the CET is not known apriori, and therefore the CET may not coincide with the position of a fixed thermocouple.

A solution to this problem is to use a heat transfer mathematical model which predicts temperatures in the ingot as a function of time and distance from the chill face. These temperatures in turn are used to determine how G_L changes throughout the course of the experiment using equation 2.24. In order to gain confidence in the model, the predicted temperatures must first agree closely with accurate temperature measurements.

The boundary conditions needed to solve the transient heat conduction equation, (2.1), are generally unknown ahead of time but are assumed to have the form given by equations 2.4 and 2.5, see section 2.4. The unknowns in equations 2.4 and 2.5, are the heat transfer coefficients at the top and bottom of the alloy, H_B and H_{Top}, and the furnace temperature above the melt, T_{Furn}. The heat transfer coefficient at the bottom of the alloy was determined first by iteration using H_{Top} equal to zero. This produced calculated temperatures which were close to the experimental temperatures at the first TC position but did not fit well with experimental temperatures at the top two thermocouple positions during cooling and solidification.

In order to obtain a good fit between calculated and predicted temperatures at all three thermocouple positions, H_{Top} was arbitrarily selected, and T_{Furn} calculated using the simplifying assumption of how T_{FURN} changes with time as shown in Figure 2.10 and discussed in section 2.4. The heat transfer coefficient at the bottom of the alloy was then adjusted until the calculated temperatures closely coincided with the measured temperatures at all three thermocouple positions.

The results of this process are shown in Figure 3.31, for test 45, in which the experimental results are shown by symbols for the three indicated distances from the chill, and the calculated temperatures by the solid and dashed lines. In these calculations it was assumed that the latent heat was released linearly between the liquidus and the solidus temperatures. Best fit between the measured and the calculated values is at 33 mm. At distances farther away from the chill the calculated values above the liquidus temperature tend to be a little lower than the measured values. As the calculated temperatures approach the liquidus, the fit improves while below the liquidus, the calculated values are higher than the measured values. On average, the fit at all points for the three curves is within ±3°C while the fit at the liquidus temperature is within ±1°C. In addition, the predicted time the liquidus is reached is within 60 seconds of the experimental time.

The temperature gradient in the melt immediately ahead of the liquidus was determined from the predicted temperatures. In general, a linear gradient is calculated for distance up to 10 mm ahead of the interface. This is shown in Figure 3.32 for test 45 at two different positions, one, when the liquidus has reached a distance of 61 mm from the chill face, where TC2 is located, and two, at a distance of 76 mm from the chill where the CET occurred for test 45. At these two distances the gradient in the liquid is different and has decreases as the position of the liquidus temperature increasingly progresses away from the chill. The gradient, G_L, assumed to affect the CET, is obtained over one node length,(0.5 mm), ahead of the interface and for test 45 is shown as a function of distance in Figure 3.33. Included in Figure 3.33, are the two measured values, G_{LX}, and the

position of the CET. As expected, G_L is high at distances close to the chill face and decreases with increasing distance from the chill until finally at 76 mm reaching a value of 0°C/mm.

The predicted values of $G_L$at 33 and 61 mm from the chill are close to the measured values at those two distances. At 33 mm from the chill, the measured value of G_{LX} is below the calculated value by 0.05°C/mm while at 61 mm, the two values coincide. At the CET, the calculated G_L is 0°C/mm.

The same values for H_B, H_{Top}, and T_{Furn}, were used in the model and compared to the experimental results from tests 46 and 47 in the same way as described for test 45 with similar results. The same is not true for test 48. As can be seen in Figure 3.34 which shows the calculated and experimental temperatures at TC1 which is closest to the chill at 36 mm and for TC3 which is furthest from the chill at 93 mm, the results are very different. The experimental temperatures for TC3 are appreciably lower than the calculated temperatures by up to 20°C. At 36 mm from the chill, the discrepancy between the experimental temperatures and the calculated temperatures is not as large and shows a reversal at 300 seconds. The experimental temperatures are higher than the calculated temperatures at the start but as the temperatures decrease the experimental temperatures become lower than the calculated temperatures. The calculated and experimental temperatures for TC2 at 61 mm from the chill are not shown for sake of clarity.

In order to bring the predicted temperatures in line with the experimental temperatures, it was necessary to increase the heat loss from the top of the melt by changing T_{FURN} in equation 2.5 until a reasonable fit was again obtained between the calculated and the experimental temperatures. The fit between the experimental and the

calculated temperatures shown in Figure 3.35 was obtained using the same constant heat transfer coefficient at the bottom used for test 45, 46 and 47. These results show that the cooling curves are very sensitive to the heat loss from the top of the melt.

The calculated temperature gradient in the melt ahead of the liquidus, G_L, from test 48 also started high at distances close to the chill face but decreases much more rapidly than G_L for test 45 as shown in Figure 3.36. The measured values, G_{LX}, for test 48, also shown in Figure 3.36, are also much lower than those for test 45, but, they still agree with the predicted values.

The position of the CET in test 48 was observed to occur at 60 mm from the chill where G_L is calculated to be less than 0.01°C/mm.

Mathematical modelling was done for every experiment with the furnace off during cooling and solidification. The top and bottom boundary conditions were adjusted as discussed above in order to obtain a good fit between predicted and experimental temperatures at all three thermocouple positions. The calculated temperature gradient, G_L, and growth velocity, V, at the CET are listed in Table 3.16 along with the top and bottom boundary conditions and the position of the CET. The measured temperature gradients, G_{LX}, are not listed in Table 3.16 because in general, the measured values are taken at positions not coincident with the CET. In most cases, the calculated value of G_L at the CET is very small, 0.02°C/mm. The exceptions are tests 42 to 44 where the calculated G_L was higher and varied from 0.04 to 0.10°C/mm. In test 40, the structure was completely equiaxed, therefore no CET occurred and no G_L calculated.

The growth velocities, V, at the CET are calculated using equation 2.28 in section 2.4.9. The position of the interface, x , was plotted against the $\sqrt{time}$ to give a slope B,

TABLE 3.16
PREDICTED VALUES OF G_L AND V AT THE CET
FOR Pb-1.5%Sn

TEST N°	CHILL ASSEMBLY	HTC J/cm²-°C-sec	ΔT T_{Pure} - T_{TOP} °C		CET mm	G_L °C/mm	V mm/sec
			START	FINISH			
33	CA1	0.0105	10	-7.5	60	0.02	0.05
34	CA1	0.0090	10	-7.5	67	<0.01	0.07
35	CA2	0.0105	0	-5.0	71	<0.01	0.07
36	CA2	0.0105	0	-7.5	62	0.01	0.06
37	CA2	0.0105	0	-7.5	67	<0.01	0.07
38	CA2	0.0105	0	-7.5	72	<0.01	0.07
39	CA2	0.0105	0	-7.5	70	<0.01	0.06
40	CA3	0.0080	0	-7.5	-	-	-
41	CA3	0.0080	0	-7.5	51	0.02	0.08
42	CA3	0.0095	0	-7.5	44	0.04	0.08
43	CA3	0.0095	0	-7.5	47	0.09	0.08
44	CA3	0.0095	0	-7.5	39	0.10	0.09
45	CA1	0.0100	20	-5.0	76	<0.01	0.06
46	CA1	0.0100	15	-7.5	91	0	0.06
47	CA1	0.0105	20	-5.0	76	<0.01	0.06
48	CA1	0.0105	0	-5.0	60	<0.01	0.08

H_{Top} = 0.02 J/cm²-°C-sec
HTC LISTED AT CHILL FACE
FURNACE OFF DURING COOLING

with B ranging in values from a low of 2.7 mm/sec$^{1/2}$ to a high of 5.1 mm/sec$^{1/2}$. The average value of B is 4.2 mm/sec$^{1/2}$. The growth velocity of the interface at the CET is calculated based on the slope B, and the time it took for the interface to reach the CET. As seen in Table 3.16, the velocities are relatively constant varying between 0.05 and 0.08 mm/sec with an average of 0.07 mm/sec.

3.6.2 LATENT HEAT

As described in section 2.4.6, the latent heat release in the calculations can be based on a linear release between the liquidus and solidus temperatures, or it can be released in a non-linear fashion using either the Scheil equation, or the Lever rule to calculate the fraction solidified as a function of temperature. All three methods were used to produce the cooling curves at 33, 61, and 93 mm from the chill for test 45 as shown in Figure 3.37, 3.38 and 3.39 respectively. The cooling curves in Figure 3.37 are observed to be superimposed in the liquid as expected. Below the liquidus, the Lever rule gives slightly higher temperatures than the Scheil and linear curves which are still superimposed. At 61 mm from the chill, Figure 3.38, similar results to those at 33 mm are observed. At 93 mm, Figure 3.39, the cooling curves for all three methods are virtually identical.

The effect of changing the method to release latent heat on the temperature gradient, G_L, was examined using the calculated temperatures shown in Figures 3.37 to 3.39. The calculated values of G_L are shown in Figure 3.40 as a function of distance from the chill. The difference between the procedures is observed to be very small, the Lever rule giving slightly lower values than the other two.

3.6.3 Pb-3%Sn and Pb-6%Sn

The effect of changing the method to release latent heat on Pb-6%Sn, (test 57), at three distances from the chill is shown in Figures 3.41 to 3.43 inclusive. Similar to the Pb-1.5%Sn alloy, the calculated difference between the three methods is small with the largest difference at 36 mm from the chill face. At this position, the Lever rule

temperatures are higher than the linear values which are higher than the Scheil values. All of the calculated temperatures are higher than the observed values, with the Scheil values being the closest. At 66 mm from the chill, Figure 3.42, the temperatures using the linear method are below the other two, with all the calculated values being higher than the observed values at decreasing temperatures below the liquidus. At 93 mm, the three cooling curves are effectively superimposed and coincident with the observed values along the liquidus line. The results for Pb-3%Sn are similar to those for the Pb-6%Sn alloy.

3.7 Sn-10%Pb

Cooling curves are calculated for the Sn-10%Pb alloy, (test 60), using the phase diagram temperatures given in section 2.4.8. The same boundary condition values are applied at the bottom for the Pb-1.5%Sn alloy. At the top surface of the melt, q was taken as zero. The results for the linear release of latent heat at 34, 64 and 93 mm from the chill face are shown by the solid lines in Figures 3.44 to 3.46 respectively. The experimental results are indicated by the square symbol in the figures. In general, there is poor fit between the calculated and experimental values. Above the liquidus, there is good fit at 34 mm but poor fit at 64 and 93 mm. The calculated values at the top two TC positions are lower than the experimental temperatures. The experimental cooling curves at all three positions deviate substantially from the calculated cooling curves after the start of solidification. The experimental points show supercooling followed by a horizontal temperature plateau at all three thermocouple positions. The calculated curves show no supercooling or horizontal temperature plateau but show continuous cooling which

results in a large difference between the calculated and measured temperatures.

A comparison is made in Figure 3.47 between the calculated cooling curves using all three methods to release latent heat for a distance of 93 mm from the chill face. At temperatures well above the liquidus temperature, the three calculated cooling curves are very similar and are all below the experimental results. As the liquidus temperature is approached, the cooling curve from the linear method to release latent heat diverges from the curves produced using the Scheil equation and the Lever rule. The linear method produces temperature below those produced by the other two methods. At the liquidus temperature, the curves from the Scheil and the Lever rule exhibit a brief horizontal temperature plateau but the calculated results are still lower than the experimental results.

In contrast to the Pb-Sn results the manner of latent heat release influences the temperature gradient, G_L for the Sn-10%Pb alloy. This is shown in Figure 3.48 where G_L is shown as a function of distance from the chill for the three methods. Releasing the latent heat using the Scheil equation and Lever rule give the same calculated values of G_L, which are significantly lower than the calculated values using the linear procedure for distances up to 100 mm from the chill face.

The measured values of G_{LX} taken from the cooling curves for test 60 do not show the same relationship with distance from the chill as the calculated values. For example, the experimental point at 34 mm from the chill is between the two calculated curves at 0.14°C/mm, while the experimental point at 64 mm from the chill is well above all three calculated curves at 0.10°C/mm.

The CET in test 60 occurred at 45 mm from the chill face, see Figure 3.48. At this position, the calculated values of G_L for the three procedures to release latent heat are

listed in Table 3.17. The linear model gives a value for G_L of 0.12°C/mm, which agrees with the interpolated value of 0.125°C/mm assuming a linear temperature gradient between the thermocouples. The calculated value of G_L for the Scheil and the Lever rule procedures was 0.06°C/mm, significantly lower than the linear procedure and the estimated measured value.

TABLE 3.17
G_L AS CALCULATED AT 45 mm FROM CHILL FACE FOR TEST 60 USING THE THREE PROCEDURES TO RELEASE LATENT HEAT

CET POSITION mm	LINEAR MODEL G_L °C/mm	SCHEIL MODEL G_L °C/mm	LEVER MODEL G_L °C/mm	LINEAR APPROXIMATION G_{LX} °C/mm
45	0.12	0.06	0.06	0.125

3.8 HEAT FLUX AT BOTTOM OF MOULD

The mathematical heat transfer model uses as a bottom boundary condition a constant heat transfer coefficient, H_B, equal to 0.0105 J/cm^2-°C-sec and an ambient temperature of 25°C to solve the transient heat conduction equation, (2.1). An alternative method was attempted which utilized the temperature measurements from the two TC's in the chill assembly described in section 2.3 and illustrated in Figure 2.4. The temperature measurements were recorded along with those temperatures in the melt with the A/D board. Since the distance between thermocouples is known as well as the thermal conductivity of copper, and stainless steel, the temperature difference, ΔT_{CA}, between the

TC in the top disk, and the TC in the bottom disk could theoretically be used to determine the heat flux, $\dot{q}$, from the bottom of the mould and through the chill assembly if the following assumptions are valid:

1. There is intimate contact at all surfaces.
2. Heat flow is unidirectional.
3. Heat flow through the copper disk with holes is evenly distributed.
4. The thermocouples are positioned exactly in the middle of the disk.
5. Steady state exists.
6. The furnace does not affect the heat flux in the chill assembly.

The heat flux is calculated through the chill assembly, CA1, using the following equation:

$$\dot{q} = \frac{\Delta T_{CA}}{\frac{2\Delta x}{k_{Cu}A_{Cu}} + \frac{\Delta x}{k_{Cu}A_{eff}}} \tag{2.29}$$

where:

$\dot{q}$ = Heat flux through the chill assembly.

ΔT_{CA} = The temperature difference between the top and bottom solid copper disks.

Δx = The thickness of the copper disks.

k_{Cu} = The thermal conductivity of copper.

A_{Cu} = Cross sectional area of the solid copper disks.

A_{eff} = Effective cross sectional area of copper disk with holes.

Measurements of the temperature difference with time across the three chill assemblies were made under normal test conditions. The results are shown in Figure 3.49. The temperature difference ΔT is observed to increase sharply when the chill is put into

contact with the bottom of the mould, reach a maximum, and then slowly decrease with time for the three assemblies. As expected, the temperature difference at a given time increases with an increased thickness of stainless steel from CA1 to CA3.

A comparison of the calculated melt temperatures using equation 2.29 as the bottom boundary condition and the values of ΔT as a function of time from test 45 and the experimental melt temperatures is made in Figure 3.50. The cooling curve at 33 mm from the chill face determined in this way is shown as a solid line while the corresponding experimental values are indicated by the points. The calculated results shown by the solid line are lower than the experimental results right from the start. After 1020 seconds of cooling, the calculated results are 50°C below the experimental values. Similar results between calculated and experimental values at 61 and 93 mm were obtained but are not shown.

The results clearly indicate that the measured ΔT values cannot be used to establish the heat flux from the bottom of the mould. This is most likely due to the inapplicability of assumption 1 regarding intimate contact, and assumption 3 regarding heat flow through the copper disk with holes. Heat flow through this disk may be more complex than assumed making the true effective area for heat flow unknown.

3.9 SENSITIVITY ANALYSIS

The results shown in section 3.6.1 for the directional solidification of Pb-1.5%Sn were obtained using a node size of 0.5 mm and a time step of 0.5 seconds. Increasing the node size to 1.0 mm and the time step to 1.0 seconds, did not significantly change the calculated temperatures or temperature gradients.

Thermophysical parameters such as k, ρ, and C_p had to be assumed for the Pb-Sn alloys and the Sn-10%Pb alloy as this data is not readily available in the literature. It was assumed that the values for k,ρ, C_p, for the alloy could be determined from the values for Pb and Sn on the basis of the weighted averages of the Pb and Sn in the alloy. Therefore, it is worthwhile to perform a sensitivity analysis on these parameters to see their influence on the results of the model.

There is thermal conductivity data for Pb-10%Sn at 54°C which can be used to provide some basis for the error encountered in the model using the weighted averages assumption. At 54°C, the thermal conductivity of Pb-10%Sn is reported as 0.360 W/cm-K[43]. Using the weighted averages method, and values for Pb as 0.352 W/cm-K, and for Sn as 0.742 W/cm-K, the thermal conductivity of Pb-10%Sn at 54°C is 0.415 W/cm-K, 15% higher than the reported value. Thus, the sensitivity analysis is performed with this error limit. The values of G_L as a function of distance from the chill were calculated using three values for the thermal conductivity, the original k, 0.85k and 1.15k giving the results shown in Figure 3.51. The largest effect of k on G_L is in the region between 10 and 40 mm from the chill. Decreasing k by 15% increases G_L in this region by up to 0.1°C/mm, while increasing k by 15% decreases G_L by up to 0.07°C/mm. The values of G_L for the three values of k all converge to 0°C/mm at approximately 76 mm from the chill which is in the vicinity of the CET for this particular test. Therefore, for Pb-1.5%Sn alloys, a 15% error does not significantly affect the results at the CET.

Figure 3.1

Cast structure of test 1

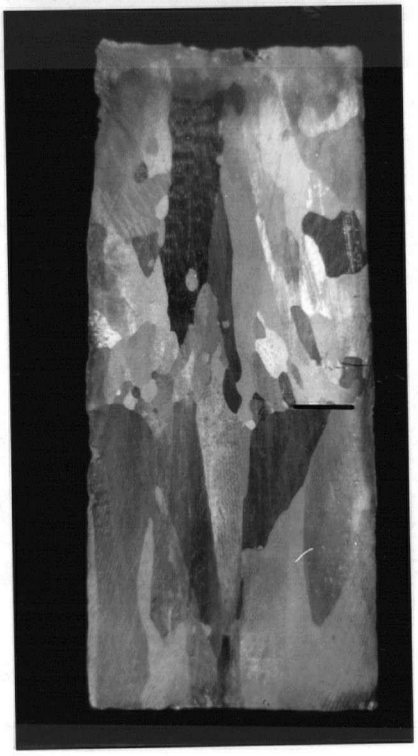

Figure 3.2

Cast structure of test 2

Figure 3.3

Cast structure of test 4

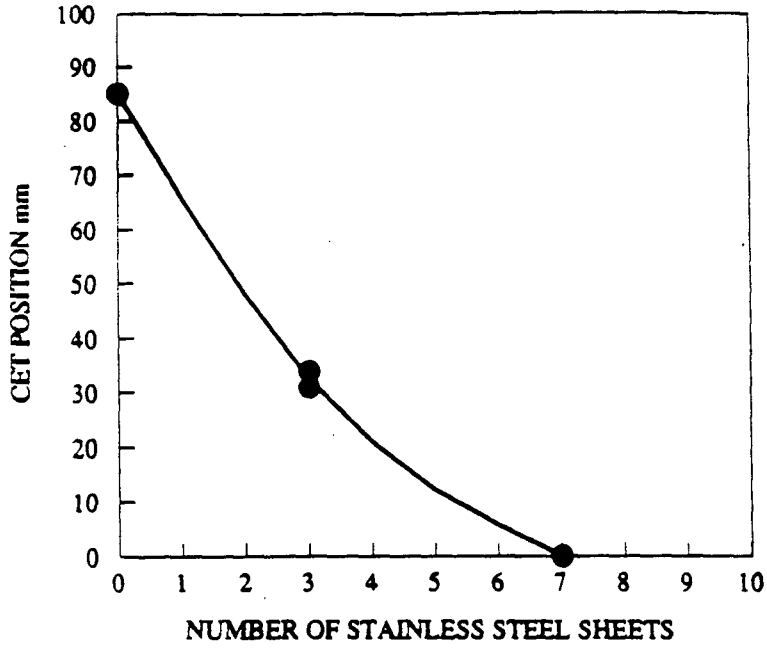

Figure 3.4

The position of the CET as a function of the number of stainless steel sheets.

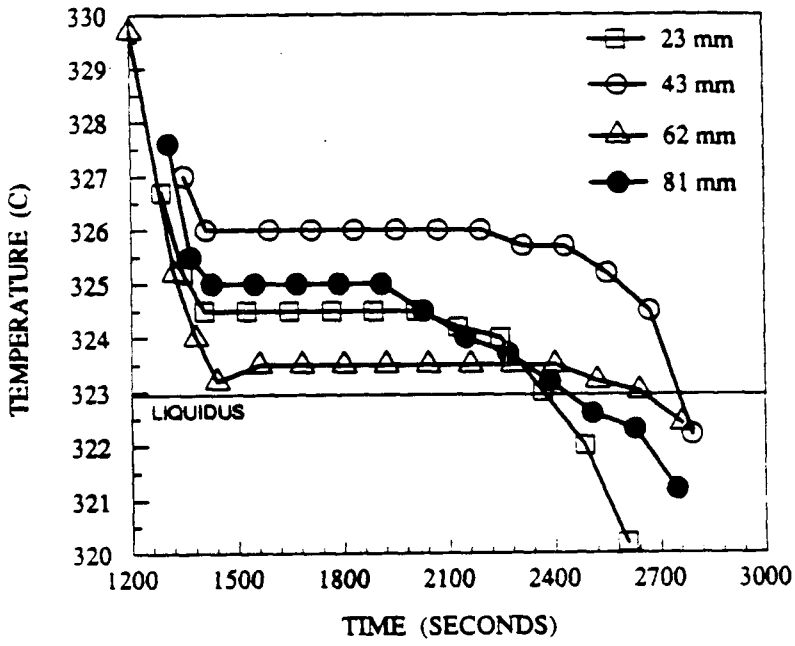

Figure 3.5

Cooling curves from test 1 at the indicated distances from the chill

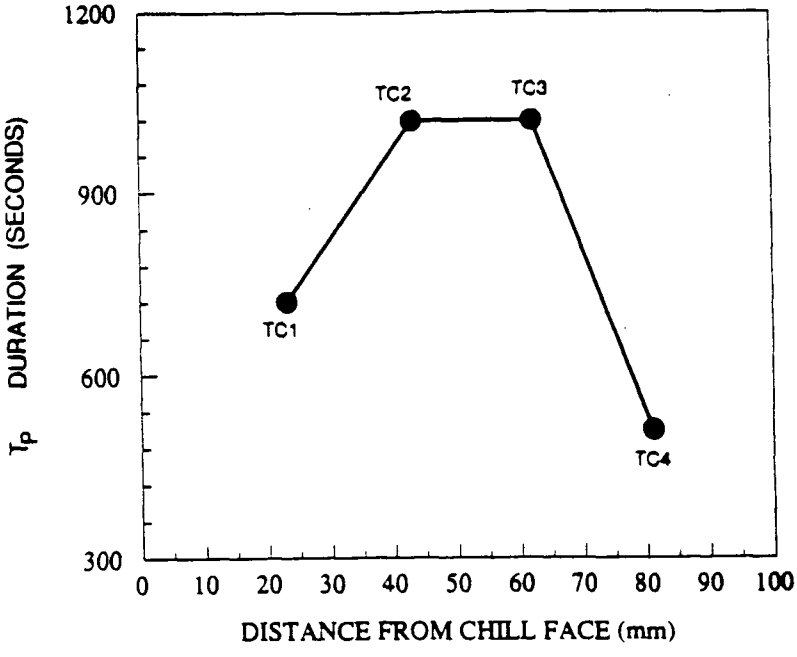

Figure 3.6

The duration of the plateau as a function of distance from the chill in test 1

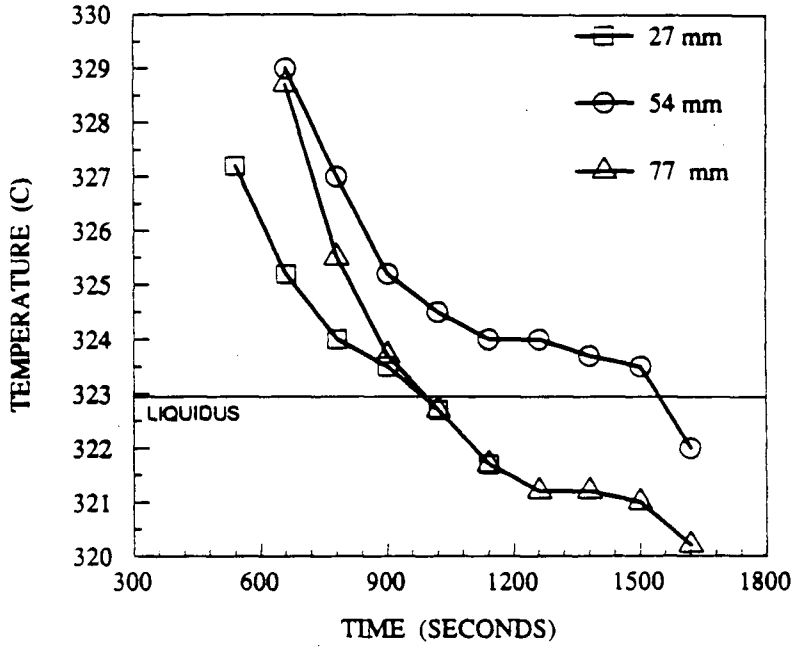

Figure 3.7

Cooling curves from test 2 at the indicated distance from the chill

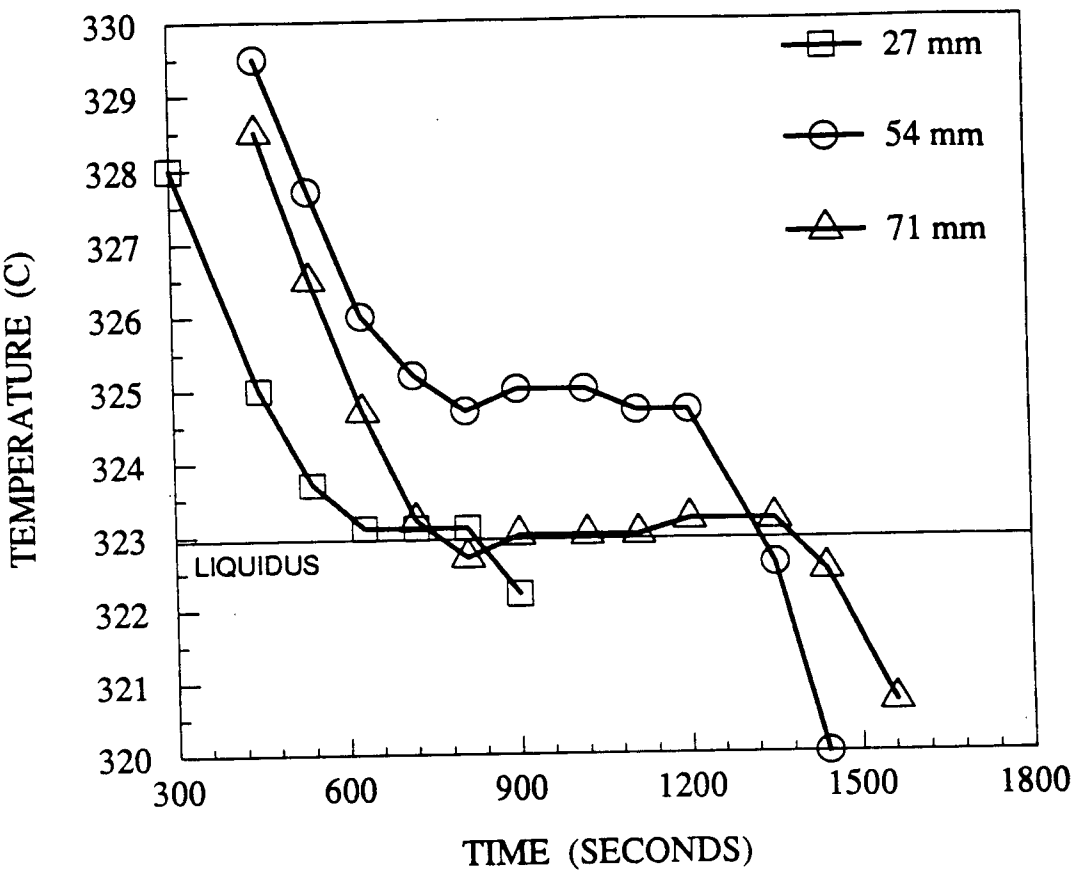

Figure 3.8

Cooling curves from test 3 at the indicated distances from the chill

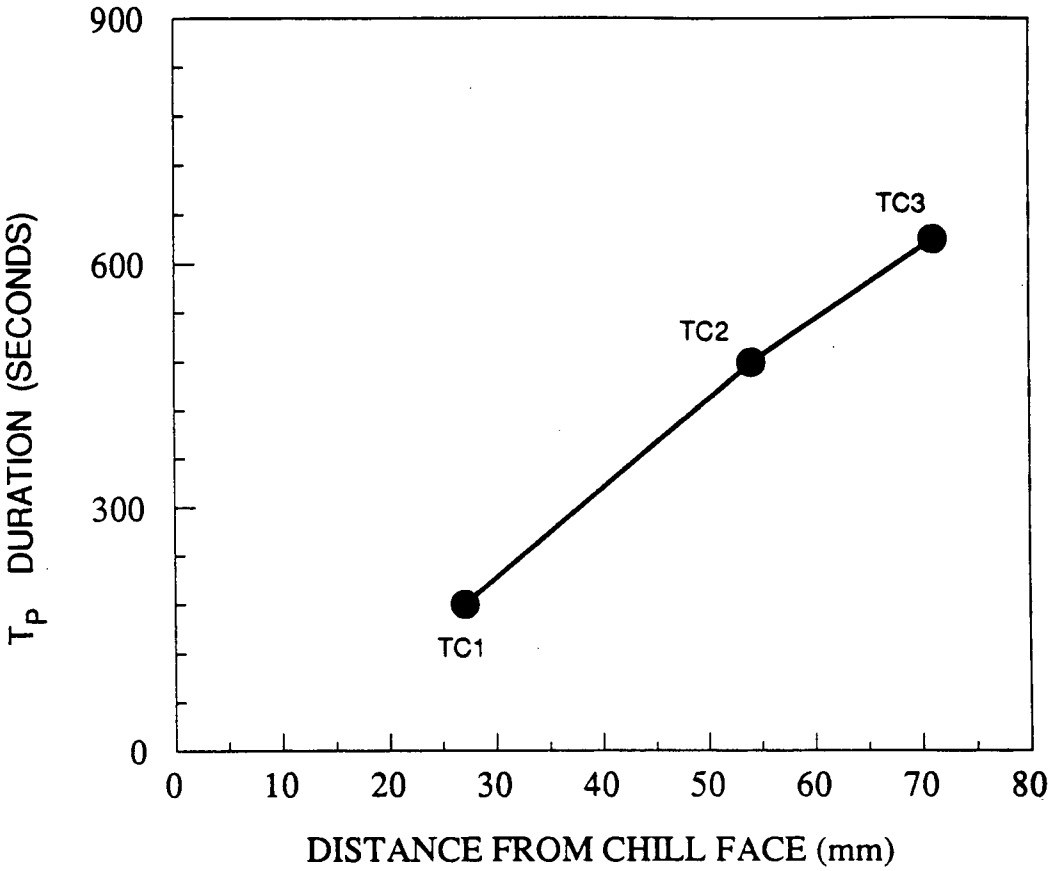

Figure 3.9

The duration of the plateau as a function of distance from the chill in test 3

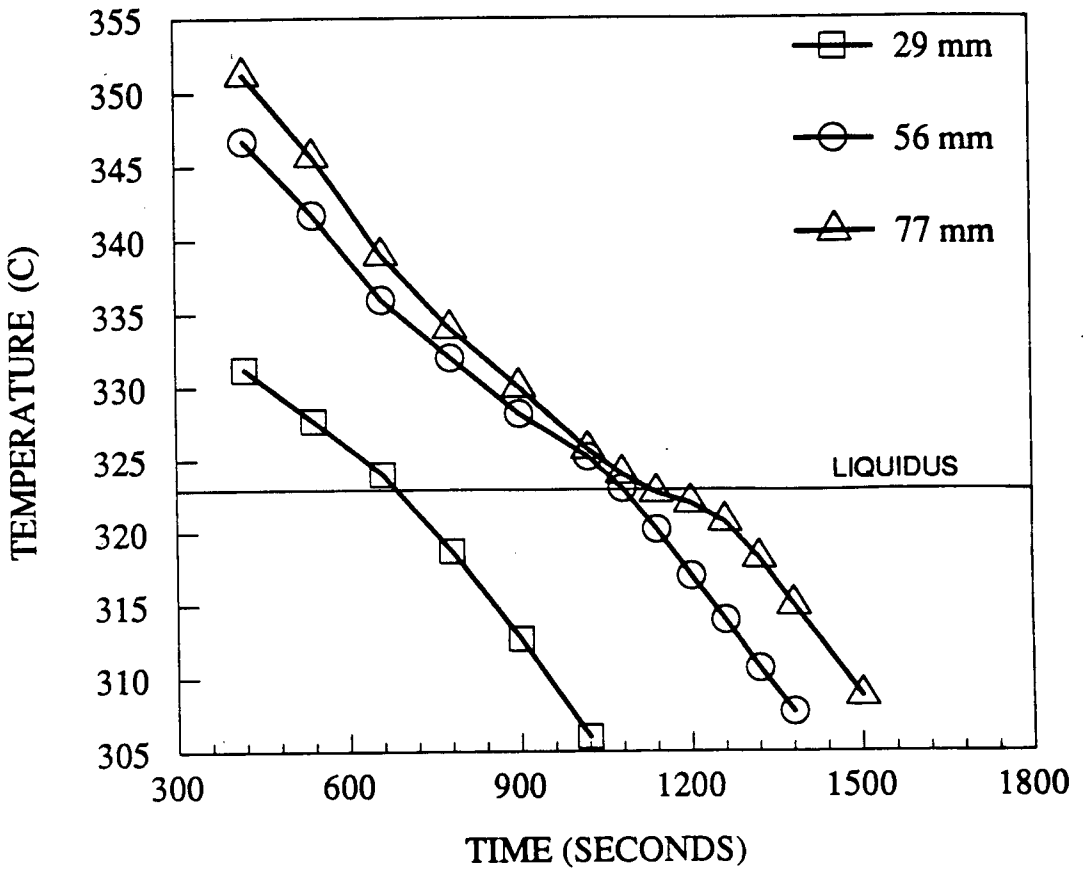

Figure 3.10

Cooling curves from test 4 at the indicated distances from the chill

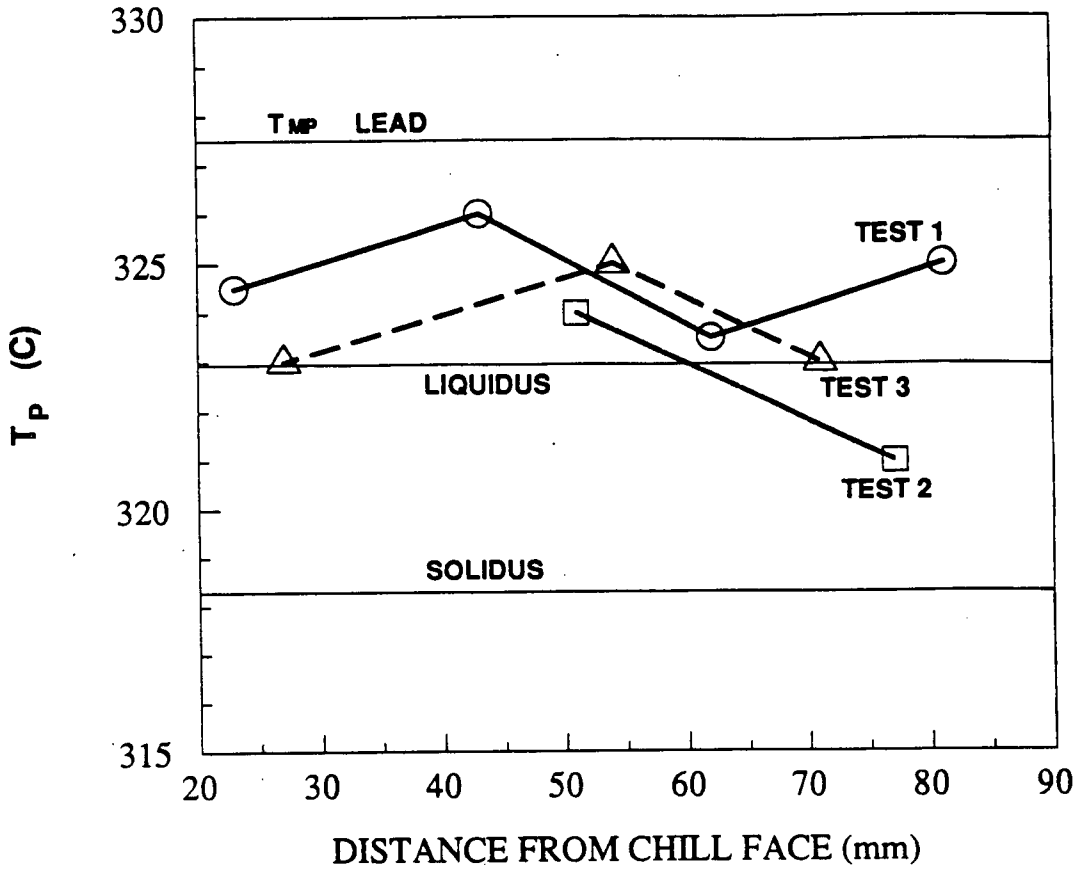

Figure 3.11

The plateau temperature from tests 1, 2, and 3 as a function of distance from the chill

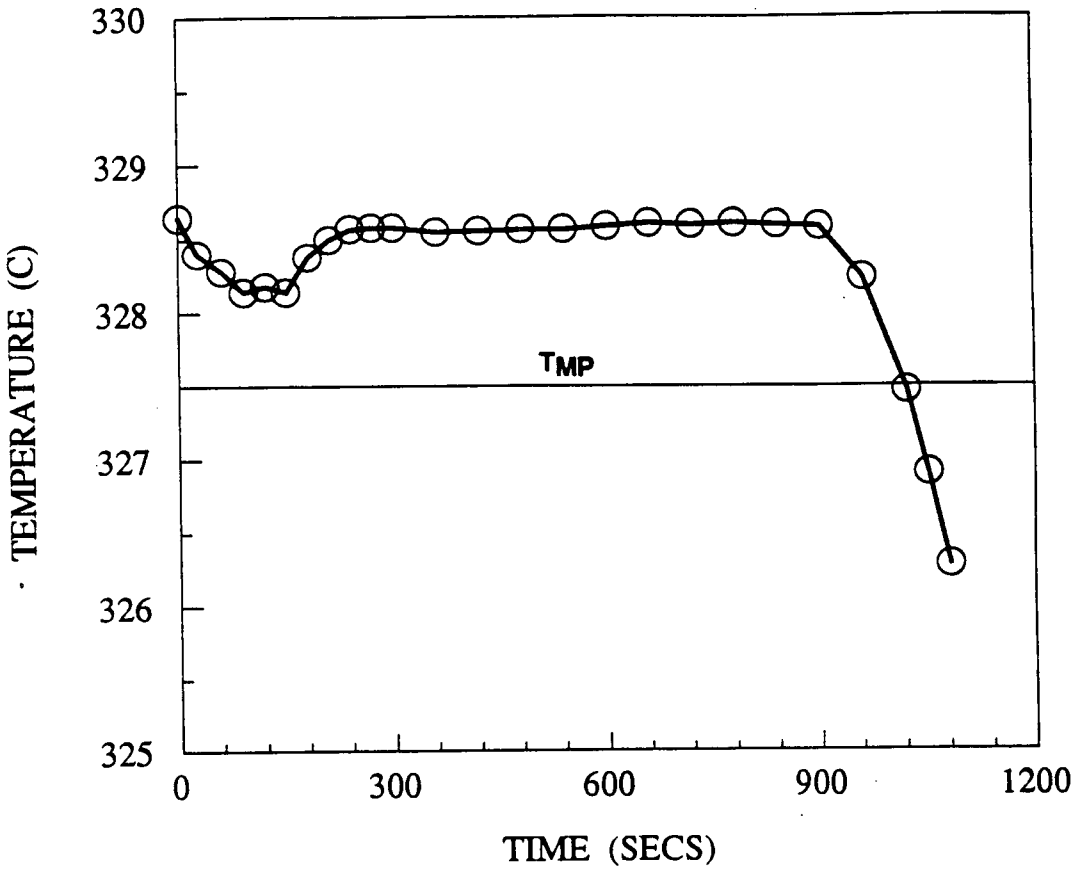

Figure 3.12

A typical cooling curve for TC1 using 99.999%Pb

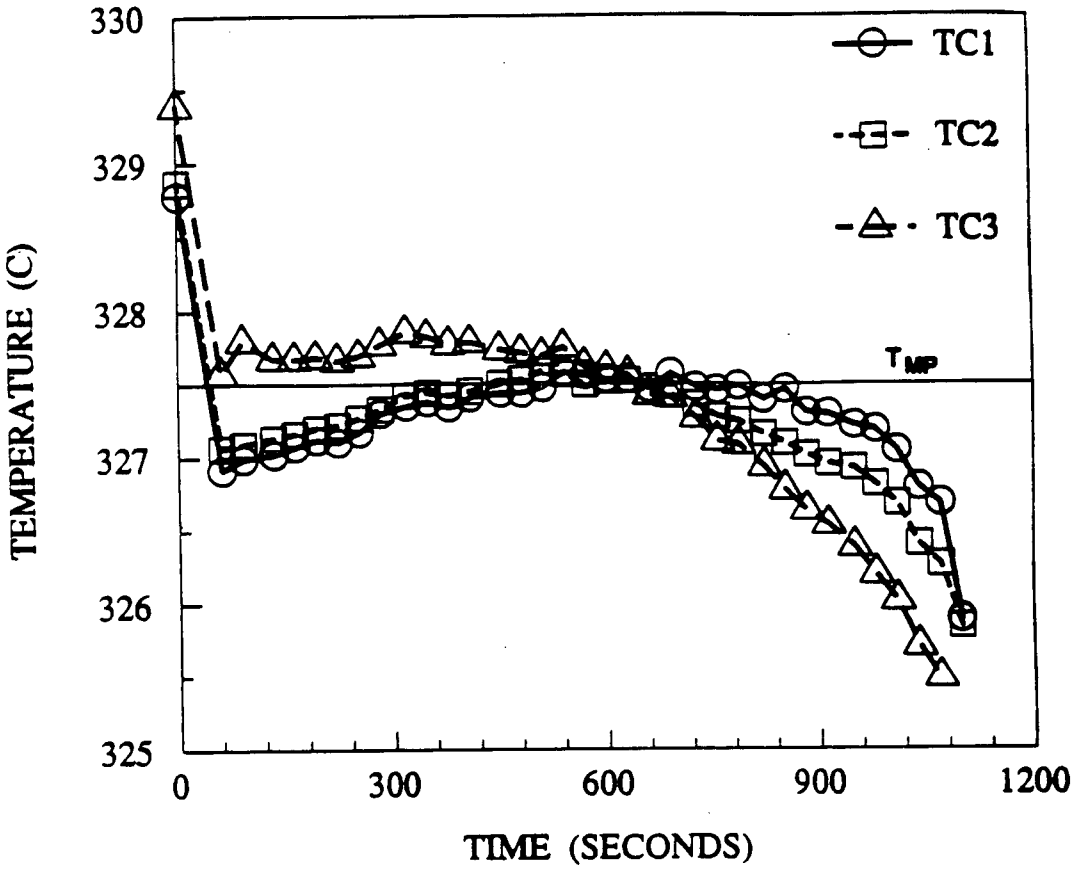

Figure 3.13

Cooling curves from TC1, TC2, and TC3 using 99.99%Pb

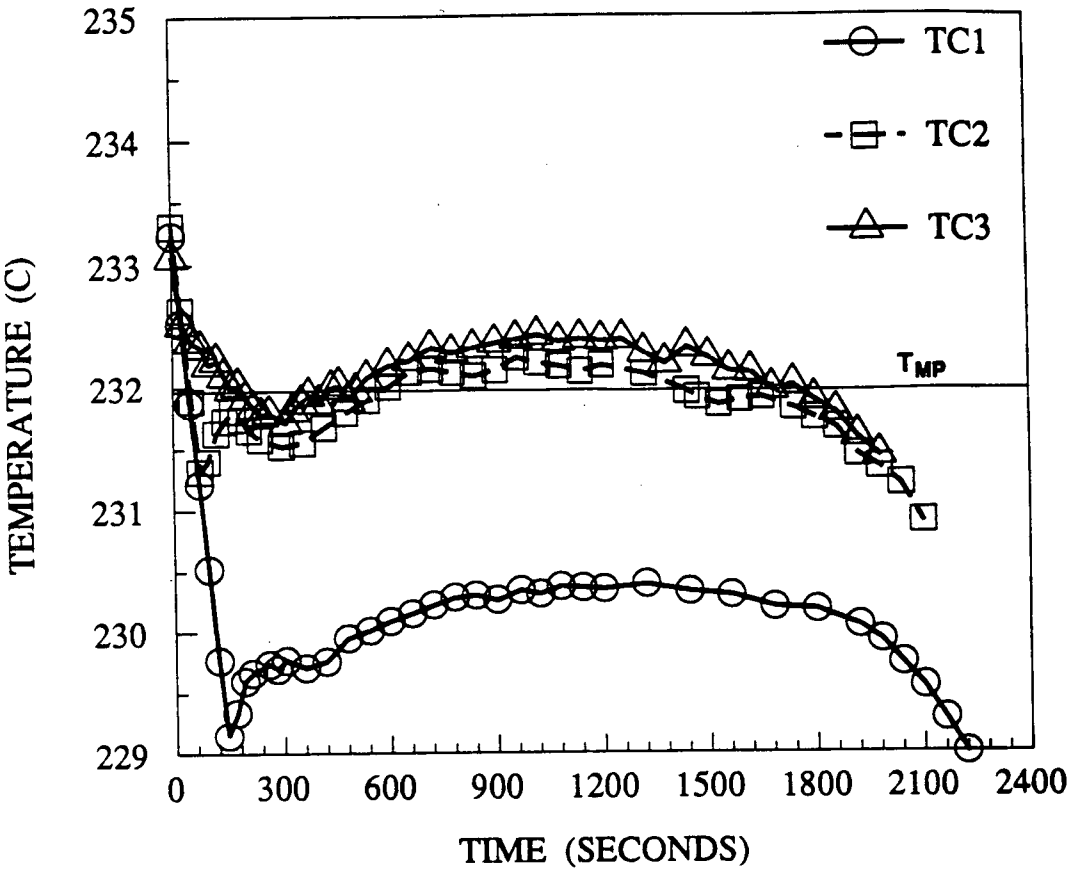

Figure 3.14

Cooling curves from TC1, TC2, and TC3 using 99.89%Sn

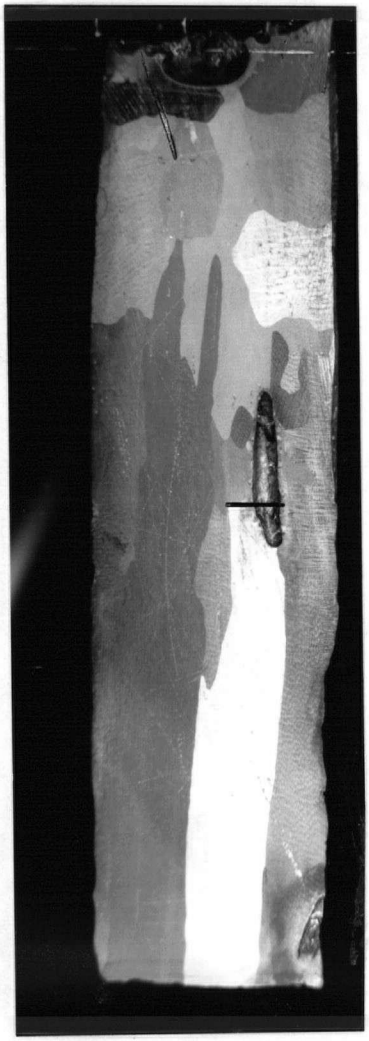

(a)

(b)

Figure 3.15

(a) Cast structure of test 34 using chill assembly CA1

(b) Cast structure of test 38 using chill assembly CA2

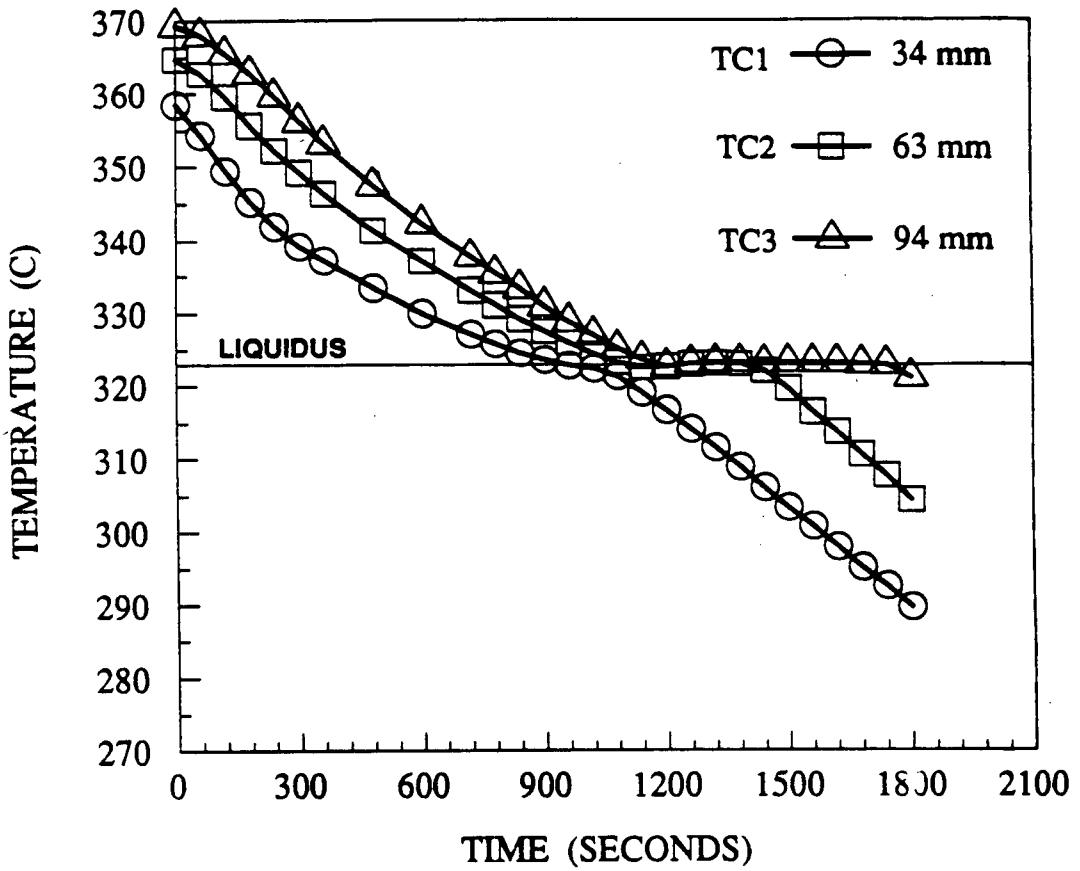

Figure 3.16

Cooling curves for test 34 at the indicated distances from the chill

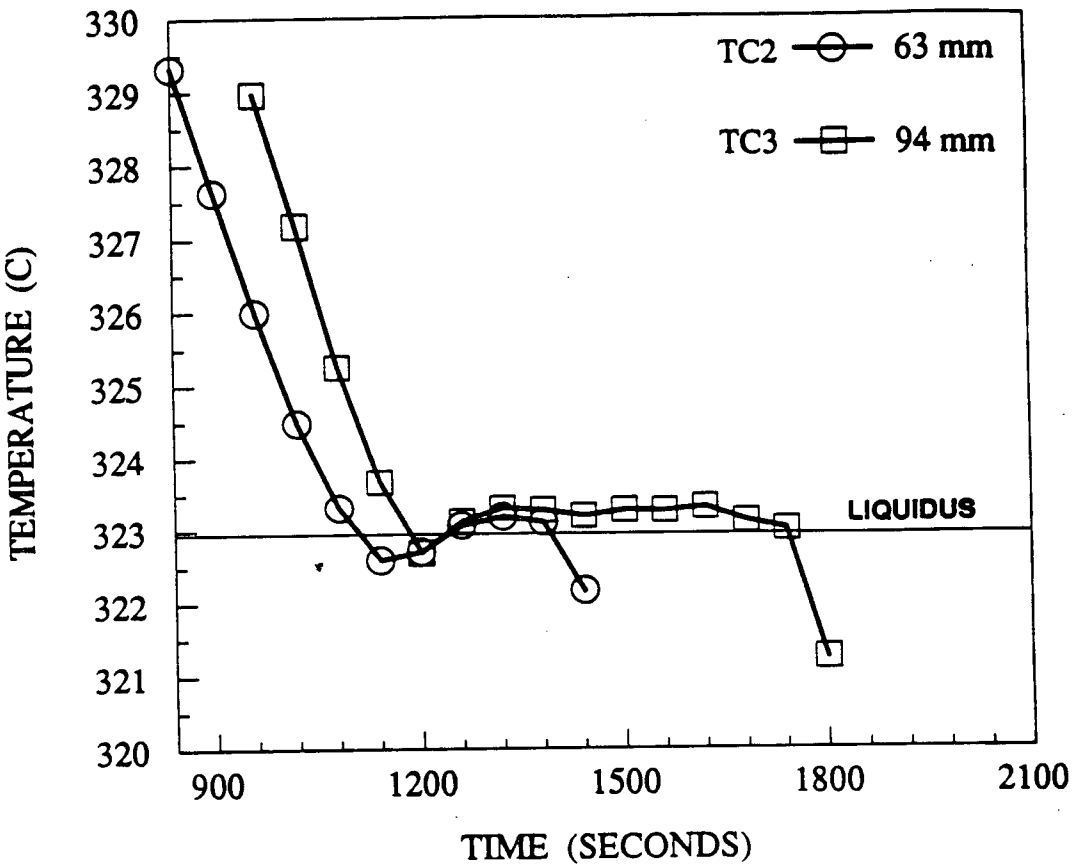

Figure 3.17

The plateau region for test 34 at the top two TC positions at the distance indicated

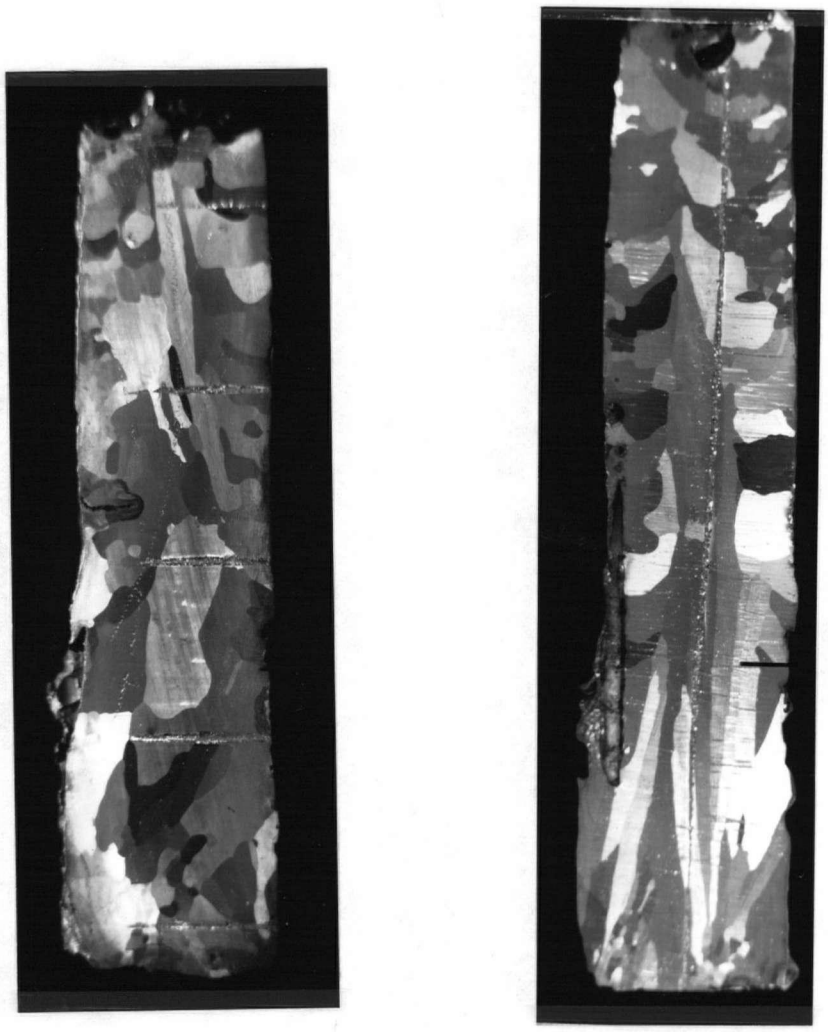

(a) (b)

Figure 3.18

(a) Cast structure of test 40 using chill assembly CA3

(b) Cast structure of test 42 using chill assembly CA3

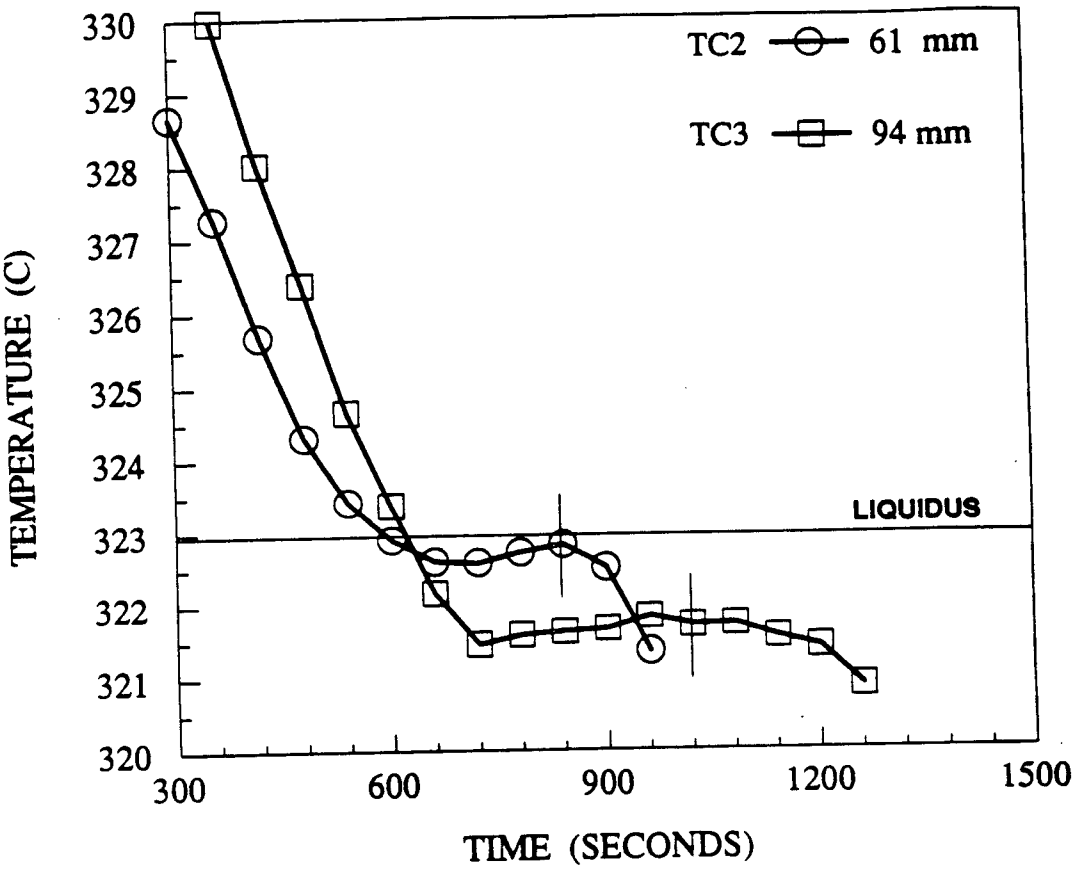

Figure 3.19

Cooling curves for test 43 at the plateau region at the indicated distances from the chill

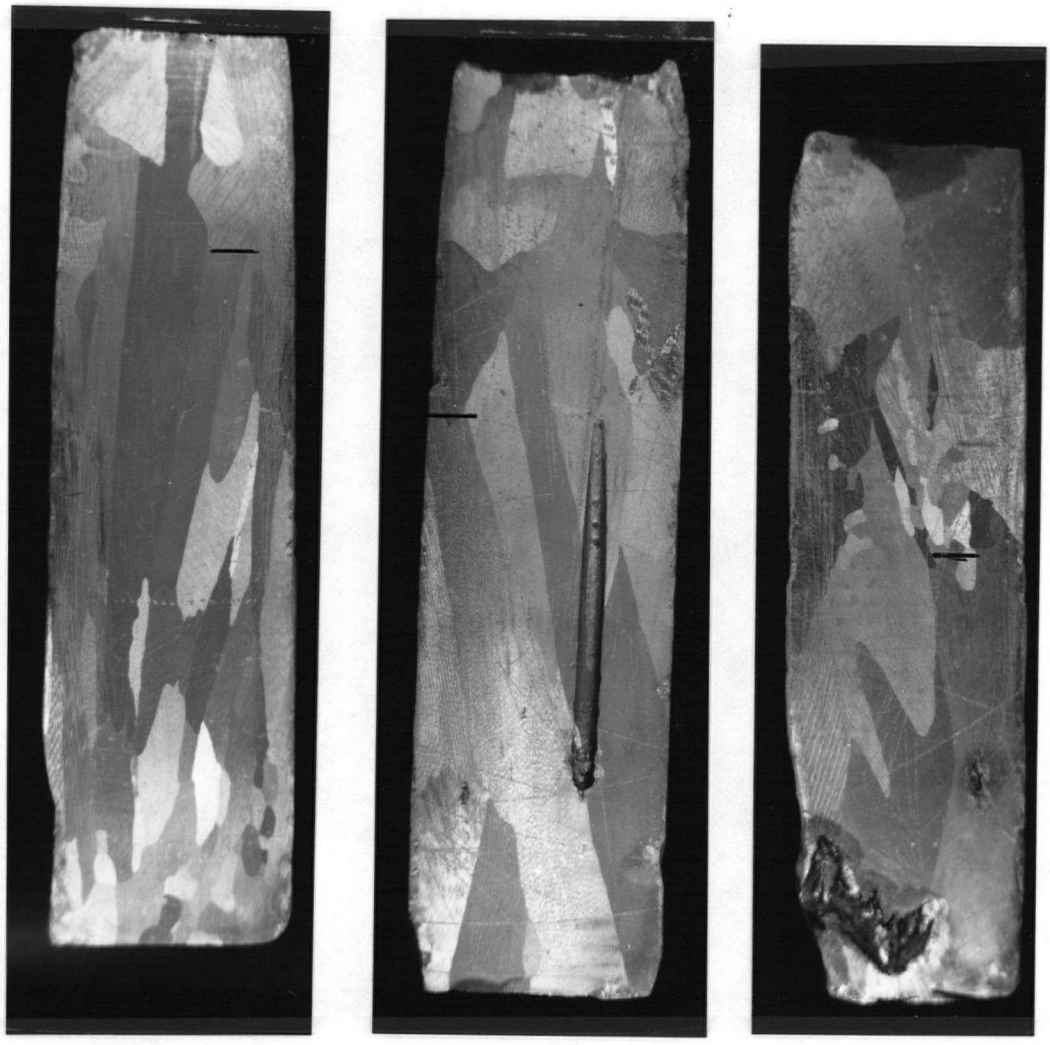

(a) (b) (c)

Figure 3.20

(a) Cast structure of test 46 using chill assembly CA1 and top of melt insulated

(b) Cast structure of test 47 using chill assembly CA1 and top of melt insulated

(c) Cast structure of test 48 using chill assembly CA1 and top of melt insulated

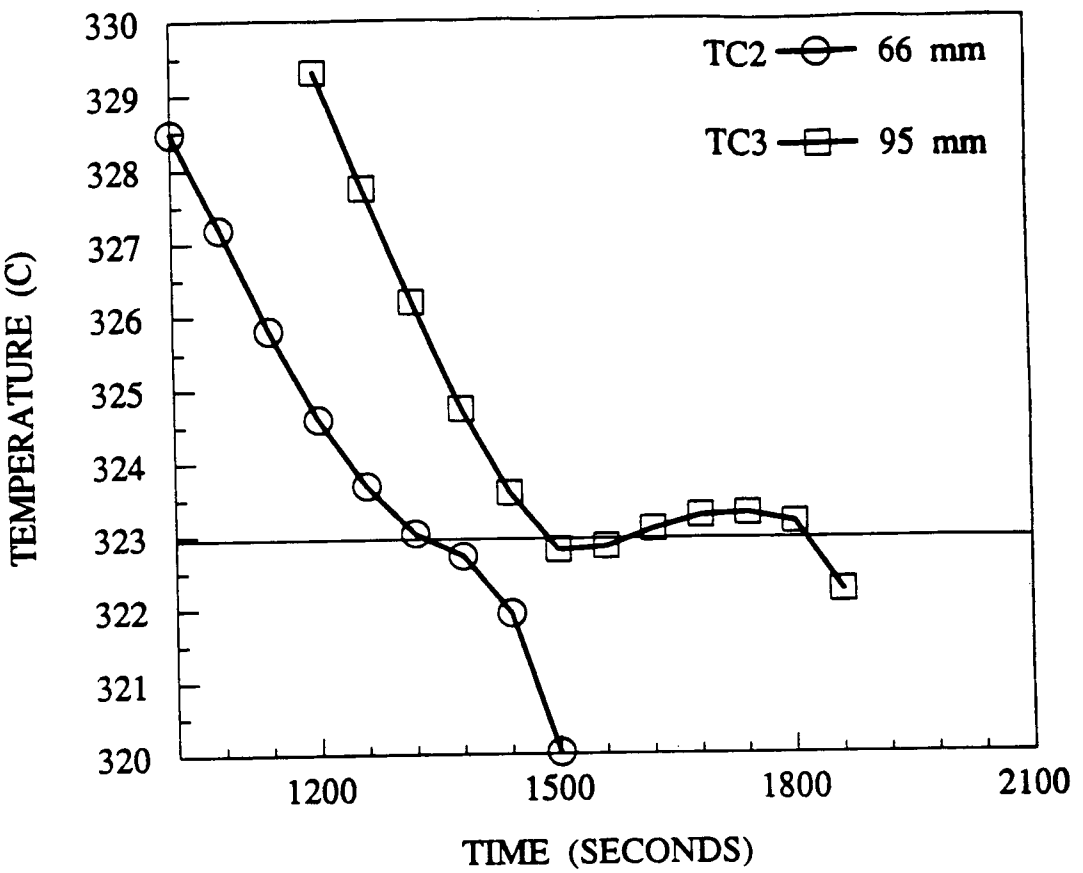

Figure 3.21

Cooling curves for test 47 at the plateau region at the indicated distances from the chill

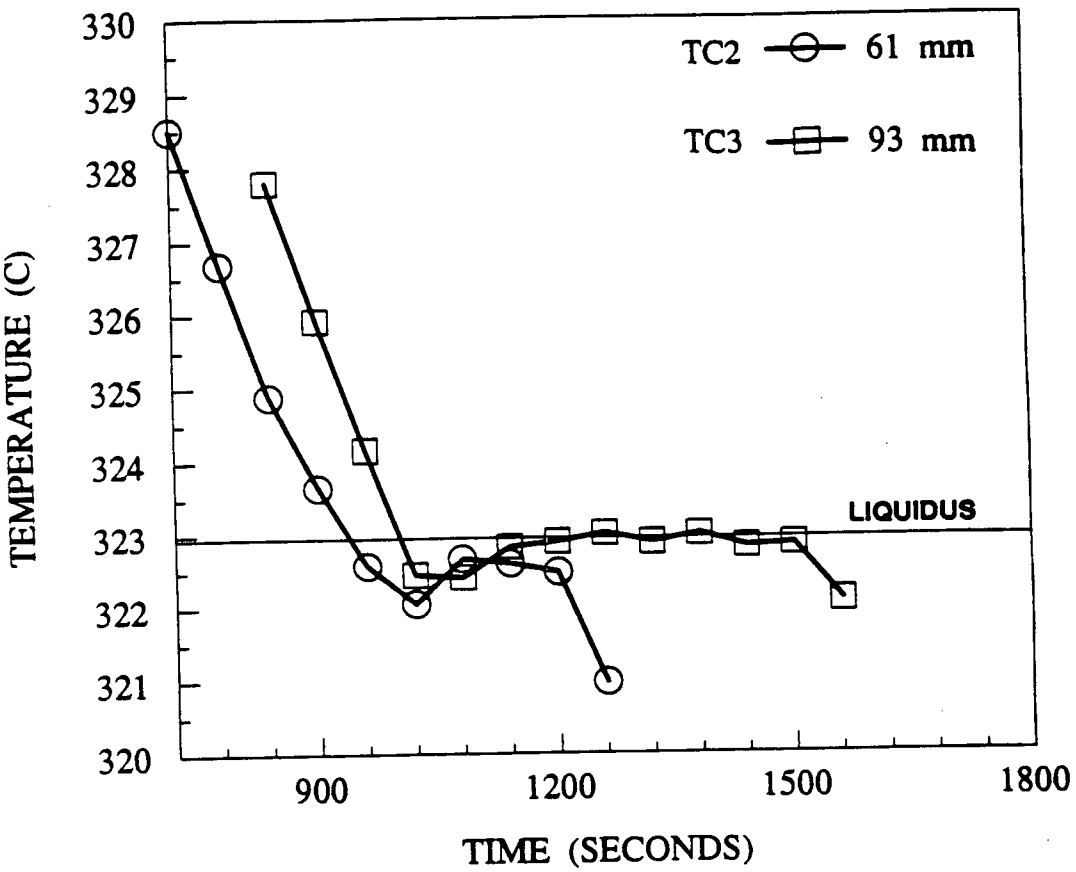

Figure 3.22

Cooling curves for test 48 at the plateau region at the indicated distances from the chill

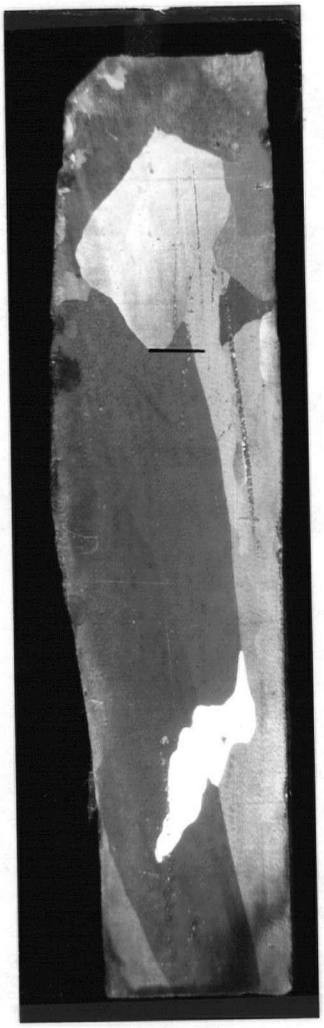

Figure 3.23

Cast structure of test 54 using chill assembly CA1 and the furnace power on during cooling, I=3.0 Amps.

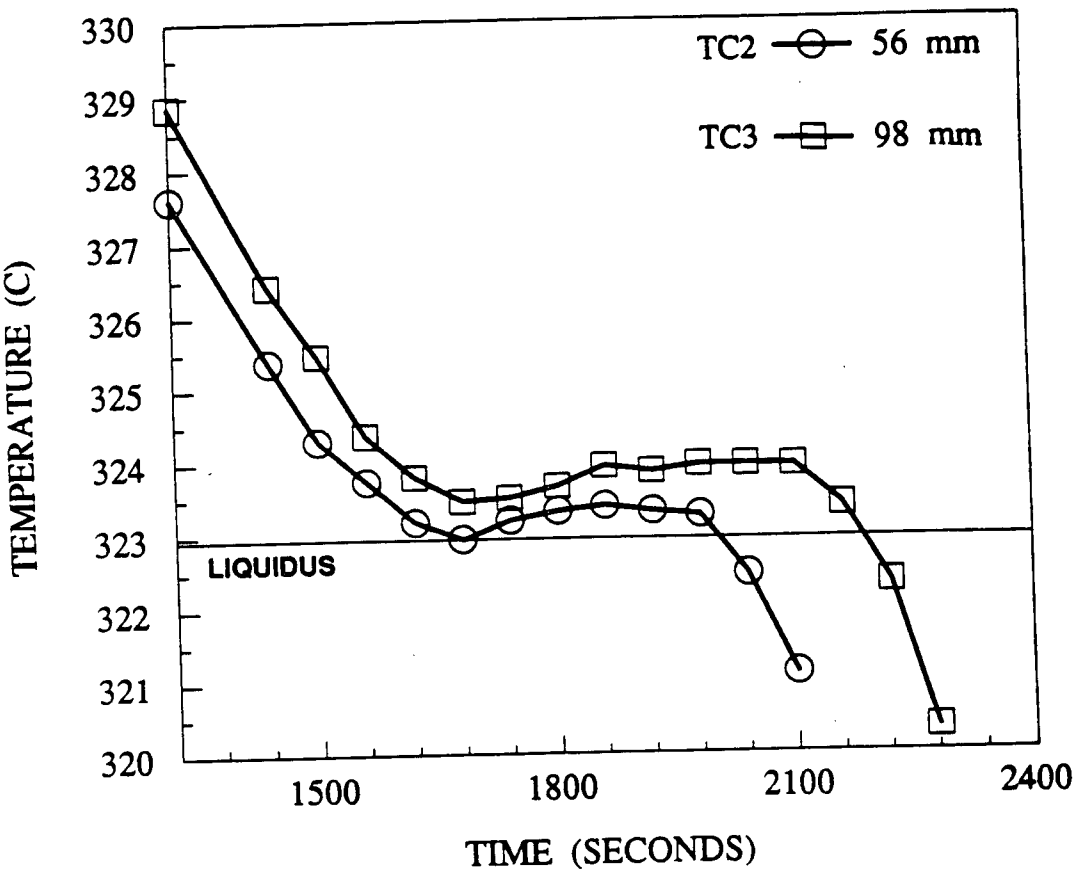

Figure 3.24

Cooling curves for test 54 at the plateau region at the indicated distances from the chill; cooling occurred with I=3.0 amps to the furnace

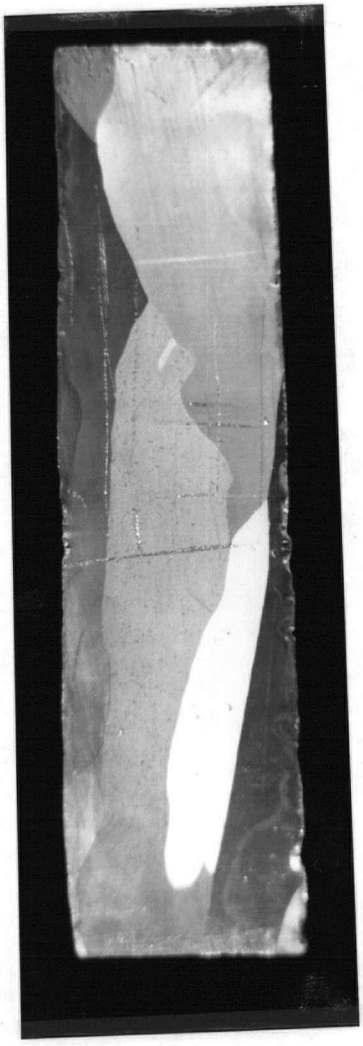

Figure 3.25

Cast structure of test 55 using chill assembly CA1 and the furnace power on during cooling; I=5.0 Amps.

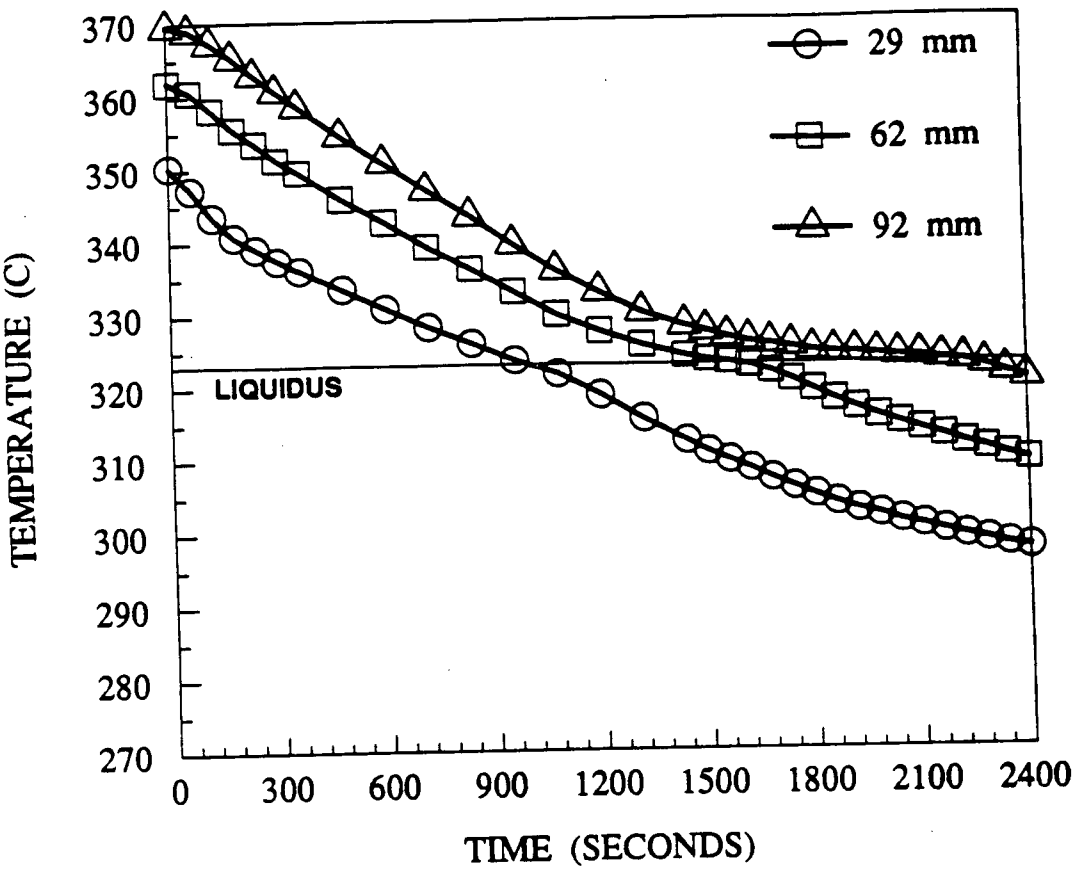

Figure 3.26

Cooling curves for test 55 at the indicated distances from the chill

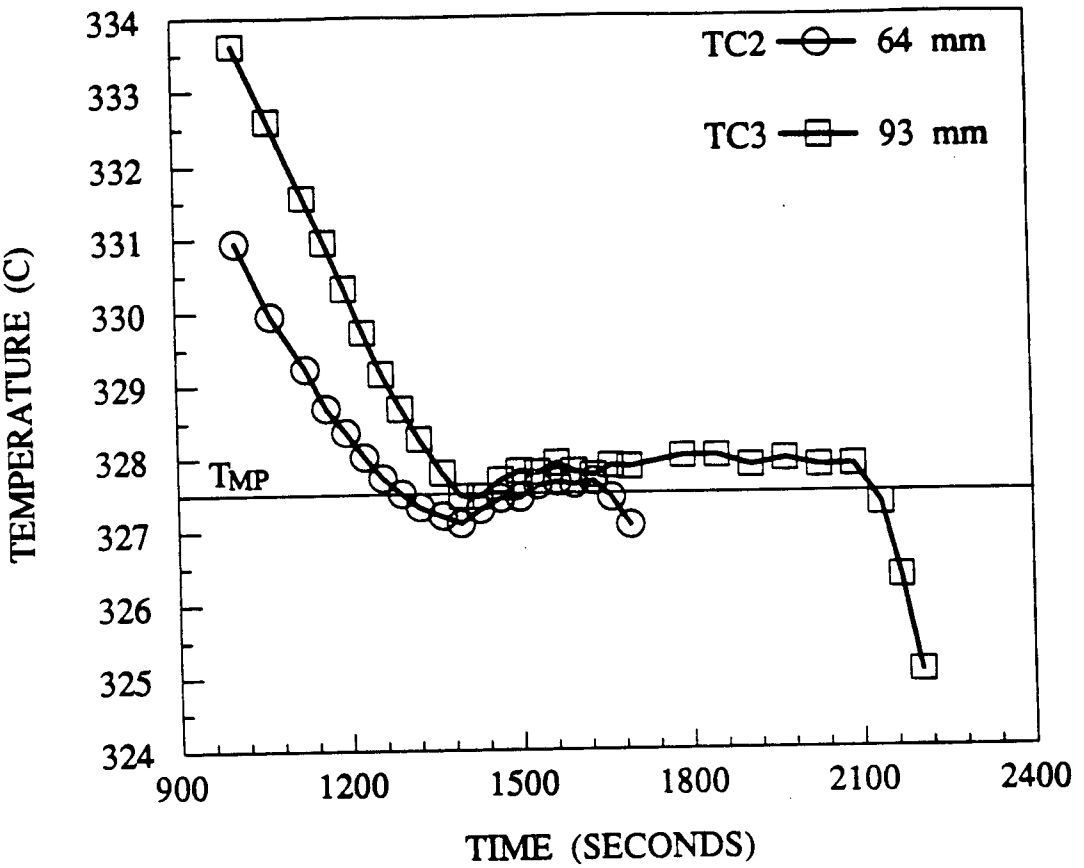

Figure 3.27

Cooling curves for test 57 (99.999%Pb) at the plateau region at the indicated distances from the chill

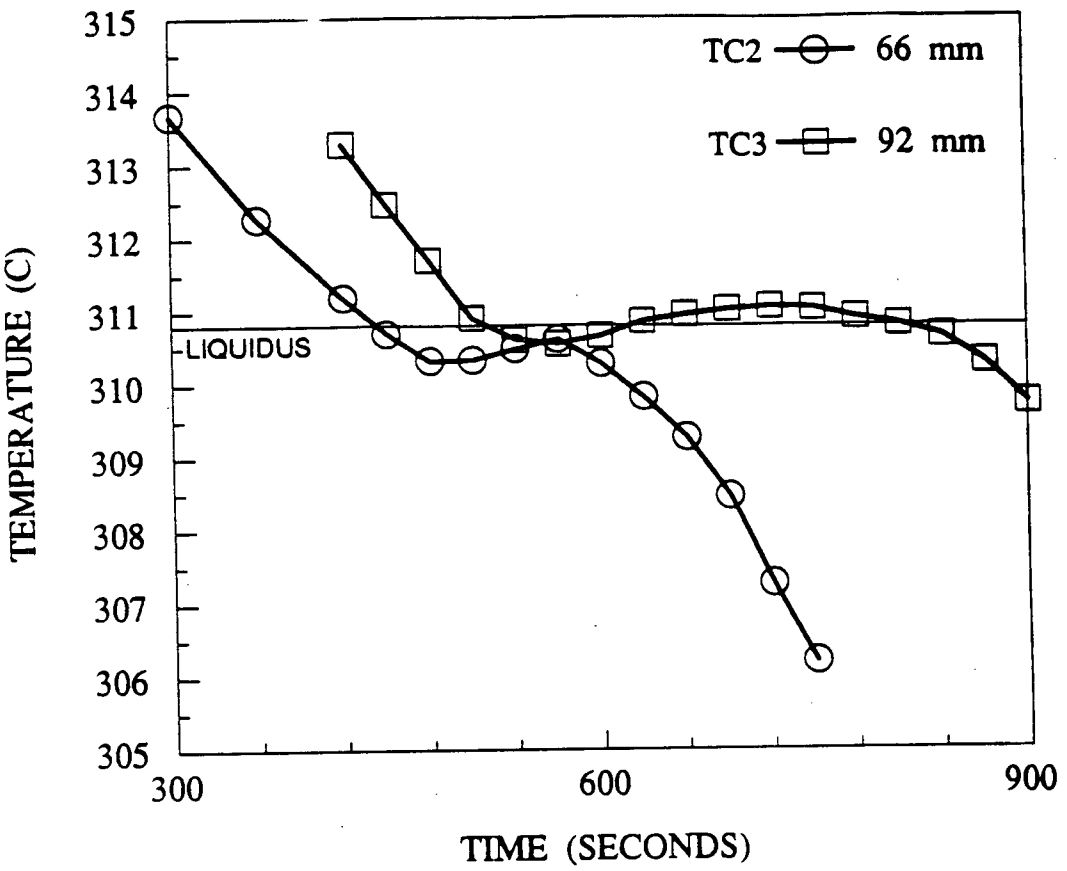

Figure 3.28

Cooling curves for test 59 at the plateau region at the indicated distances from the chill

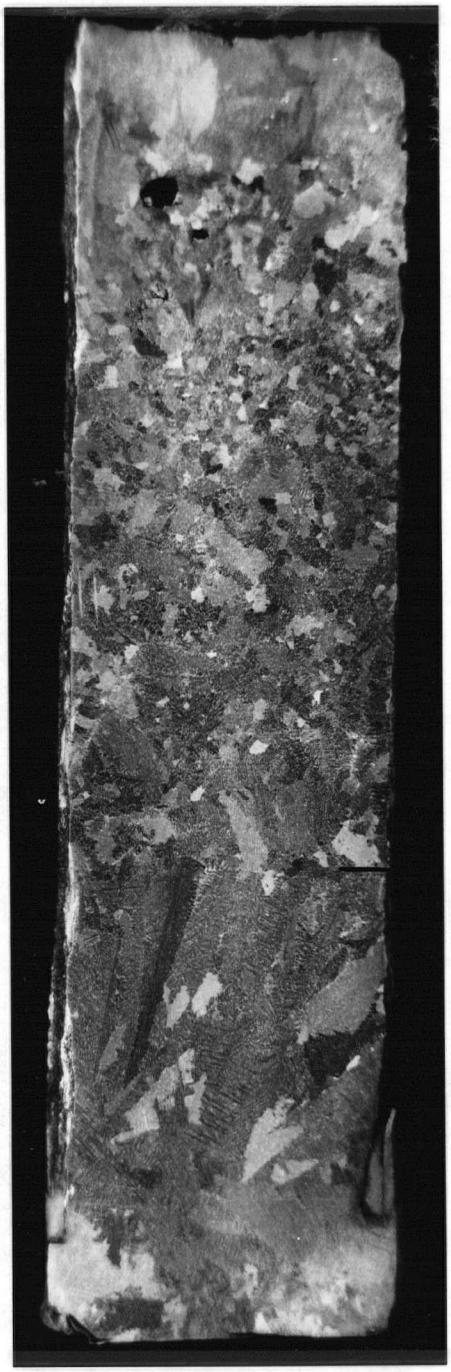

Figure 3.29

Cast structure of test 60 (Sn-10%Pb) using chill assembly CA1 and the top of the melt insulated

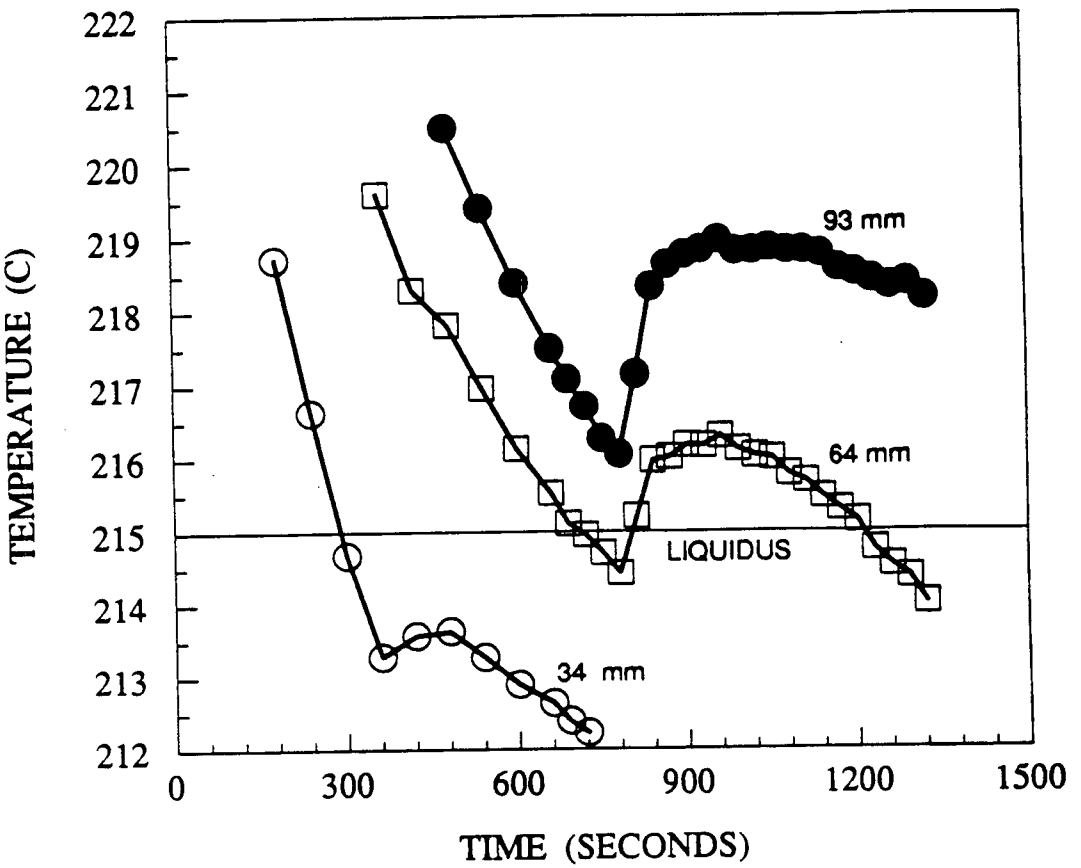

Figure 3.30

Cooling curves for test 60 at the indicated distances from the chill

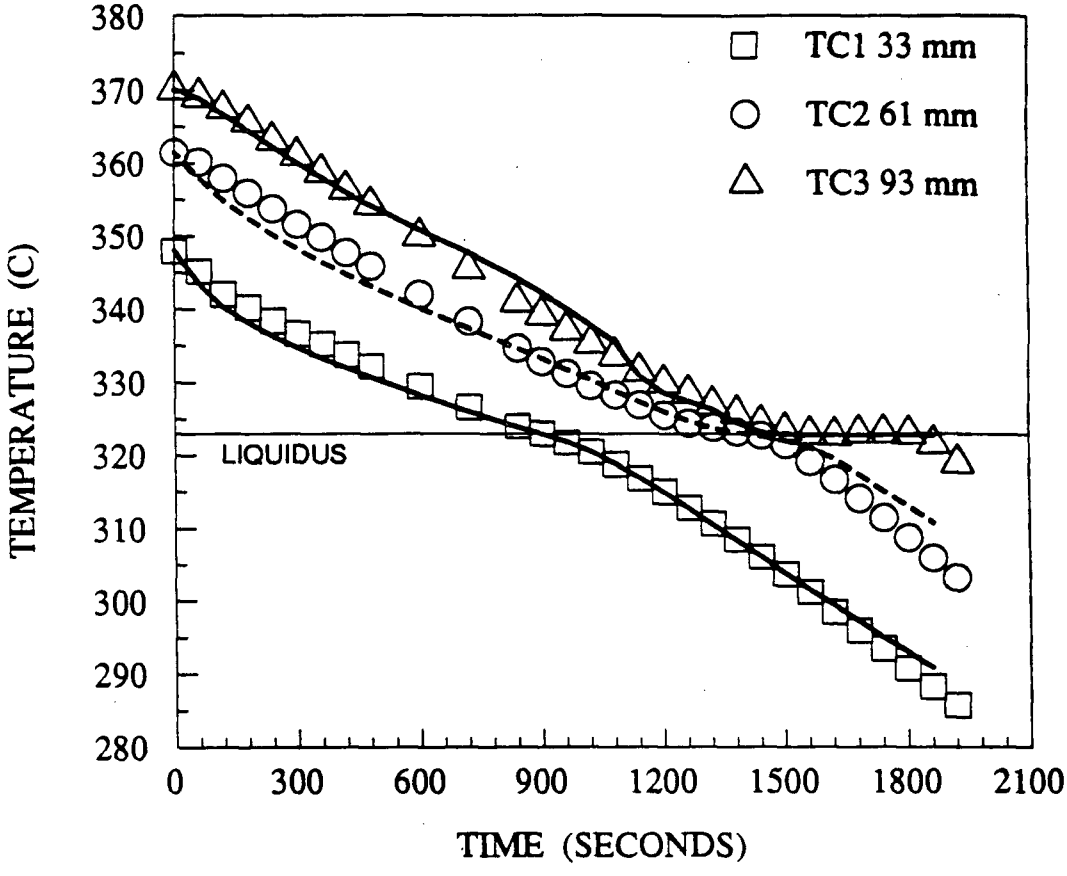

Figure 3.31

Predicted cooling curves (lines) and experimental cooling curves (symbols) for test 45.

HTC_{Bottom} = 0.0105J/cm^2-°C-sec HTC_{Top} = 0.02J/cm^2-°C-sec

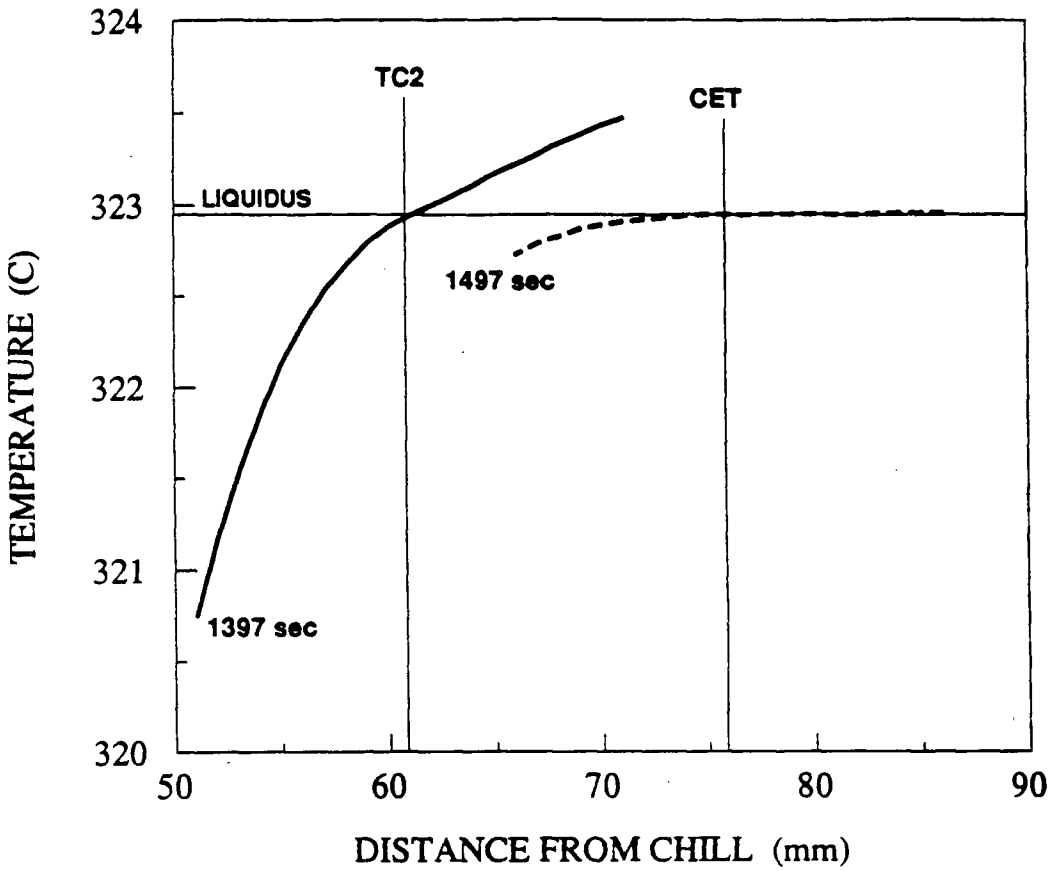

Figure 3.32

The thermal field ±10 mm from the liquidus temperature at two positions (1) when the liquidus is at TC2 61 mm for test 45 and (2) when the liquidus is at 76 mm from the chill where the CET occurs.

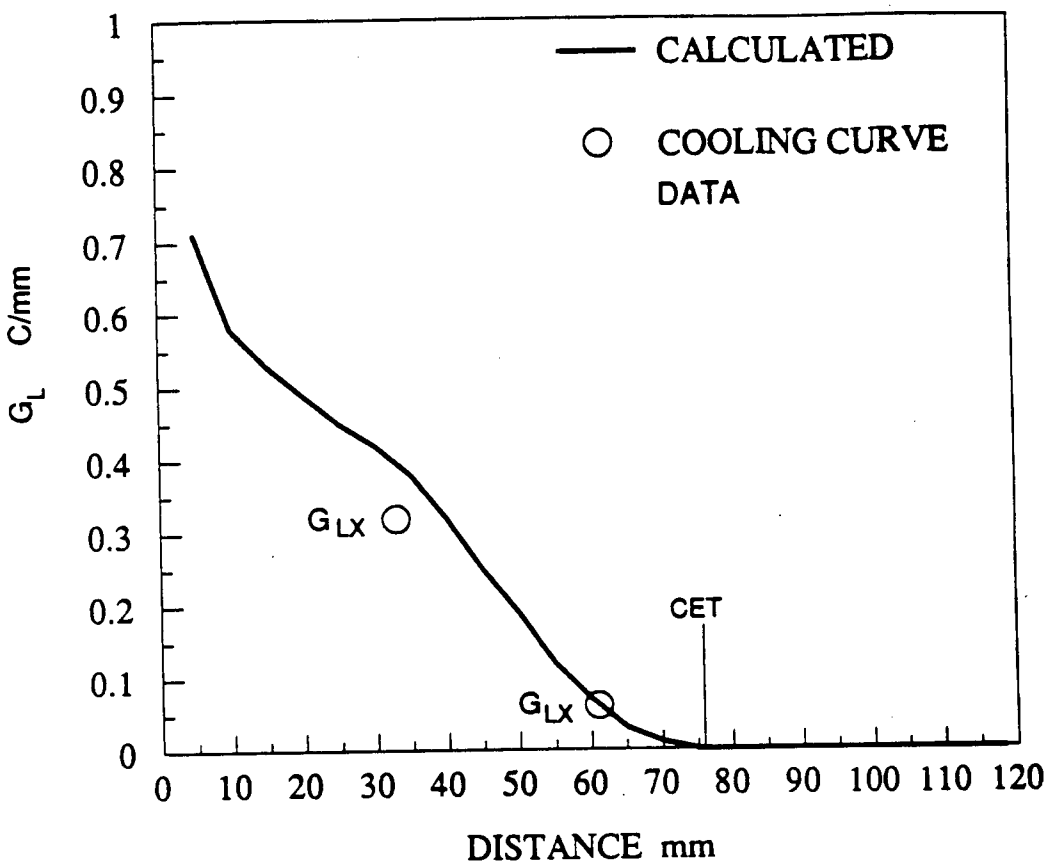

Figure 3.33

G_L as a function of distance from the chill for test 45.

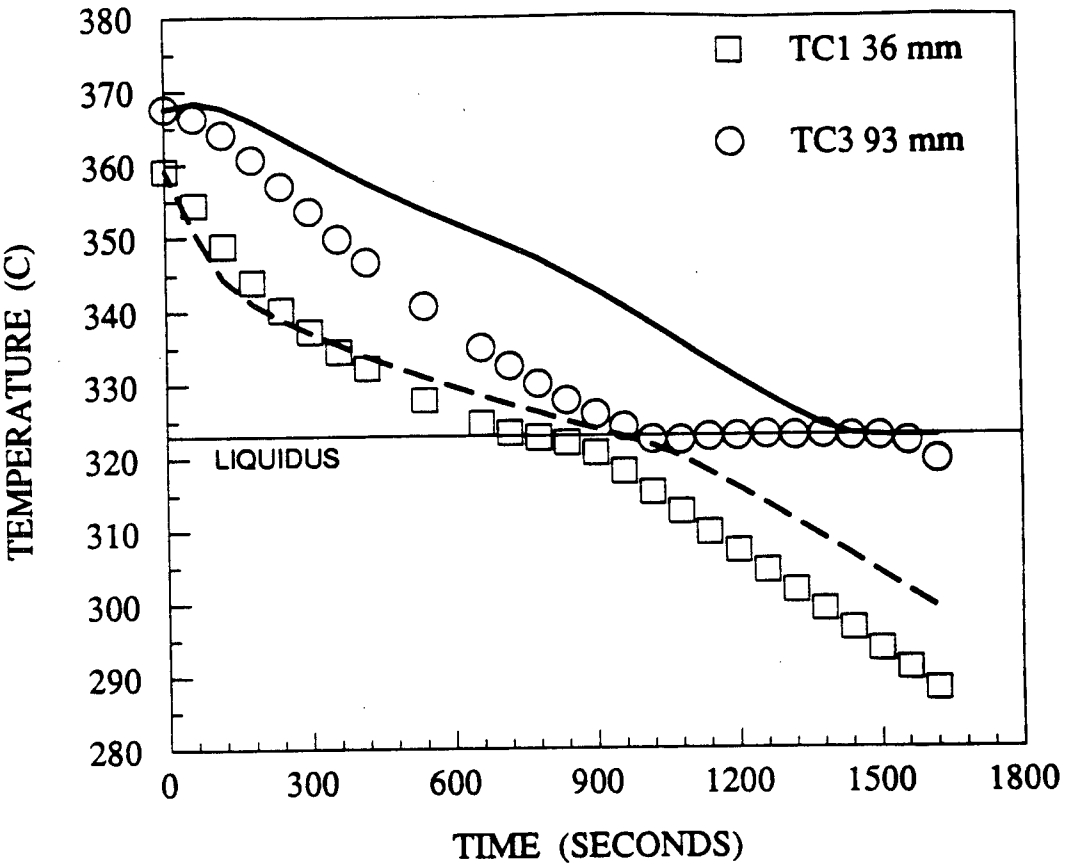

Figure 3.34

Predicted cooling curves (lines) and experimental cooling curves (symbols) for test 48.

$HTC_{Bottom} = 0.0105 J/cm^2\text{-}^{\circ}C\text{-}sec$ $HTC_{Top} = 0.02 J/cm^2\text{-}^{\circ}C\text{-}sec$

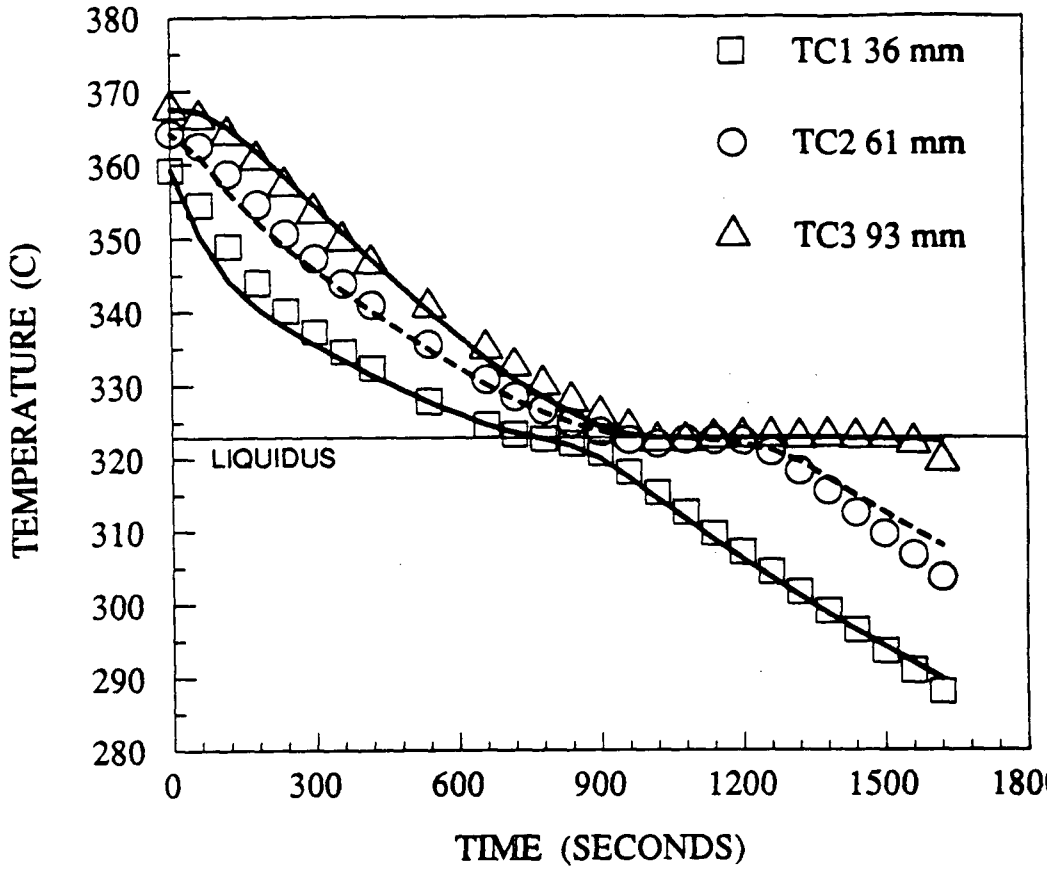

Figure 3.35

Predicted cooling curves (lines) and experimental cooling curves (symbols) for test 48 using the same heat transfer coefficients but with different T_{FURN} values.

HTC_{Bottom} = 0.0105J/cm^2-°C-sec HTC_{Top} = 0.02J/cm^2-°C-sec

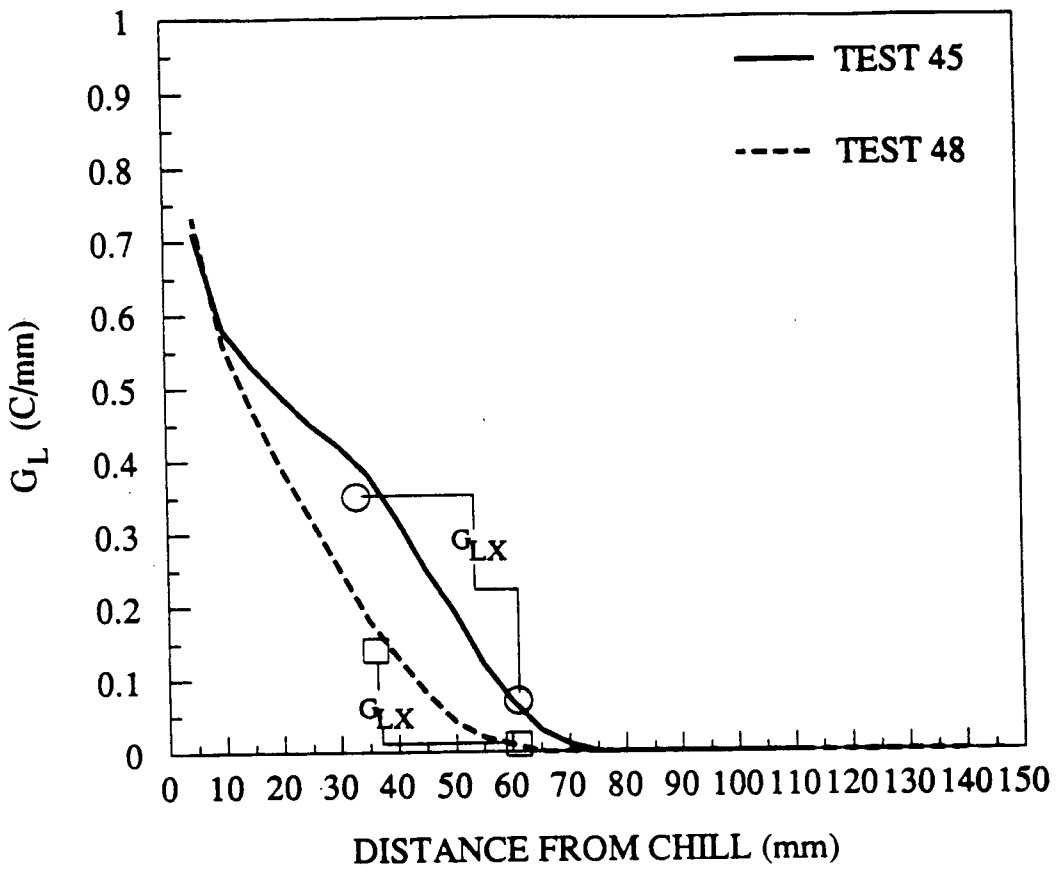

Figure 3.36

G_L as a function of distance from the chill for test 45 and for test 48.

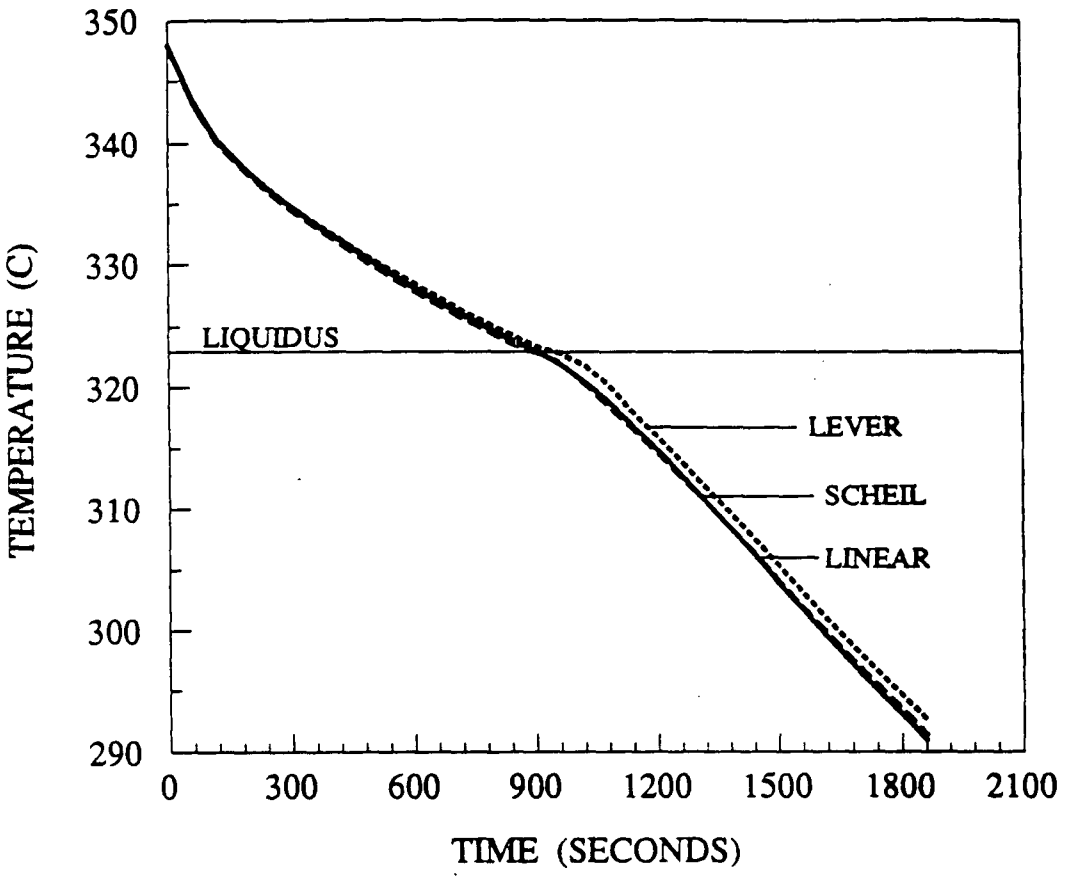

Figure 3.37

Predicted cooling curves for test 45 using the Linear model, the Scheil equation model and the Lever rule model.

Distance from chill = 33 mm

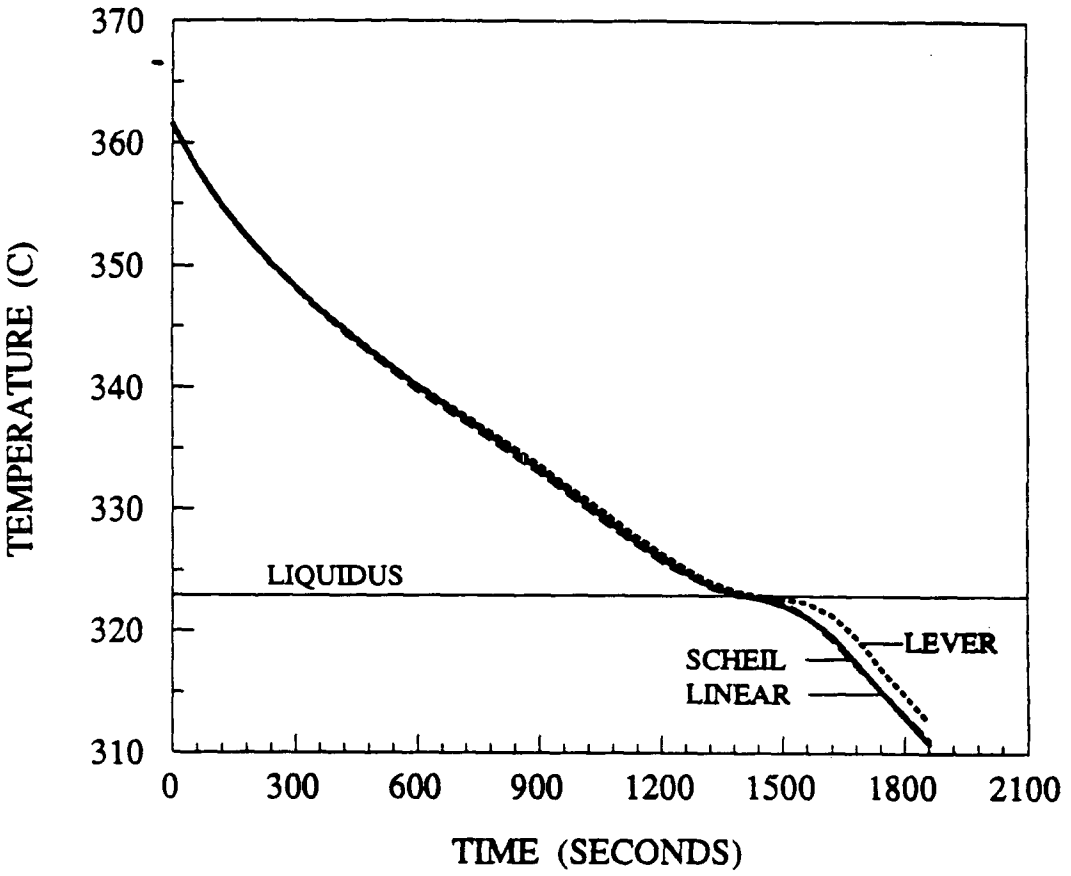

Figure 3.38

Predicted cooling curves for test 45 using the Linear model, the Scheil equation model and the Lever rule model.

Distance from chill = 61 mm

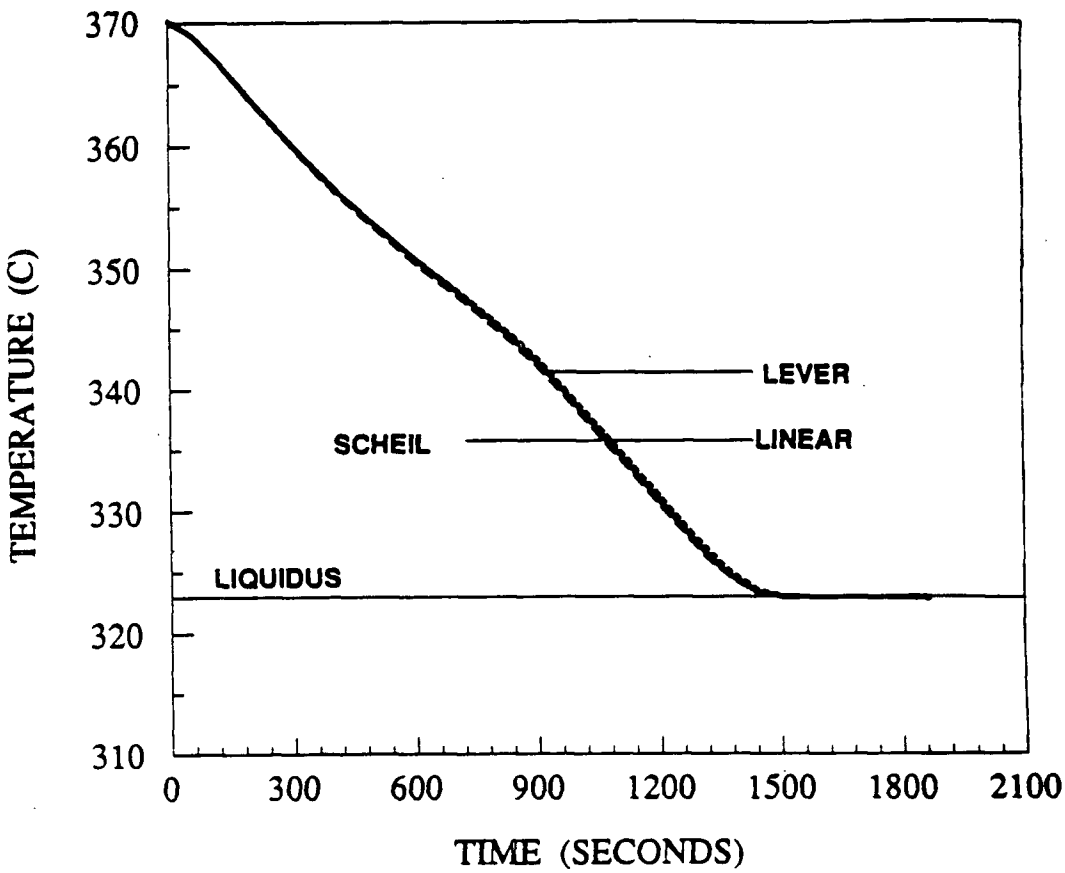

Figure 3.39

Predicted cooling curves for test 45 using the Linear model, the Scheil equation model and the Lever rule model.

Distance from chill = 91 mm

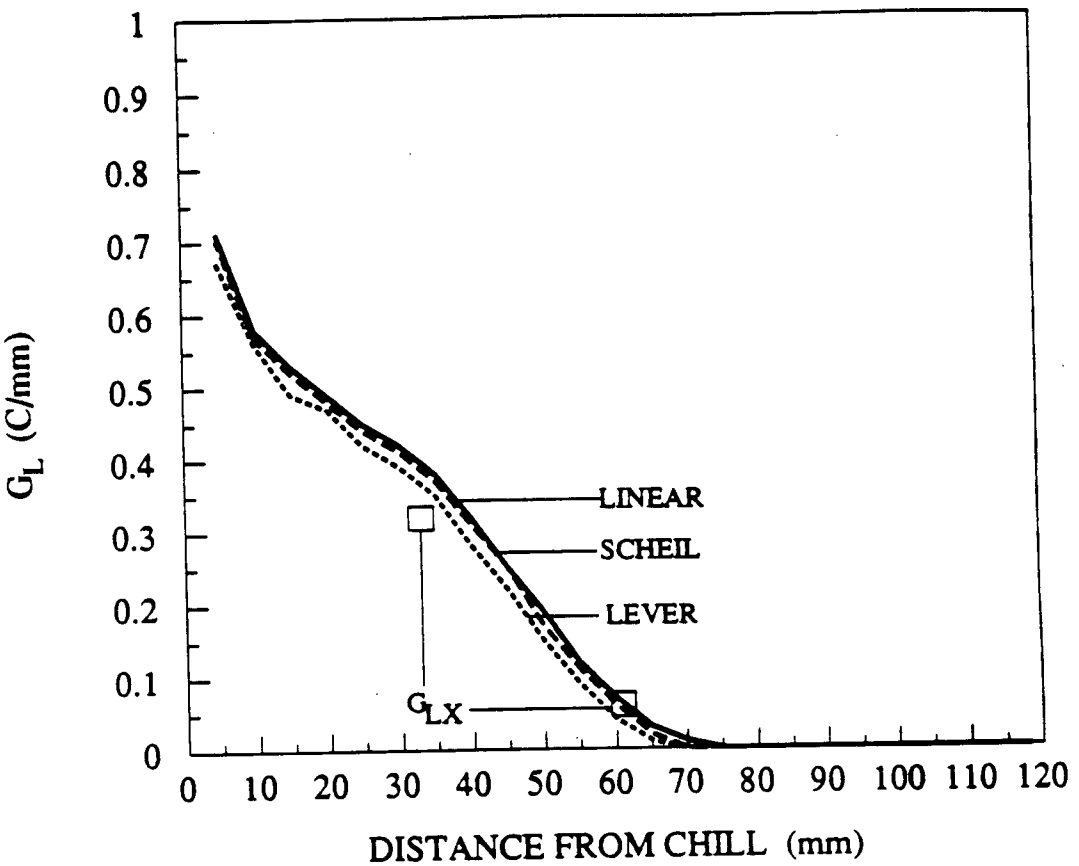

Figure 3.40

G_L as a function of distance from the chill for test 45 using the three procedures to release latent heat.

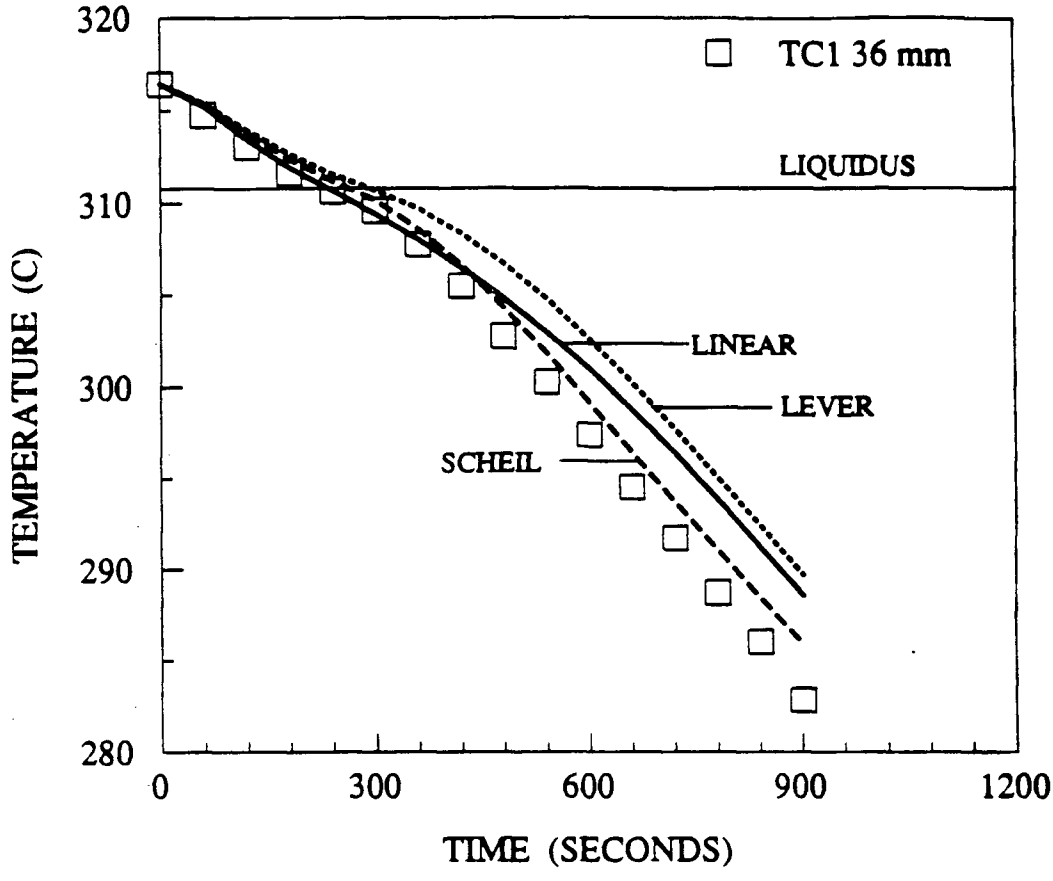

Figure 3.41

Predicted cooling curves (lines) and experimental cooling curves (symbols) for test 59 (Pb-6%Sn), using the three procedures to release latent heat for the predicted curves. HTC_{Bottom} = 0.0105J/cm^2-°C-sec HTC_{Top} = 0.02J/cm^2-°C-sec

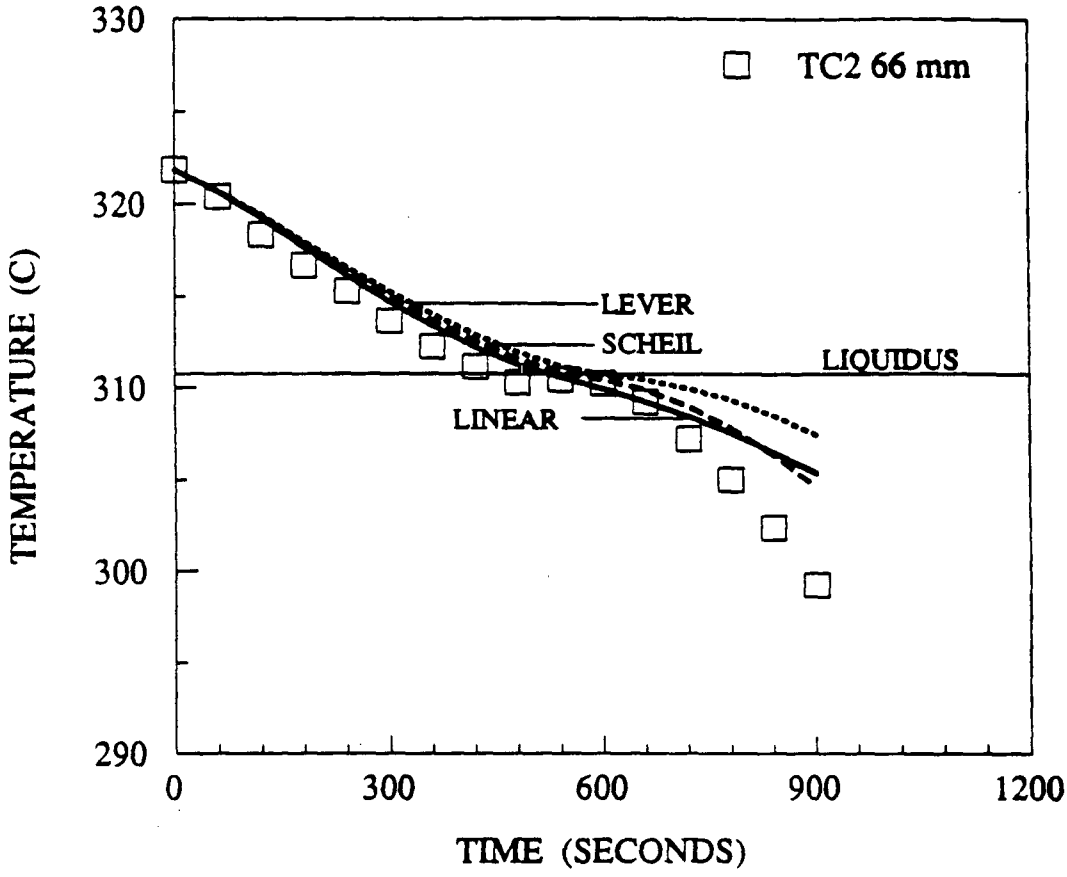

Figure 3.42

Predicted cooling curves (lines) and experimental cooling curves (symbols) for test 59 (Pb-6%Sn), using the three procedures to release latent heat for the predicted curves.

$HTC_{Bottom} = 0.0105 J/cm^2\text{-}^\circ C\text{-}sec$ $HTC_{Top} = 0.02 J/cm^2\text{-}^\circ C\text{-}sec$

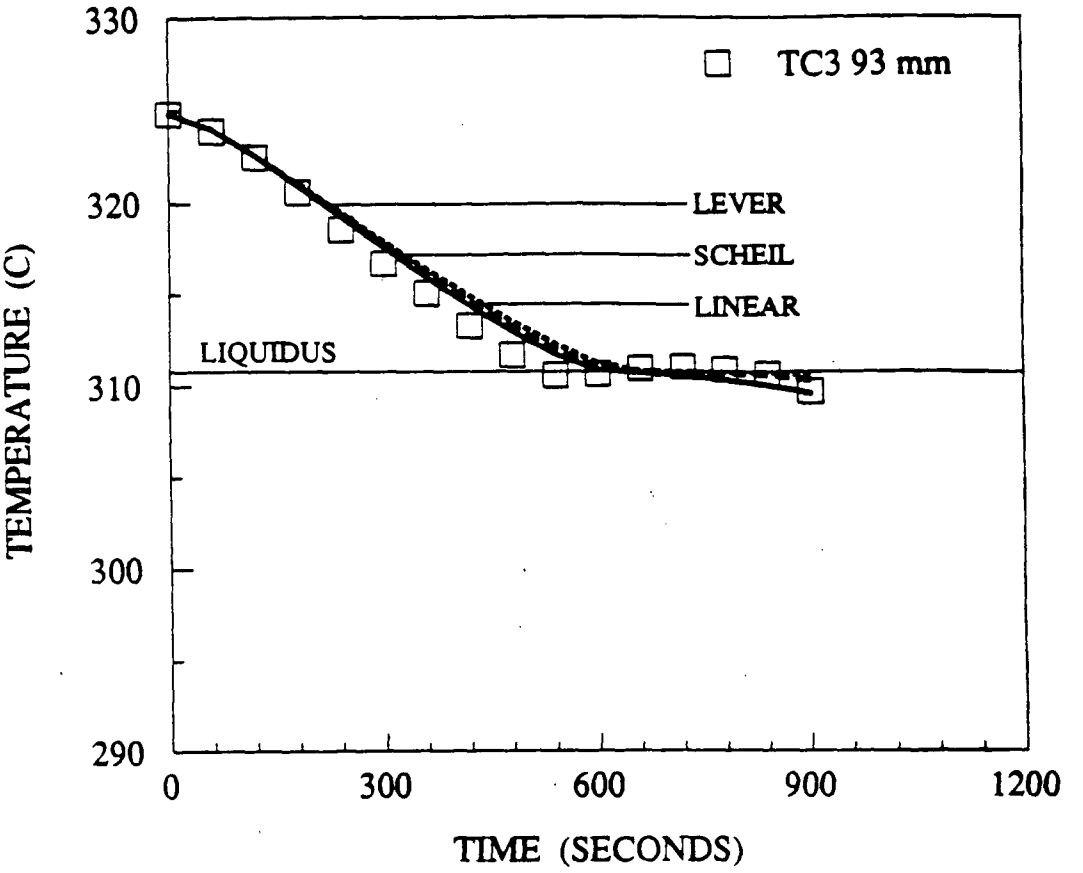

Figure 3.43

Predicted cooling curves (lines) and experimental cooling curves (symbols) for test 59 (Pb-6%Sn), using the three procedures to release latent heat for the predicted curves. HTC_{Bottom} = 0.0105 J/cm^2-°C-sec HTC_{Top} = 0.02 J/cm^2-°C-sec

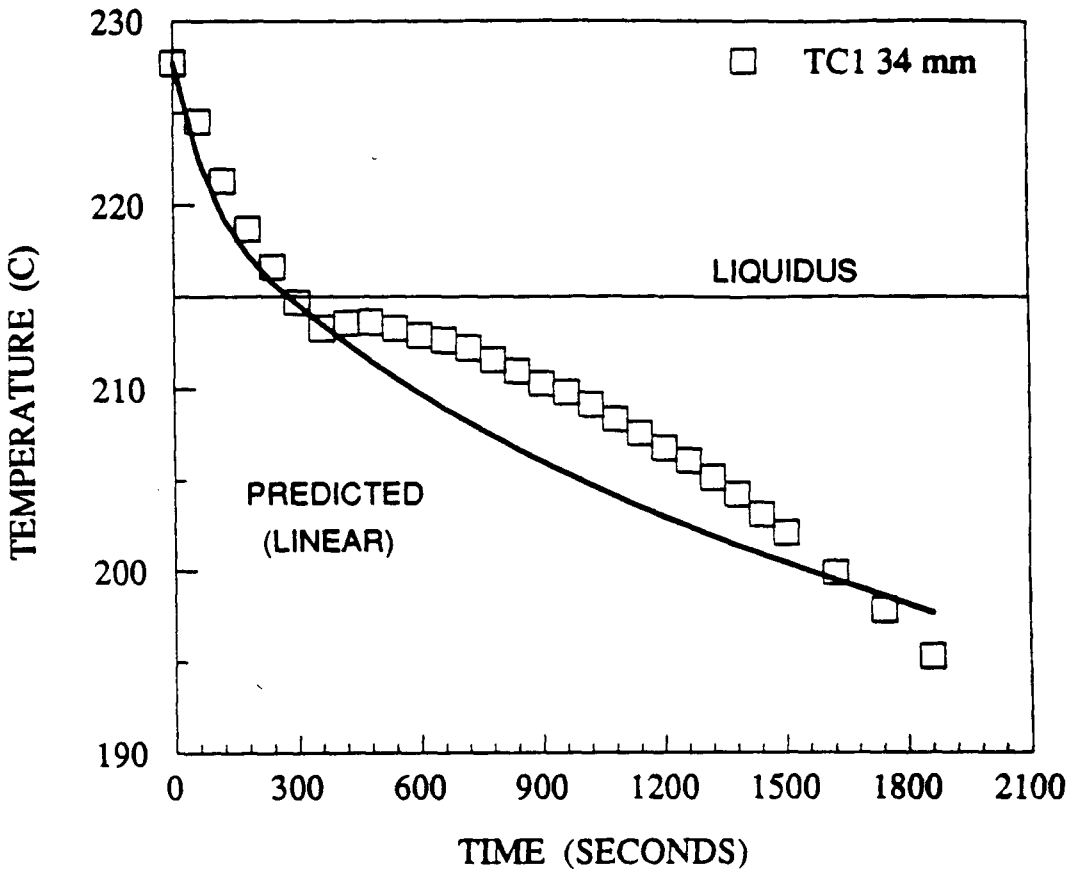

Figure 3.44

Predicted cooling curves (lines) and experimental cooling curves (symbols) for test 60 (Sn-10%Pb), using the linear method to release latent heat for the predicted curves.

HTC_{Bottom} = 0.0105 J/cm^2-°C-sec HTC_{Top} = 0 J/cm^2-°C-sec

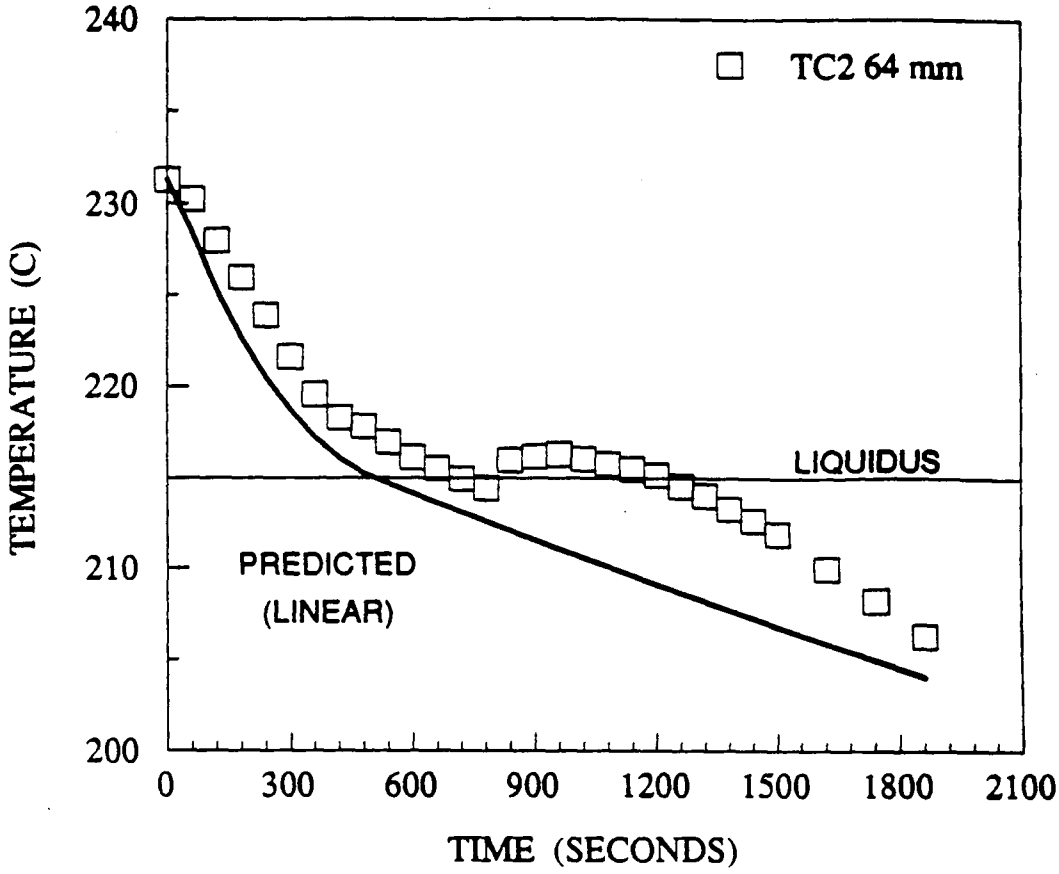

Figure 3:45

Predicted cooling curves (lines) and experimental cooling curves (symbols) for test 60 (Sn-10%Pb), using the linear method to release latent heat for the predicted curves.

HTC_{Bottom} = 0.0105 J/cm^2-°C-sec HTC_{Top} = 0 J/cm^2-°C-sec

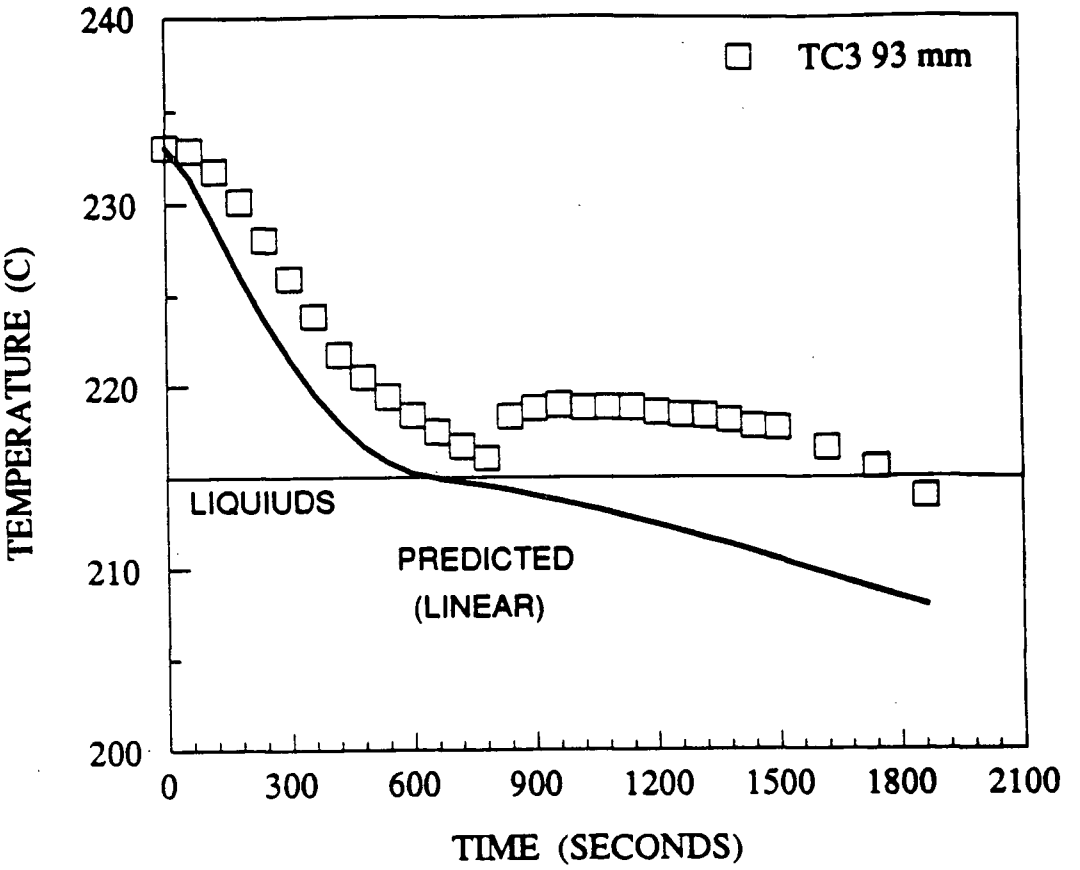

Figure 3.46

Predicted cooling curves (lines) and experimental cooling curves (symbols) for test 60 (Sn-10%Pb), using the linear method to release latent heat for the predicted curves.

HTC_{Bottom} = 0.0105 J/cm^2-°C-sec HTC_{Top} = 0 J/cm^2-°C-sec

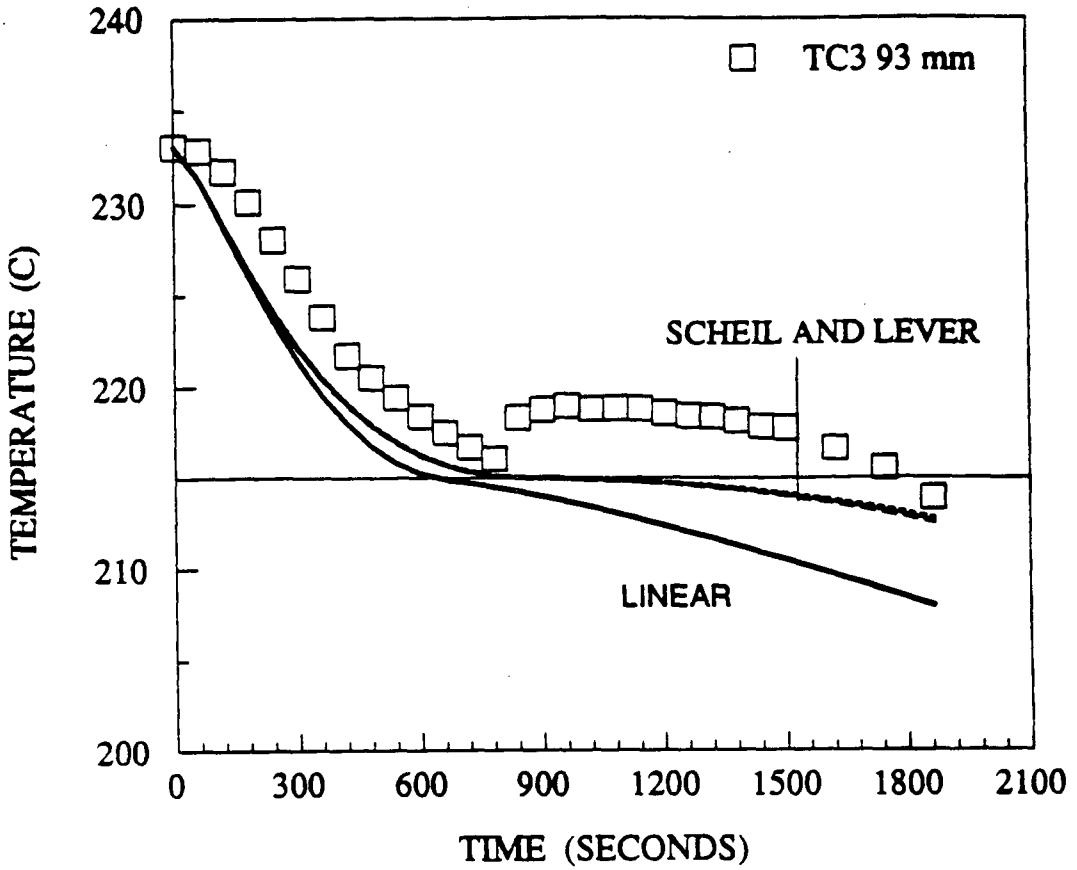

Figure 3.47

Predicted cooling curves (lines) and experimental cooling curves (symbols) for test 60 (Sn-10%Pb), using the three procedures to release latent heat for the predicted curves. HTC_{Bottom} = 0.0105 J/cm^2-°C-sec HTC_{Top} = 0 J/cm^2-°C-sec

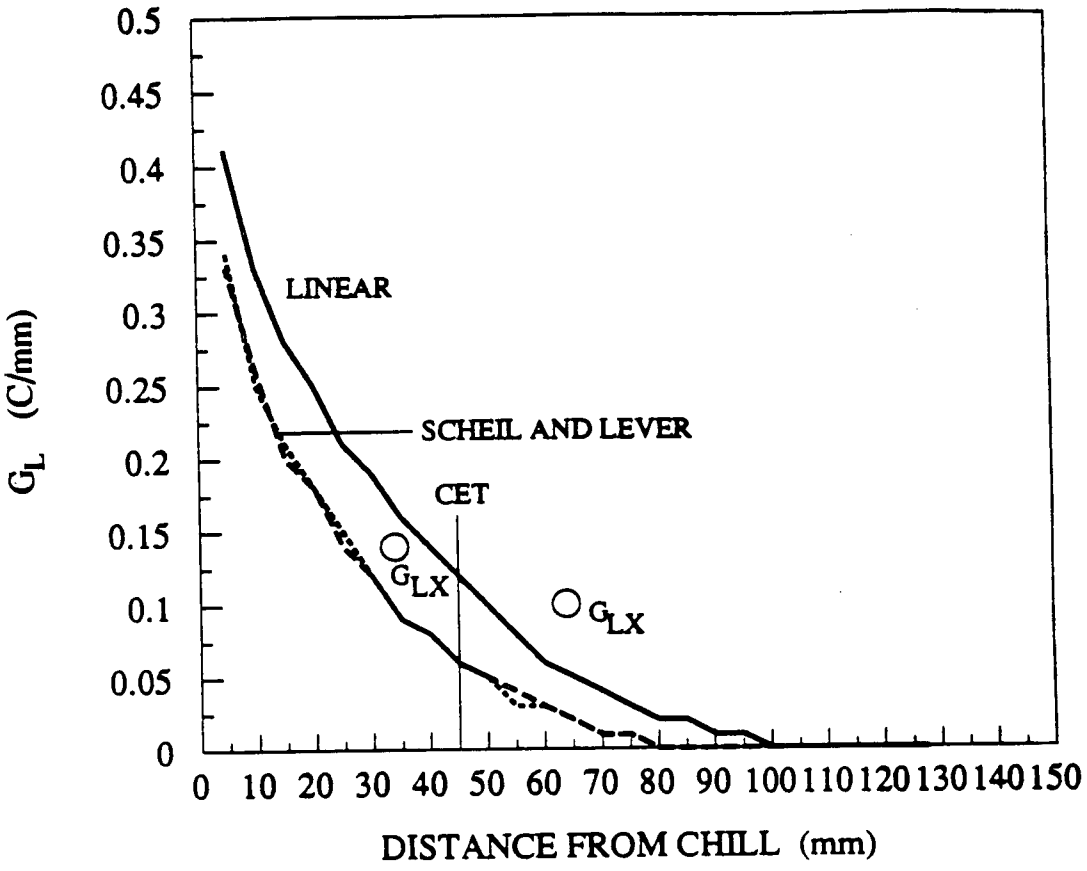

Figure 3.48

G_L as a function of distance for the chill for test 60 (Sn-10%Pb) using the three procedures to release latent heat.

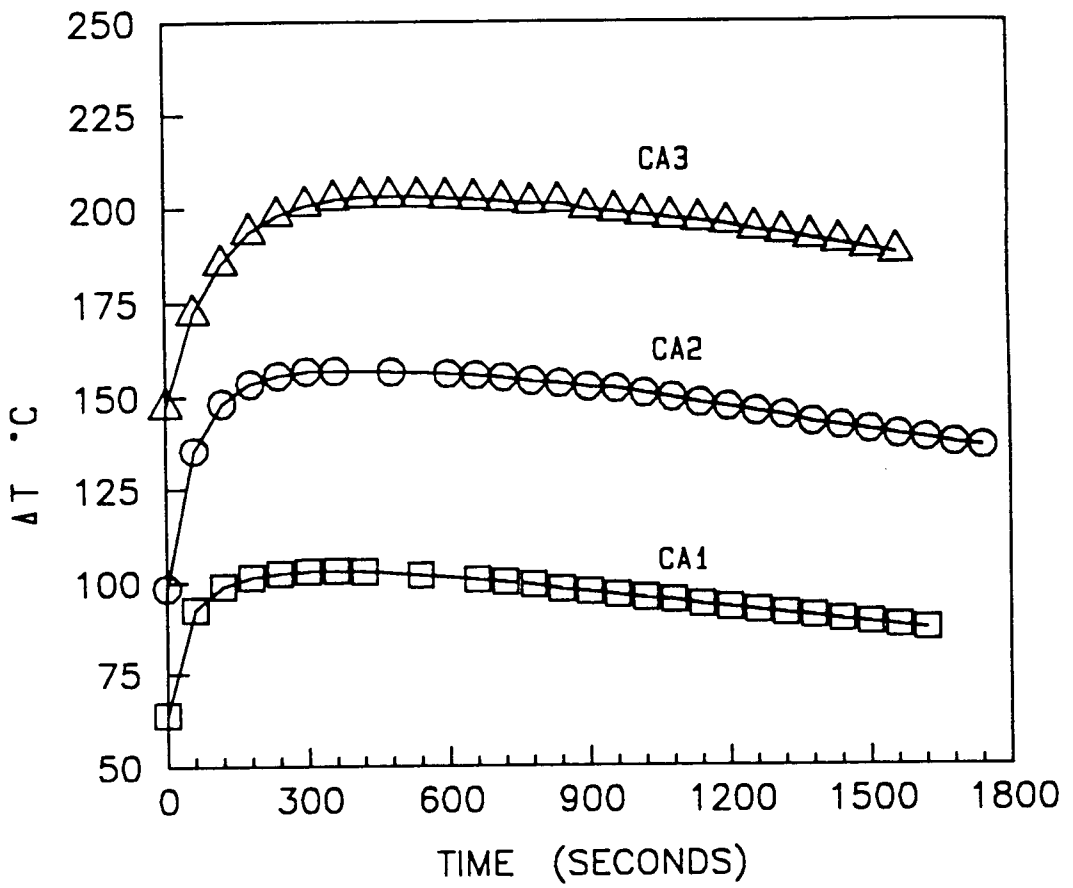

3.49 Measured Temperature Differences in the Three Chill Assemblies as a Function of Time

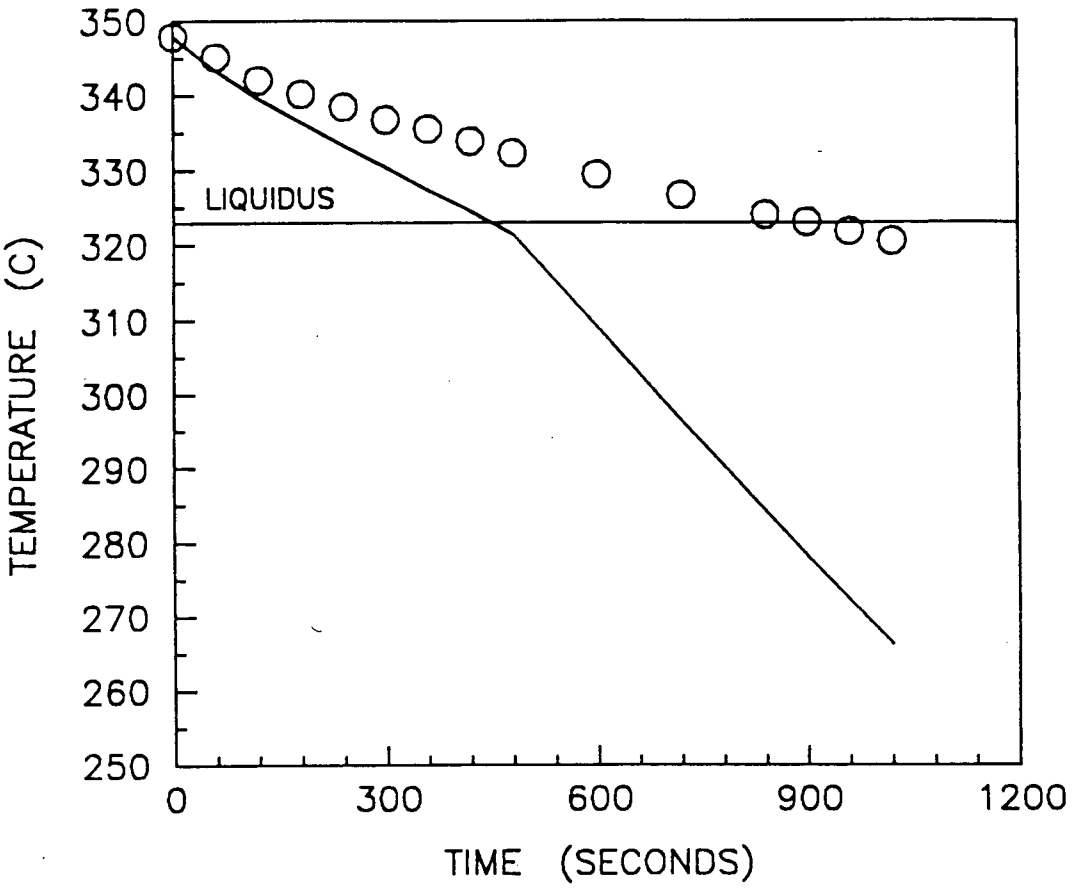

3.50 Predicted Versus Experimental Cooling Curve for Test 45 at 33 mm from the Chill Using the Calculated Heat Flux Instead of a Heat Transfer Coefficient

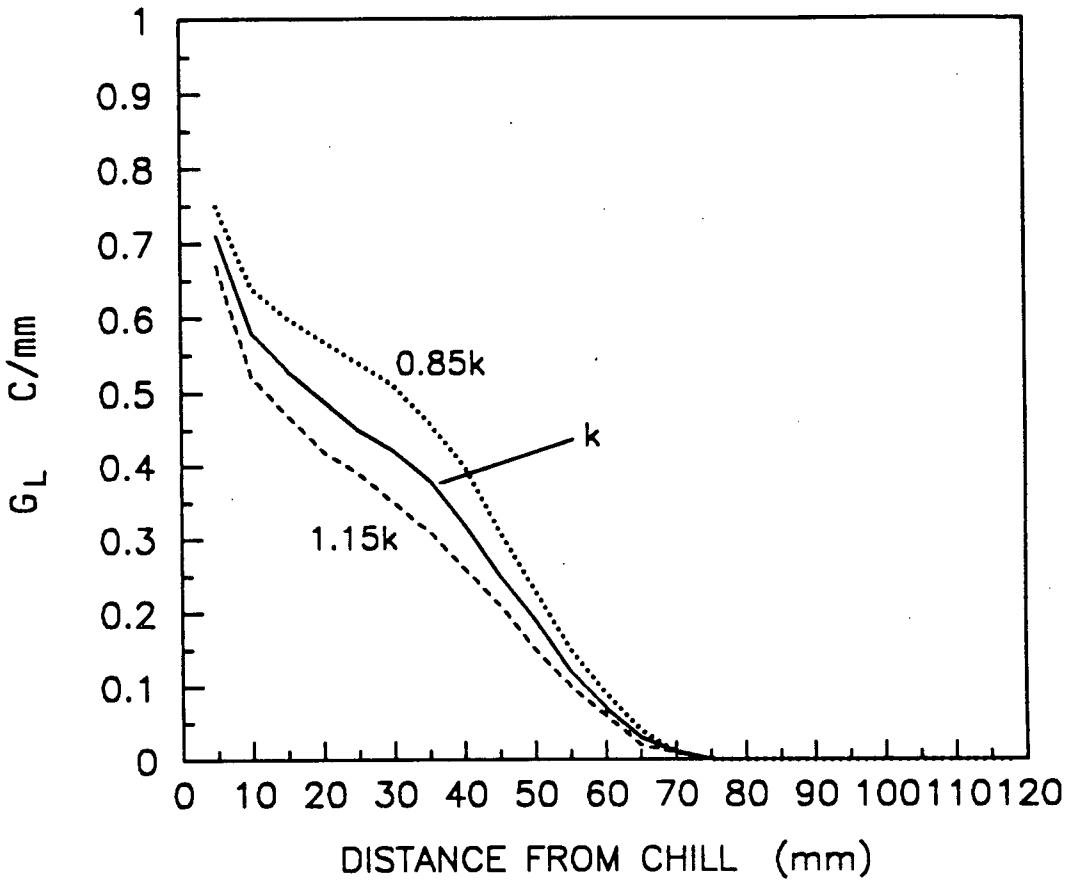

3.51 G_L as a Function of Distance Using Three Different Values for the Thermal Conductivity

Chapter 4

DISCUSSION

4.1 TEMPERATURE MEASUREMENTS

Thermocouples are inherently inaccurate and their use for precise, and accurate temperature measurements requires careful calibration. It is clearly evident in tests 1-4 where the thermocouples were calibrated once, prior to test 1 using 99.99% Pb, that the thermocouples were not calibrated carefully enough. The correction factors applied to the thermocouple output, in °C, produced erroneous results as shown in Figure 3.11. The different plateau temperatures, T_P, should all be the same given that the alloy composition was held constant at Pb-1.5%Sn. In addition, it is expected that all the horizontal temperature plateaus occur at the liquidus temperature for the alloy, approximately 323°C.

The errors which occurred in tests 1-4 can be explained by reviewing the results from tests 5 to 32, ie, the temperature measurements made with high purity lead, 99.999%. In these tests the melting point of the lead, T_{MP}, is constant at 327.5°C and so the horizontal temperature plateau observed in the cooling curves should be at this precise value. Any deviation from this value , (T_P-T_{MP}), may be attributable to errors in the chemical composition in the thermocouple wires, errors associated with the cold junction, and the degree of cold worked material after the thermocouple is made[21]. It is quite clear that these errors are not constant as the difference between T_P and T_{MP} changes from test to test for a given thermocouple. Therefore, it is reasonable to expect that this occurred in tests 1-4 as well so that the correction factor established independently, no longer applied. The end result is that of Figure 3.11 with the measured T_P for Pb-1.5%Sn ranging from 321°C to 326°C, an error of approximately ±2.5°C. Improving the accuracy further using a single calibration experiment is not possible.

In order to use the results of tests 5 to 32 and improve the accuracy of the temperature measurements beyond the value mentioned above, it was decided to use a mean correction factor based on the values of T_P-T_{MP} in tests 5 to 16 inclusive for TC1, in tests 16 to 23 inclusive for TC2, and in tests 24 to 32 for TC3. In using this procedure, it is assumed that the correction factor in subsequent directional solidification tests do not deviate outside the range established in Tables 3.2, 3.3, and 3.4. In this way, the absolute error using the three thermocouples is expected to be in the order of ±0.7°C while the relative error between two thermocouples is expected to be ±1.4°C.

This approach was met with limited success for subsequent directional soldification tests using Pb-1.5%Sn, in that the T_P in Table 3.7 for tests 33 to 39 does not deviate from the T_{LIQ} of the alloy by more than 0.5°C. However, in later tests shown in Table 3.8, the

T_P deviates from the T_{LIQ} up to 1.4°C indicating that the correction factors established in tests 5 to 32 may no longer apply. When more than one T_P was measured from the three thermocouples, see Figure 3.19, the relative error did not exceed 1.4°C. This means that the difference in the two temperatures can be taken as negligible.

Further improvements in the accuracy of the temperature measurements using the three thermocouples are possible by eliminating the correction factor which is established independently of the directional solidification test. In this way, the three thermocouples are calibrated simultaneouly to the liquidus temperature of the alloy by performing immediately prior to directional solidification, an "in-situ" calibration test as described in section 2.3. The correction factor for each thermocouple becomes specific for this test and is not applied to any other tests. The deviation between T_P and T_{LIQ} in Pb-1.5%Sn tests is ±0.2°C as shown in Table 3.9. Applying this technique to the Pb-3%Sn and the Pb-6%Sn produced a deviation between T_P and T_{LIQ} between 0.2°C and 0.4°C which is still better than the results from Table 3.7 for Pb-1.5%Sn using the mean correction factor.

In establishing a mean correction factor for TC1, TC2, and TC3 using the 99.999% Pb melting point as a basis of comparison, an average supercooling of 0.6°C is measured. This is a small amount and in order to establish its credibility, the precision of the temperature measurements must be briefly discussed. In Tables 3.2 to 3.4 inclusive, the temperature measurements are reported using a precison of ±0.1°C. This is based on the temperature range recorded while the temperature was on the plateau. On average, the temperature range was 0.2°C, with an equal balance of temperatures above and below the

average T_p. Thus, each T_p can be determined within ±0.1°C. The same external and internal electrical noise is expected to influence temperatures not on the plateau with the same degree of precision.

Since each recorded temperature is an average of 32 measurements taken 10 ms apart, a statistical analysis can be made using the mean, the standard deviation, and the variance of each measurement to confirm the precision of the temperature measurements observed on the temperature plateau. The analysis concerns the significance of the difference of the means of two sets of independent data. the analysis, shown in Appendix 2, determines that the smallest significant difference is 0.07°C. This is very close to ±0.1°C and well below 0.6°C. Therefore, the supercooling is indeed present and at the value reported.

In the directional solidfication tests of Pb-1.5%Sn, the measured supercooling decreased to a range from 0.2°C to 0.4°C. While this is still above the ±0.1°C limit set for the pure Pb tests discussed above, the precision of the temperature measurements decreases because the number of measurements per temperature decreases, see Appendix 2. The difference becomes 0.16°C which is now close to 0.2°C, the bottom range of the supercooling. This may raise some questions as to the realilty of the measurements. However, even with the very small supercooling there is a consistent rise in temperature from the maximum supercooling value to the plateau and not just a single spike which indicates that supercooling does exist at that point.

4.2 Sn-10%Pb

In a previous study[18], there is a degree of uncertainty regarding the value of G_L of 0.11°C/mm at the CET for Sn-10%Pb. The value was determined primarily on the predicted temperatures from a one dimensional heat transfer mathematical model validated by fitting the predicted temperatures to within ±3°C of the experimental temperatures taken over a 600 second time period. On this basis, the relative error between two thermocouples positions could be as high as 6°C. The error in the determination of the temperature gradient over 20 mm, the distance between two thermocouples, could therefore be as high as 0.3°C/mm which is three times the value of the critical temperature gradient. There was no mention of an experimentally determined temperature gradient to assist in validating the model.

An attempt is made in this study to address this uncertainty as the Sn-10%Pb alloy is reexamined, test 60, using carifully calibrated thermocouples with a high degree of accuracy to produce experimental values of G_L in front of two fixed positioned thermocouples straddling the CET. It was found that the CET occurred between experimental values, denoted in this study as G_{LX}, of 0.14°C/mm and 0.10°C/mm. Linearly interpolating between these two values results in an experimentally determined value at the CET of 0.12°C/mm which is very close to the original value found by Mahapatra and Weinberg[18]. Therefore, to a first approximation, this verifies the earlier finding. It is also interesting to note that the one dimensional mathematical heat transfer model using the linear assumption of latent heat release predicted a value of G_L of 0.12°C/mm even though the fit between the predicted cooling curves and the experimental cooling curves is not good. The redeeming feature of the fit could be in that

all the predicted values are lower than the experimental values rather than being on either side of the experimental cooling curve. In this way, the absolute temperatures are incorrect but the relative temperatures are close but only for times before the CET takes place. After that time, the model predictions are not valid. The model predicts that the G_L continues to decrease until reaching 0°C/mm at 100 mm from the chill face whereas there is some indication from Figure 3.30 that the temperature gradient remains positive. The three cooling curves show that the temperature in the ingot increase as the distance from the chill increases until solidification is complete at 1320 seconds.

An important feature of the CET in the Sn-10%Pb test performed in this study is that it resembles the CET in the previous study. That is, the CET is abrupt and flat and is very easy to identify. In addition, the entire cast structure is reminiscent of the cast structure found by Mahapatra and Weinberg[18]. The equiaxed grain size is small and decreases as the distance from the CET increases.

However, two very prominent features in the cooling curves found in this study were not reported by Mahapatra and Weinberg. They are, supercooling followed by a horizontal temperature plateau. It was found that both the amount of supercooling and the temperature of the plateau increased as the distance from the chill increases. The reason this was not previously reported could lie in the method and duration of the temperature measurements made by Mahapatra and Weinberg. In their study, four thermcocouples were used to measure temperatures during cooling and solidification and were connected to a two pen Kipp and Zonen chart recorder via a switching device. Therefore, only two thermocouples could be monitored simultaneously leaving open the possibilty of important information such as the small amount of supercooling and short plateaus at

distances close to the chill being missed. In addition, terminating temperature measurements after 600 seconds would not allow the large supercoolings and significant temperature plateaus observed in this work at 780 seconds to be observed.

Unfortunately, no repeat work was done using Al-3%Cu alloy and the carefully calibrated thermocouples to verify the findings of Ziv and Weinberg[19] that the G_L is 0.06°C/mm at the CET.

4.3 Pb-1.5%Sn

The results of the Pb-1.5%Sn work show that the G_L does not influence the position of the CET as it does for Sn-10%Pb. There are many instances in the experimental data where the G_L goes to 0°C/mm before the CET occurs. Test 35 is an example where at 67 mm from the chill, the experimental value, G_{LX}, is 0°C/mm while the CET occurs at 71 mm from the chill. However, there are cases where this trend is not followed. This is most clearly seen in the results of test 40 which features a completely equiaxed structure yet the G_{LX} does not go to 0°C/mm until somewhere between 35 and 65 mm from the chill face. With inconsistent results such as these, it is difficult to detect a critical temperature gradient for Pb-1.5%Sn.

It would be much easier to determine a temperature gradient at which the CET occurs if the structures in test 33 to 48 resembled those in tests 1 to 4 where the CET is abrupt and flat. Unfortunately, the poor temperature measurements prevent this from happening. The major differences are in the grain size and and the shape of the CET. Therefore, the difficulty in detecting a critical temperature gradient for Pb-1.5%Sn is attributed to the irregular shape of the CET and the very large equiaxed grain size. The

large equiaxed grain size infers that there were very few effective nuclei in the melt ahead of the advancing solid/liquid interface prior to directional solidification. The small number of nuclei are also responsible for the irregular shape of the CET in tests 33 to 48.

The appearance of the CET in the Pb-1.5%Sn tests is described as being irregular as some columnar grains continue to grow into a predominantly equiaxed zone as shown in Figures 3.15(a) and (b). The columnar grains which continue to grow do so because there are no equiaxed grains growing immediately ahead them. Adjacent to these columnar grains, which are generally situated in the middle of the ingot, are equaixed grains which have stopped the columnar growth at a distance closer to the chill. In order to have an equiaxed grain growing ahead of the columnar grain two conditions must be met. The liquid has to be supercooled and must contain nuclei with a nucleation temperature, ΔT_N, less than the amount of supercooling. The first condition is always met for alloys, as a small region of constitutionally supercooled liquid is present ahead of the dendrite tip due to the rejection of solute, since the partition coefficient is less than 1. Intuitively, it is felt that equiaxed grains should nucleate in this region if condition two is met. With Pb-1.5%Sn, this zone is especially small since the amount of solute used is low and given the results it is concluded that it is not met for every columnar dendrite. Therefore there are an insufficient number of nuclei in the melt to produce a flat CET.

Another reason for the irregular shape of the CET is possible. This could occur if there was a very steep radial temperature gradient such that temperatures in the middle of the ingot are much higher than on the outside edge. This possibility is discarded given the results shown in Table 3.12. There is a small temperature gradient observed between the outside edge of the ingot and the centre starting at 0.06°C/mm, (1.0°C/15 mm), which decreases gradually with time to 0.02°C/mm when the temperature plateau is recorded.

The gradient though is in the opposite direction with temperatures being hotter on the outside and cooler in the centre. Since there is not a steep radial temperature gradient, the isotherms across the face of the ingot are considered to be flat which leaves the lack of nuclei responsible for the irregular shape of the CET in Pb-1.5%Sn alloys.

Supercooling is observed consistently in the cooling curves for Pb-1.5%Sn at distances of approximately 95 mm from the chill. Since directional solidification of an alloy is occurring, it is reasonable to consider at first that the supercooling is constitutional. This conflicts with the above argument. However, there are results which indicate that the supercooling is thermal. First, there is the fact that when directionally solidified, pure Pb, (99.999%), supercools by approximately the same amount and in the same general location, ie, towards the top half of the ingot, see Table 3.13. Second, if enough power to the furnace is supplied such that heat is added to the melt to maintain a positive temperature gradient, the supercooling disappears as shown in Table 3.10. This would not occur if the supercooling were constitutional.

It is surprising to see a directionally solidifed alloy thermally supercool. This is only possible if there were another avenue for the heat to escape other than from top of the ingot to the chill block. The two other sources of heat loss are radially through the fibrefrax and into the furnace, and vertically out from the top surface of the melt and into the furnace assuming that a layer of fibrefrax has not been put on the top surface. There is some experimental evidence to show that heat is being lost in these directions, see Figure 2.10. It is difficult though to determine the magnitude of each but a good fit can be obtained in the model assuming heat is lost only from the top surface of the melt. This suggests that the radial heat loss is much lower than the heat lost vertically out the top of the melt.

4.4 MECHANISM FOR THE CET IN Pb-1.5%Sn AND Sn-10%Pb ALLOYS

The irregularity of the CET and the existence of thermal supercooling in tests 33 to 48 are explained by the lack of nuclei in the melt prior to solidfication, yet it is difficult to account for the presence of sufficient nuclei in tests 1 to 4 without considering the showering of dendrites theory proposed by Southin to produce nuclei for all the Pb-1.5%Sn tests. An integral part of the showering of dendrites theory is heat loss from the top surface of the melt. This clearly happened in test 2 as shown in Figure 3.7. The thermocouple situated at the top of the melt, 77 mm from the chill face, cools faster than the other two thermocouples situated closer to the chill face. It is felt that this occurs in test 1 as well because the duration of the horizontal temperature plateau 81 mm from the chill face, see Figure 3.5, is shorter than the other three. It is felt that heat loss from the top surface occurred in tests 33 to 48 since thermal supercooling is observed in these particular tests yet in these tests there were a lack of nuclei. The difference to account for the small grain size and abrupt CET in tests 1 to 4 is in the amount of heat being lost from the top surface. In tests 1 to 4 a greater amount of heat is being loss from the top surface than in tests 33 to 48. In only one test, (test 35), is the duration of the horizontal temperature plateau at the top thermocouple shorter than than the duration of the plateau measured at a distance closer to the plateau. In addition, the cooling rate of the thermocouples located 95 mm from the chill face is approximately equal to the cooling rate of the thermocouple located 65 mm from the chill face. Thus in accordance to the showering of dendrites theory, increasing the heat loss from the top surface increases the likelihood of surface dendrite formation. This in turn should increase the number of

nuclei that detach and increase the number of nuclei in the melt ahead of the advancing columnar grains. It is also felt that the smaller size ingots used in tests 1 to 3 are more conducive to the survival of detached surface dendrites as the distance they travel to the growing columnar front is much shorter. This would make them less likely to melt.

Not all aspects of the showering of dendrites theory is supported in this work. Growing equiaxed grains still have to release their latent heat into a supercooled environment. In the case of Pb-1.5%Sn the liquid thermally supercools which allows this to occur. Therefore, it is proposed that thermal supercooling is required for the showering of dendrites mechanism to take effect which conficts with the original theory proposed by Southin. It is felt that the melt in tests 1 to 4 also thermally supercooled but that it could not be measured due to improper techniques and equipment. As such, the showering of dendrites mechanism was active for these tests.

It must be emphasized that thermal supercooling of an alloy is phenomenon that probably only occurs in a laboratory experiment as described in this study and may not occur in a commercial casting application such as the continuous casting of steel billets. The difficulty is in visualizing how the central portion of a steel billet loses heat other than to the surrounding solid shell in order to thermally supercool. Therefore, the mechanism to account for the CET in Pb-1.5%Sn alloys can not be extended to commercial applications. It is also felt that this mechanism is not applicable even to the case of Sn-10%Pb performed in this study. In this test the large number of small equiaxed grains in the equiaxed zone indicate that there were a sufficient number of nuclei present in the melt prior to directional solidification such that the nuclei were activated in the constitutionally supercooled zone which is ahead of the dendrite tips in the columnar grains. In addition, the cooling curve data indicate that there was no loss of heat from the

top surface. First of all, the duration of the plateau increases with distance from the chill as discussed previously. Second, the slope of the cooling curves obtained from TC2 and TC3 are almost identical which means that the cooling rate is almost identical at these two positions. Without a loss of heat from the top surface, the showering of dendrites mechanism can not take place. Finally, the relative density of the initial equaixed grains to the solute enriched liquid causes them to rise and not fall.

The rise of the inital equiaxed grains is seen in the Sn-10%Pb test in the variation of the temperature of the horizontal plateau, T_P, and perhaps in the decrease in grain size in the equiaxed zone with distance from the CET. Equiaxed grains which rise cause a depletion of solute towards the top of the ingot, and an enrichmnet of solute toward the CET. This is easily calculated based on the T_P, the composition at 93 mm from the chill is calculated to be Sn-7.6%Pb while at 64 mm, it is Sn-9.3%Pb. It is expected that if the initial equiaxed grains do move upward after nucleation then one would see more and smaller equiaxed grains toward the top of the ingot which is exactly what is shown in Figure 3.29. In contrast to this if the initial equiaxed grains do not move then there should be no relationship between distance from the CET and equiaxed grain size. It is unfortunate that there are so few grains in the Pb-1.5%Sn ingots that this relationship can not be explored.

4.5 MATHEMATICAL MODELLING

In order to fulfill the mandate to fit the predicted temperatures to the experimental temperatures as closely as possible, the supercooling has to be comnpletely ignored while the temperature at the top of the melt, T_{FURN}, has to be changed. Fortunately, for

Pb-1.5%Sn the supercooling is small, <0.5°C, and the changing of T_{FURN} only illustrates the lack of precise knowledge on how heat is lost or gained using a vertical mould in a resistance heating furnace. General knowledge on the fact that heat is first gained by the melt and then lost by the melt to the furnace is all that is needed to use the model to interpolate temperatures between the fixed position thermocouples.

Even though the model does have its shortcomings it is still able to show that in most cases, at the CET the G_L is essentially 0°C/mm, see Table 3.13. There are however a few cases where the G_L is substantially higher ranging from 0.04°C/mm to 0.10°C/mm. With this kind of inconsistency it is still difficult to determine a critical G_L at the CET for Pb-1.5%Sn. It appears that given the very few effective nuclei in the melt, it is a hit and miss situation to form the CET.

The experimentally determined values, G_{LX}, assumed that the temperature gradient between two thermocouples is linear. The results shown in Figure 3.32 show that this is a good assumption as the temperature gradient in front of TC2 is linear for up to 10 mm. It is not known if the gradient remains linear beyond this distance. The very close match between G_{LX} and G_L in Figures 3.33 and 3.36 suggest that it does remain linear.

The effect of releasing latent heat in a different fashion for Pb-1.5%Sn is observed to have very little effect. Using the Scheil equation or the Lever rule to calculate the amount of latent heat released does not result in significatntly different predicted temperatures from the linear assumption as shown in Figures 3.37 to 3.39 inclusive. In both the Scheil equation and the Lever rule model, a greater proportion of the latent heat is released closer to the liquidus temperature. In turn, one would expect that the predicted temperatures around the liquidus be higher for models incorporating the Scheil equation

or the Lever rule. It is obvious that this is not so. If the temperatures are higher at the liquidus the one would expect that the G_L would be lower than using the linear assumption. As shown in Figure 3.40, this does happen but again the difference is negligble. There are two principal reasons that proportioning the latent heat release differently does not result in different predicted temperatures. The first reason is due the low amount of latent heat released overall. The calculated value listed in Table 2.1 is only 24.5 J/gm. The second is due to the very short freezing range of the alloy which is only 4.6°C. Increasing the solute content of the alloy does increase the freezing range over from 4.6°C to 9.3°C for Pb-3%Sn and 18.6°C for Pb-6%Sn. This does have some effect on the predicted temperatures as shown in Figure 3.41. The predicted temperatures from the three models are now separated by a greater amount. The change in the way latent heat is released does not change the overall shape of the cooling curves. For example, a horizontal temperature plateau does not appear using the Scheil equation or the Lever rule when one does not appear using the linear assumption. It is also interesting to note that at very low temperatures in Figure 3.41 the Scheil equation model predicts the lowest temperatures. This is due to the fact that using the Scheil equation means that the temperature range over which the alloy solidifies is extended to the eutectic temperature and at some temperature within the liquidus to solidus temperatures, the fraction solid versus temperature plot levels off. As a result, the linear method releases more latent heat at the lower temperatures than the Scheil equation which produces higher predicted temperatures.

Changing the alloy system to Sn-10%Pb greatly affects the ability to fit the predicted temperatures to experimental temperatures using all three methods to release latent heat as shown in Figures 3.44 to 3.46 inclusive. The predicted temperatures are

always lower than the experimental temperatures but more importantly, the shape of the predicted cooling curve does not resemble the experimental cooling curve. The difference in the shape of the curve is magnified as the distance from the chill face increases. The predicted cooling curves have a concave up shape while the experimental cooling curves show a change in the concavity from concave up while the alloy is liquid to concave down while the alloy is solidifying. This is felt to be important as it signifies that the model is not solidifying in the same way as the alloy solidifies. The situation is improved only slightly when the method to release latent heat is changed to using the Scheil equation or the Lever ruleThis is shown for the case at 93 mm from the chill face, where the predicted cooling curve from the Scheil equation and the Lever rule do show some change in the concavity of the curve but this does not significantly improve the fit between predicted and experimental temperatures. The predicted temperatures are still lower than the experimental temperatures at the liquidus temperature.

The problem in obtaining a good fit for Sn-10%Pb is not one of latent heat release but one concerning the supercooling and the deviation of the horizontal temperature plateau from the liquidus temperature observed in the experimental cooling curve. Assuming that no supercooling is required for solidification to occur is extremely erroneous in this case as the supercooling in the Sn-10%Pb alloy is measured up to 2.8°C which is now a very significant amount when compare to <0.5°C for Pb-1.5%Sn. The experimental conditions state that supercooling must be considered and that it varies with distance from the chill. In order to incorporate this condition into the model, the nature of the model must be changed from one involving heat transfer alone to one involving nucleation and growth processes. An example of such a model is the Hunt model which provides a nucleation condition, equation 1.4, and a growth condition, equation 1.3. In

addition, for the model to be successful, it must also account for the increase in the horizontal temperature plateau caused by the movement of light equiaxed grains and heavy solute enriched liquid. Accomodating these observations into a model is difficult as not much is known about why the supercooling varies with distance, and how fast the nuclei rise.

Despite the inaccuracies of the linear, the Scheil and the Lever rule models, comments should be made on the influence of the release of latent heat on the predicted G_L for the Sn-10%Pb alloy. In Figure 3.48 releasing more of the latent heat closer to the liquidus temperature, as the Scheil equation and Lever rule methods do, decreases the predicted G_L significantly. This does change the value of G_L predicted to occur at the CET. However, increasing the amount of latent heat released closer to the liquidus temperature does not prevent the G_L from decreasing to 0°C/mm. In fact, the Scheil equation and the Lever rule models show that the G_L reaches 0°C/mm faster than the linear assumption.

The major difference between the Sn-10%Pb system and the Pb-1.5%Sn system, to produce the differences observed in the predictions from the three methods to release latent heat, is in the total amount of latent heat released. The Sn-10%Pb alloy is calculated to release 56J/gm which is twice as much as the Pb-1.5%Sn alloy. Thus, any change in the proportioning of the latent heat is expected to have a greater influence on the amount that is released at various temperatures between the liquidus and the solidus temperatures. In addition, the Sn-10%Pb alloy has a much wider temperature range than the Pb-Sn alloys. For a given amount of latent heat using the linear assumption, increasing the temperature range decreases the amount of latent heat released per °C. The Sn-10%Pb alloy also shows the Lever rule and the Scheil equation model to predict

identical temperatures and temperature gradients whereas the Pb-1.5%Sn shows a small difference. This is due to the fact that with Sn-10%Pb the solidus temperature and the eutectic temperature are the same and therefore the range over which the latent heat is released is the same. This is not true for Pb-1.5%Sn which has a solidus temperature of 318.3°C and an eutectic temperature of 183°C.

It is expected given the difference in the predicted temperatures and temperature gradients of the Pb-Sn and Sn-Pb alloys using the three methods to release latent heat that the differences would be even more with an alloy that has a very large amount of latent heat released over a very wide solidification range. For example, Al-3%Cu has a calculated latent heat of 382J/gm and solidifies over a 55°C range. Both of these values are greater than Sn-10%Pb alloy's values so that the predicted results using a linear assumption of latent heat should be vastly different than the predicted results using either the Scheil equation or the Lever rule.

Chapter 5

CONCLUSIONS

1). Temperature measurements as accurate as ±0.2°C are possible using chromel-alumel thermocouples if an "in-situ" calibration is performed immediately prior to the experiment.

2). The "in-situ" calibration technique is complimented by taking multiple data points and using the mean of the data points as the recorded temperature when using an A/D data acquisition board.

3). Calibrating thermocouples once prior to testwork performed over a prolonged period results in inaccurate temperature measurements because of the errors associated with the thermocouples change with time in a non predictable fashion.

4). The CET in a Sn-10%Pb alloy has been found to occur at approximately 0.1°C/mm as determined by accurate temperature measurements. This confirms to a first approximation the results of Mahapatra and Weinberg[18].

5). Supercooling is observed in directionally solidified Sn-10%Pb and varies with distance from the chill ranging from 0.3°C to 2.8°C.

6). A horizontal temperature plateau is also observed in Sn-10%Pb and also varies with distance from the chill due to the initial equiaxed grains rising and the Pb enriched solute sinking during equiaxed growth.

7). The CET in a Pb-1.5%Sn alloy must wait for the liquid ahead of the solid/liquid interface to thermally supercool because of the lack of nuclei in the melt prior to directional solidification. The G_L at the CET is usually close to 0°C/mm as determined experimentally and verified from a heat transfer model.

8). The maximum amount of thermal superooling is approximately 0.4°C in directionally solidified a Pb-1.%Sn.

9). Horizontal temperature plateaus are also seen with the Pb-1.5%Sn alloy but unlike the Sn-10%Pb alloy, the temperature of the plateau does not vary with distance from the chill. The temperature of the plateau occurs at the liquidus temperature of the alloy. This is due to the fact that the initial equiaxed grains do not rise in the liquid during their growth but probably remain motionless.

10). The CET in Pb-1.5%Sn occurs following the showering of dendrites theory as proposed by Southin[6]. However, thermal supercooling is intrinsically involved in the CET for this alloy which does not follow the original theory.

11). The showering of dendrites mechanism for Pb-1.5%Sn is not transferable to Sn-10%Pb because of the difference in the number of nuclei in the melt and their behaviour after the initial grains form.

12) A heat transfer model is successful in predicting temperatures for Pb-1.5%Sn because of the small amount of supercooling and no movement of equiaxed grains during growth.

13). A heat transfer model is not successful in predicting temperatures for Sn-10%Pb because of the large amount of supercooling and the movement of light equiaxed grains after they initially form. A better approach to take to model this alloy when directionally solidifying this alloy is to use a nucleation and growth model in conjunction with the heat transfer model.

14). The effect of changing the method to release latent heat on the predicted temperatures and temperature gradients is dependent on the amount of latent heat to be released and the freezing range of the alloy. Increasing both has a tendancy to increase the effect as higher temperatures and lower gradients are predicted using the Scheil equation or the Lever rule compared to the results using a linear assumption.

REFERENCES

1. B.Chalmers, Principles of Solidification, John Wiley and Sons, 1964

2. G.J.Davies, Solidification and Casting, Applied Science Publishers Ltd.,1973

3. B.Chalmers, Journal of Metals, Transactions AIME, May 1954

4. B.Chalmers, W.C.Winegard, Transaction of The ASM, Vol. 46, 1954, p1214

5. B.Chalmers, D.Walton, Transactions of The Metallurgical Society of Aime, Vol. 215, June 1959

6. R.T.Southin, Transactions of The Metallurgical Society of Aime, Vol.239, Feb. 1967, p220

7. J.L. Walker, Phys. Chem. of Proc. Met. II, G.R. St. Pierre ed, p 845, 1961

8. K.A.Jackson, J.D.Hunt, D.R.Uhlman, T.P.Seward III, Transactions of The Metallurgical Society of Aime, Vol. 236, Feb. 1966, p149

9. G.S.Cole, G.F.Bolling, Transactions of The Metallurgical Society of AIME, Vol.239, Nov.1967, p1824

10. G.S.Cole, G.F.Bolling, Transactions of The Metallurgical Society of AIME, Vol.233, Aug.1965, p1568

11. A.Ohno, T.Motegi, H.Soda, Transactions ISIJ, Vol.11, 1971, p18

12. J.D.Hunt, Material Sciences and Engineering, Vol. 65, 1984, p75

13. J.D.Hunt, S.C.Flood, Modelling of Welding and Casting II, 1983, p207

14. J.D.Hunt, S.C.Flood, Modelling of Welding and Casting Processes, 1986, p607

15. M.H.Burden, J.D.Hunt, Metallurgical Transactions A, Vol. 6A, Jan. 1975, p240

16. M.H.Burden, J.D.Hunt, Journal of Crystal Growth, Vol. 22, 1974, p99

17. M.H.Burden, J.D.Hunt, Journal of Crystal Growth, Vol. 22, 1974, p109

18. R.B.Mahapatra, F.Weinberg, Metallurgical Transactions B, Vol. 3, N°2, June 1987, p425

19. I. Ziv, F. Weinberg, Metallurgical Transactions B, Vol 20B, 1989, p731

20. J.Lipton, M.E.Glicksman, W.Kurz, Material Science and Engineering, 65, (1984), 57-63

21. P.A.Kinzie, Thermocouple Temperature Measurement, John Wiley and Sons, 1973

22. R.J.Schaefer, M.E.Glicksman, Transactions of The Metallurgical Society of AIME, Vol. 239, Feb. 1967, p257

23. G.S.Cole, K.W.Casey, G.F.Bolling, Metallurgical Transactions, Vol. 1, May 1970, p1413

24. G.S.Cole, G.F.Bolling, Transactions of The Metallurgical Society of AIME, Vol. 242, Jan. 1968, p153

25. J.Lipton, W.Henemann, W.Kurz, Arch. Eisenhuttnwes, 55, 1984,p195

26. L.A.Tarshis, J.L.Walker, J.W.Rutter, Metallurgical Transactions, Vol. 2, Sept. 1971, p2589

27. J.Lipton, W.Kurz, W.Henenmann, Concast News Technology, Vol. 22, N°2, 1983, p4

28. H.Fredriksson, M.Hillert, Metallurgical Transactions, Vol. 3, Feb. 1972, p565

29. H.Fredriksson, M.Hillert, Material Sciences and Technology, Vol. 2, May 1986, p508

30. S.Witzke, J.P.Riquet, Acta Metallurgica, Vol. 30, 1982, p1717

31. S.Witzke, J.P.Riquet, F.Durand, Acta Metallurgica, Vol. 29, 1981, p365

32. L.Beitelman, Transactions of The ISS, Aug. 1988, p43

33. J.K.Brimacombe, K.Sorimachi, Metallurgical Transactions B, Vol. 8B, Sept. 1977, p489

34. G.A.Chadwick, Metals and Materials, March 1969, p77

35. T.W.Clyne, Materials Science and Engineering, 65, 1984, p111

36. C. Schesvov, M.A.Sc. Thesis, 1983, U.B.C.

37. S.E.Kisakurek, Journal of Material Science, Vol. 19, 1984, p2289

38. D.R.Croft, D.G.Lilley, Heat Transfer Calculations Using Finite Difference Equations, Applied Science Publishers Ltd., 1977

39. L.Backerud, B.Chalmers, Transactions of The Metallurgical Society of AIME, Vol. 245, Feb.1969, p309

40. G.S.Cole, W.C.Winegard, Journal of The Institute of Metals, Vol.93, 1964-65, p153

41. D. Poirier, M. Salcudean, ASME Conference, December, 1986

42. Handbook Of Chemistry and Physics, 57th Edition

43. Thermophysical Properties of Matter, Vol. 1, Thermal Conductivity, IFI/Plenum, New-York, Washington, 1970

APPENDIX 1

The heat balance on the interior node, ie: i=2, N, shown below is given as:

Heat In - Heat Out + Heat Generated - Heat Consumed = Heat Accumulated

Heat In:

$$(k\Delta y\,1)\frac{(T'(i-1)-T'(i))}{\Delta x}$$

Heat Out:

$$(k\Delta y\,1)\frac{(T'(i)-T'(i))}{\Delta x}$$

For a node in the liquid state cooling then, Heat Generated = Heat consumed = 0

Heat Accumulated:

$$\rho C_p(\Delta x\Delta y\,1)\frac{(T'(i)-T(i))}{\Delta t}$$

After all terms are combined, allowing $\Delta x = \Delta y$, and dividing by Δx^2, the heat balance equation for the interior nodes become:

$$\frac{k}{\Delta x^2}T'(i+1)-\left(\frac{2k}{\Delta x^2}+\frac{\rho C_p}{\Delta t}\right)T'(i)+\frac{k}{\Delta x^2}T'(i-1)=\frac{-\rho C_p}{\Delta t}T(i)$$

The heat balance on the bottom node where i=N is given by:

Heat In:

$$(k\Delta y\,1)\frac{(T'(i-1)-T'(i))}{\Delta x}$$

Heat Out:

$$H_B \Delta y 1 (T'(i) - T_{AMB})$$

Heat Accumulated:

$$\rho C_p \left(\frac{1}{2} \Delta x \Delta y 1 \right) \frac{(T'(i) - T(i))}{\Delta t}$$

Again, if all terms are combined and $\Delta x = \Delta y$, and divide by Δx^2, the bottom heat balance equation becomes:

$$\frac{2k}{\Delta x^2} T'(i-1) - \left(\frac{2k}{\Delta x^2} + \frac{2H_B}{\Delta x} + \frac{\rho C_p}{\Delta t} \right) T'(i) = \frac{-\rho C_p}{\Delta t} T'(i) - \frac{2H_B}{\Delta x} T_{AMB}$$

Similarly, the heat balance at the top node where i=1 is given by:

Heat In:

$$k \Delta y 1 \left(\frac{T'(i+1) - T'(i)}{\Delta x} \right.$$

Heat Out:

$$H_{Top} \Delta y 1 (T'(i) - T_{Furn})$$

Heat Accumulated:

$$\rho C_p \left(\frac{1}{2} \Delta x \Delta y 1 \right) \frac{(T'(i) - T(i))}{\Delta t}$$

The final heat balance at the top node where i=1 after all terms are combined and $\Delta x = \Delta y$ and the entire equation is divided by Δx^2 is:

$$\frac{2k}{\Delta x^2}T'(i+1)-\left(\frac{2k}{\Delta x^2}+\frac{2H_{Top}}{\Delta x}+\frac{\rho C_p}{\Delta t}\right)T'(i)=\frac{-\rho C_p}{\Delta t}T(i)-\frac{2H_{Top}}{\Delta x}T_{AMB}$$

As stipulated, the above equations do not consider the situation where a node releases a portion of the latent heat of solidification upon cooling through the mushy zone. To incorporate the latent heat of solidification term, consider heat a node loses as it cools:

$$H=\rho CV\Delta T$$

If a node is undergoing solidification, the heat lost is given as:

$$H=\rho CV\Delta T+L\rho V\Delta FS$$

To bring in the latent heat into the implicit finite difference equations, the temperature of the node is first allowed to cool from the liquid state to the mushy state without the latent heat being brought in as depicted below.

The heat lost is then given by:

$$H=\rho VC(T_1-T_2)$$

Reality states that T_2 is not reached at this time because latent heat is released after the temperature falls below T_{Liq}. Therefore, the heat lost by the node undergoing solidification should be given by:

$$H=\rho VC_1(T_1-T_{Liq})+\rho VC_2(T_{Liq}-T_3)+L\rho V\Delta FS$$

The amount of heat lost by the node is identical, therefore the heat balance is given by:

$$\rho VC_1(T_1-T_2)=\rho VC_1(T_1-T_{Liq})+\rho VC_2(T_{Liq}-T_3)+L\rho V\Delta FS$$

The equation reduces to:

$$T_3 - \left(\frac{L}{C_2}\right)\Delta FS = T_{Liq} - \left(\frac{C_1}{C_2}\right)(T_{Liq} - T_2)$$

A problem appears in that to calculate ΔFS using the Scheil equation one has to know what the C_s, and C_l at the new corrected temperature T_3 are, to solve the heat balance. This is accomplished by using the Secant convergence technique which uses two simultaneous guesses at T_3 to calculate C_s, and C_l, which produce two guesses at ΔFS in order to solve the heat balance. The procedure is repeated until convergence is reached. When convergence is reached, T_3 becomes the new temperature for the node.

The same situation is encountered when the node goes from one mushy state to another as depicted below.

The total heat lost by the node in this situation is given by equation XX while reality states that the heat lost by the node is given by:

$$H = \rho V C_2(T_1 - T_3) + L\rho V\Delta FS$$

The heat balance is:

$$\rho V C_2(T_1 - T_2) = \rho V C_2(T_1 - T_3) + L\rho V\Delta FS$$

This equation reduces to:

$$T_3 - \left(\frac{L}{C_2}\right)\Delta FS = T_2$$

The Secant convergence technique is also used to solve the heat balance.

APPENDIX 2

This analysis is concerned with two hypotheses at a 1% level of significance regarding the ratio of variances from two sets of samples. The hypotheses one is testing is whether or not the ratio of:

$$\frac{\sigma_1^2}{\sigma_2^2} = 1$$

or

$$\frac{\sigma_1^2}{\sigma_2^2} = \lambda \neq 1$$

where:

σ_1^2, σ_2^2 are the variances of the two sets of samples in question.

The hypotheses are tested by calculating a critical region of values which are given by:

$$\frac{S_1^2}{S_2^2} < F_{n_1-1, n_2-1, 1-\alpha/2}$$

or

$$\frac{S_1^2}{S_2^2} > F_{n_1-1, n_2-1, \alpha/2}$$

where:

$F_{n_1-1, n_2-1, \alpha/2}$ is the Snedecor F ratio with (n_1 - 1, n_2 - 1) degrees of freedom at the α level of significance, and $\alpha = 0.01$.

If S_1^2 and S_2^2, satisfy either of the above inequalities then the variances of the two sets of samples are significantly different.

The data from two selected temperatures on the cooling curve shown in Figure 17 corresponding to a temperature in the supercooled portion of the curve and to a temperature on the plateau are chosen for the analysis, and are shown below.

Set 1. (from the supercooled portion of the cooling curve)

$n_1 = 32$

$\bar{x}_1 = 13.3821mV = (328.15°C)$

$s_1 = 0.0051$ mV

Set 2. (from the temperature plateau)

$n_2 = 32$

$\bar{x}_2 = 13.3987mV = (328.39°C)$

$s_2 = 0.0037$

where:

n_1, n_2 = the number of samples taken for data points 1 and 2

$\bar{x}_1, \bar{x}_2$, = the mean of the 32 samples for data points 1 and 2

s_1, s_2 = the standard deviation of the 32 samples for data points 1 and 2

The above data produces a ratio of $\frac{s_1^2}{s_2^2} = 1.9$

The value of $F_{31,31;.005} \sim F_{30,30;.005} = 2.6278$ is from the $F_{m1,m2}$ Distribution Table in Guttman, Wilks and Hunter, while the value of $F_{31,31;.995} = \frac{1}{F_{31,31;.005}} \sim \frac{1}{F_{30,30;.005}} = .38$.